



# Control and Non-Payload Communications Generation 7 Radio Flight Test Report

*Kurt Shalkhauser and Joseph Ishac  
Glenn Research Center, Cleveland, Ohio*

*Brian Frantz  
HX5, LLC, Brook Park, Ohio*

*Michael Cauley  
Glenn Research Center, Cleveland, Ohio*

*Steven Bretmersky  
MTI Systems, Inc., Cleveland, Ohio*

*Dennis Iannicca  
Glenn Research Center, Cleveland, Ohio*

*Christine Chevalier and David Stewart  
HX5, LLC, Brook Park, Ohio*

*Robert Dimond and Evan Hanau  
Peerless Technologies Corporation, Fairview Park, Ohio*

This Revised Copy, numbered as NASA/TM-20205011515/REV1, March 2023, supersedes the previous version, NASA/TM-20205011515, October 2021, in its entirety.

## NASA STI Program . . . in Profile

Since its founding, NASA has been dedicated to the advancement of aeronautics and space science. The NASA Scientific and Technical Information (STI) Program plays a key part in helping NASA maintain this important role.

The NASA STI Program operates under the auspices of the Agency Chief Information Officer. It collects, organizes, provides for archiving, and disseminates NASA's STI. The NASA STI Program provides access to the NASA Technical Report Server—Registered (NTRS Reg) and NASA Technical Report Server—Public (NTRS) thus providing one of the largest collections of aeronautical and space science STI in the world. Results are published in both non-NASA channels and by NASA in the NASA STI Report Series, which includes the following report types:

- TECHNICAL PUBLICATION. Reports of completed research or a major significant phase of research that present the results of NASA programs and include extensive data or theoretical analysis. Includes compilations of significant scientific and technical data and information deemed to be of continuing reference value. NASA counter-part of peer-reviewed formal professional papers, but has less stringent limitations on manuscript length and extent of graphic presentations.
- TECHNICAL MEMORANDUM. Scientific and technical findings that are preliminary or of specialized interest, e.g., “quick-release” reports, working papers, and bibliographies that contain minimal annotation. Does not contain extensive analysis.
- CONTRACTOR REPORT. Scientific and technical findings by NASA-sponsored contractors and grantees.
- CONFERENCE PUBLICATION. Collected papers from scientific and technical conferences, symposia, seminars, or other meetings sponsored or co-sponsored by NASA.
- SPECIAL PUBLICATION. Scientific, technical, or historical information from NASA programs, projects, and missions, often concerned with subjects having substantial public interest.
- TECHNICAL TRANSLATION. English-language translations of foreign scientific and technical material pertinent to NASA's mission.

For more information about the NASA STI program, see the following:

- Access the NASA STI program home page at <http://www.sti.nasa.gov>
- E-mail your question to [help@sti.nasa.gov](mailto:help@sti.nasa.gov)
- Fax your question to the NASA STI Information Desk at 757-864-6500
- Telephone the NASA STI Information Desk at 757-864-9658
- Write to:  
NASA STI Program  
Mail Stop 148  
NASA Langley Research Center  
Hampton, VA 23681-2199



# Control and Non-Payload Communications Generation 7 Radio Flight Test Report

*Kurt Shalkhauser and Joseph Ishac  
Glenn Research Center, Cleveland, Ohio*

*Brian Frantz  
HX5, LLC, Brook Park, Ohio*

*Michael Cauley  
Glenn Research Center, Cleveland, Ohio*

*Steven Bretmersky  
MTI Systems, Inc., Cleveland, Ohio*

*Dennis Iannicca  
Glenn Research Center, Cleveland, Ohio*

*Christine Chevalier and David Stewart  
HX5, LLC, Brook Park, Ohio*

*Robert Dimond and Evan Hanau  
Peerless Technologies Corporation, Fairview Park, Ohio*

This Revised Copy, numbered as NASA/TM-20205011515/REV1, March 2023, supersedes the previous version, NASA/TM-20205011515, October 2021, in its entirety.

National Aeronautics and  
Space Administration

Glenn Research Center  
Cleveland, Ohio 44135

## Acknowledgments

This report was prepared under the Unmanned Aircraft Systems Integration in the National Airspace System (UAS in the NAS) Project in coordination with Radio Technical Commission for Aeronautics (RTCA) Special Committee (SC) 228 Working Group 2. The authors acknowledge the members of the UAS in the NAS Command and Control (C2) Subproject team who have contributed to this report and to the extensive flight test activities it describes. They include Daniel Young (Peerless Technologies Corporation) and Donna Clements (HX5, LLC). The project would not have been possible without the support of the pilots Kurt Blankenship, James Demers, Mark Russell, and Aaron Swank; the flight engineers Jeff Polack and Matt Fakler; and the entire maintenance staff. Additionally, the research conducted throughout the C2 Subproject would not have been possible without the capabilities of NASA601, the Lockheed Corporation model S-3B Viking aircraft owned by NASA Glenn Research Center (aircraft registration number N601NA). This twin-turboprop jet research aircraft was used extensively for all of the dual-band channel sounding measurements, developmental Control and Non-Payload Communications (CNPC) radio flight tests, CNPC radio validation flight tests, and site surveys required under the UAS C2 efforts. Built in 1978, this venerable aircraft was the last S-3B assembled by Lockheed Corporation and was the only S-3B still in service throughout the NASA UAS in the NAS Project. This aircraft has now been decommissioned and is enjoying full retirement at the San Diego Air and Space Museum.

## Revised Copy

This Revised Copy, numbered as NASA/TM-20205011515/REV1, March 2023, supersedes the previous version, NASA/TM-20205011515, October 2021, in its entirety.

An incorrect version of NASA/TM-20205011515 was published in October 2021. Modifications to this Revised Copy address errors, omissions, and inconsistencies to the text and figures. The acknowledgments section has been revised, and an authorship note has been inserted.

### Authorship note:

The authorship of this Technical Memorandum was updated in September 2022. Based on an analysis/investigation by the NASA Glenn Research Center Research Integrity Officer into the contributors to this report, the updated order of the authors reflects the best estimate of their contributions.

Trade names and trademarks are used in this report for identification only. Their usage does not constitute an official endorsement, either expressed or implied, by the National Aeronautics and Space Administration.

*Level of Review:* This material has been technically reviewed by technical management.

# Contents

Summary .....	1
1.0 Introduction .....	1
2.0 Control and Non-Payload Communications (CNPC) Radio Development and Evolution .....	1
2.1 Control and Non-Payload Communications (CNPC) Service Classes and Waveforms.....	2
2.2 Radio Physical Platform .....	3
2.3 Radio Transmission Profile .....	4
2.4 Laboratory Radiofrequency Testing.....	4
2.4.1 High-Power Amplifiers.....	5
2.4.2 Spectral Mask.....	7
2.4.3 Power Stability and Temperature Compensation.....	8
2.4.4 Power Adjustment.....	8
2.4.5 Receiver Sensitivity Measurement Methodology .....	9
2.4.6 Received Signal Strength Indicator Calibration, Sensitivity, and Linearization.....	9
2.4.7 Signal Threshold and Noise Floor Removal .....	10
3.0 Flight Test System Description .....	11
3.1 Airborne Radio System Description.....	12
3.2 Ground Radio System Description .....	16
3.2.1 Transmit and Receive Switching .....	17
3.2.2 Ground Radio System Support Systems .....	17
3.2.3 Ground Station Antennas.....	19
3.3 Flight Test Planning.....	22
3.3.1 Flight Range.....	22
3.3.2 Ground Station Networking Equipment.....	23
3.4 Flight Test Operations Center.....	23
4.0 Generation 7 Control and Non-Payload Communications Radio Propagation Flight Test Results .....	24
4.1 Flightpath General Description.....	26
4.2 Validation Flight Test Data Format Description .....	27
4.3 Validation Flight Test Data for Flat Terrain Setting, October 8, 2019.....	29
4.4 Validation Flight Test Data for Hilly Terrain Setting, December 11 and 12, 2019.....	36
4.5 Validation Flight Test Data for Open Water Setting, December 3, 5, and 6, 2019 .....	40
4.6 Excess Path Loss Data Processing and Fade Analysis .....	45
4.6.1 Fade Analysis Results .....	48
4.7 Validation Test Data for Airport Surface Operations, February 19, 2020.....	49
4.8 Generation 7 Control and Non-Payload Communications Radio Data Latency Test Results .....	52
5.0 Generation 7 Control and Non-Payload Communications Network Switchover Test Results.....	56
6.0 Conclusions .....	63
References.....	64



# **Control and Non-Payload Communications Generation 7 Radio Flight Test Report**

Kurt Shalkhauser\* and Joseph Ishac  
National Aeronautics and Space Administration  
Glenn Research Center  
Cleveland, Ohio 44135

Brian Frantz  
HX5, LLC  
Brook Park, Ohio 44142

Michael Cauley\*  
National Aeronautics and Space Administration  
Glenn Research Center  
Cleveland, Ohio 44135

Steven Bretmersky  
MTI Systems, Inc.  
Cleveland, Ohio 44135

Dennis Iannicca  
National Aeronautics and Space Administration  
Glenn Research Center  
Cleveland, Ohio 44135

Christine Chevalier and David Stewart  
HX5, LLC  
Brook Park, Ohio 44142

Robert Dimond and Evan Hanau  
Peerless Technologies Corp.  
Fairview Park, Ohio 44126

## **Summary**

This report presents a description and test results of a seventh-generation prototype radio developed for Control and Non-Payload Communications (CNPC) between a ground-based pilot and an unmanned aircraft. Radios were prepared under a cooperative agreement between the NASA Glenn Research Center and Collins Aerospace (formerly Rockwell Collins, Inc.) and were used to support the development and validation of air-to-ground CNPC radio system standards. The CNPC radios operated in the 5,030- to 5,091-MHz frequency range. This report describes radio waveforms, laboratory testing, flight test systems, and flight test results.

---

\* Retired.

## 1.0 Introduction

Unmanned aircraft (UA) continue to show promise for application in numerous future Government, commercial, and civil aeronautical systems. To help address the significant technical challenges associated with UA development, NASA Glenn Research Center has been working with other U.S. Government agencies to investigate communication technology solutions that will enable safe operation of UA in the national airspace. Data from previous NASA testing has directly supported the RTCA, Inc. Special Committee (SC)-228 development of the baseline Command and Control (C2) Data Link Minimum Operational Performance Standards (MOPS) (Terrestrial) document, which was prepared for the Federal Aviation Administration (FAA) as RTCA Paper No. DO-362 (Ref. 1). The Generation 7 (Gen 7) flight test data presented in this report directly supports Revision A of the DO-362 standard.

This work was conducted under NASA's Unmanned Aircraft Systems Integration in the National Airspace System (UAS in the NAS) Project. The C2 Subproject work was performed at Glenn Research Center in Cleveland, Ohio.

Working closely with the RTCA, academic, and industry partners, NASA engineers executed a multiyear investigation of C2 radio communications systems for UA. This work included systems studies and prototype radio development, as well as execution of flight tests in multiple environments to accumulate data needed for UA-related analyses, link budget development, and MOPS requirements validation. Under the initial Phase 1 effort (2012 to 2017), the Glenn and Collins cooperative agreement produced five incremental advancements of a software-defined radio that were used as a testbed and demonstrator for the UA Control and Non-Payload Communications (CNPC) links (Refs. 2 to 4). The fifth and final generation Phase 1 CNPC radio was utilized to validate the DO-362 requirements through a series of managed flight tests.

In the subsequent Phase 2 tasks (2017 to 2020), Glenn directed efforts at the technical challenges of reducing the size, weight, and power (SWaP) of the CNPC radio, with the intent to demonstrate compatibility with smaller, or midsize, UA operating in higher-density, lower-altitude, flight environments. Working again with Collins and utilizing an extension of the Government and industry cooperative research agreement (NNC11AA01A), two additional CNPC radio development cycles were completed, producing Gen 6 and Gen 7 radios.

This report describes the operation and testing of the Gen 7 CNPC radio and radio waveform, which was the final iteration under the C2 Subproject. NASA goals for the Gen 7 radio were (1) to demonstrate the MOPS-like CNPC functional operation on a radio platform that is smaller volume, lower weight, and utilizes less electrical power than the previous platform and (2) to demonstrate a CNPC radio that is on a path to commercialization and without constraints of International Traffic in Arms Regulations (ITAR) restrictions. Operational refinements flowing from the RTCA DO-362A (Ref. 5) studies were incorporated into the Gen 7 radio waveform, and performance was validated in a rigorous flight test campaign. Data from the NASA flight tests validated the requirements and formed the basis for many performance specifications in Reference 5.

Data from the complete flight testing campaign has been archived by NASA. Representative data has been included in this report to demonstrate the test methodology and to highlight various test results.

## 2.0 Control and Non-Payload Communications (CNPC) Radio Development and Evolution

Over the course of the two phases of the UAS in the NAS C2 Subproject, the prototype CNPC radio development followed an evolutionary path. The first phase of the subproject concentrated on the characteristics of the transmitted signals, that is, the waveform design and not the physical radio

hardware. For efficiency, the NASA/Collins team used existing software-defined radio (SDR) hardware to form and produce the transmitted radiofrequency (RF) signal for testing. The Phase 1 radios operated under temporary, experimental frequency authorizations in the L- and C-bands. In the second phase of the subproject, the testing was focused within the C-band frequencies, but the scope expanded to include evaluation of the waveform on a smaller physical platform.

The major enhancements to the waveform and radio capabilities throughout the project are summarized in Table 1.

## 2.1 Control and Non-Payload Communications (CNPC) Service Classes and Waveforms

The waveforms implemented in the Collins CNPC–5000E radios evolved throughout the term of the UAS in the NAS project. Extensive analysis and modeling, along with data from NASA testing, resulted in a consensus refinement of the signal characteristics by the RTCA DO–362 MOPS C2 Working Group. The CNPC radio waveforms used in the Gen 7 NASA tests were consistent with the final MOPS-defined signal characteristics. A complete discussion of the CNPC waveform evolution can be derived from References 2 to 5.

RTCA SC–228 recognized that different UA would have varying capabilities for differing CNPC data requirements. As a first step to identifying those requirements, SC–228 defined four service classes (Table 2) based on the types of UA communications traffic that would be used. For example, a small UA operating in a remote area at low altitude may only require uplink control and downlink telemetry services (Service Class 1), but a larger UA operating over a long range and high altitude would require all types of communications services (Service Class 4).

Glenn performed an extensive analysis of the traffic types for each service class of UA to determine the minimum data rates required. The analysis included data requirements for the airfield departure, en route, and airfield arrival phases of flight, when varying data loads are placed on the communications link. The analysis also included UA operations in both manual modes (by a ground-based pilot manipulating UA control surfaces in near realtime) and automatic mode (by adjustments of flight waypoints for an autopiloted UA). This analysis accounted for the raw payload data, header compression, and overhead for transport and network layer headers and security protocols. These required data rates were then converted to user payload bytes per CNPC frame assuming 20-Hz communication between the UA and ground station for the departure and arrival phases, and 15-Hz operation for the en route phase (5 Hz are reserved for the en route acquisition of other ground stations to enable network switchovers). The user payload sizes identified in the analysis were then verified using a combination of specialized testing.

TABLE 1.—CONTROL AND NON-PAYLOAD COMMUNICATIONS (CNPC) PROTOTYPE EVOLUTION

Phase	Generation	Description
1	1	L-band frequencies only on existing software-defined radio (SDR), point-to-point, single aircraft, and single ground station
	2	Added C-band frequencies on existing SDR, networked mode, single aircraft, and multiple ground stations; Demonstrated in-flight “switchovers” between ground stations
	3	Added capability for multiple aircraft on single ground station
	4	Added capability to restrict data rates for preliminary Command and Control (C2) Data Link Minimum Operational Performance Standards (MOPS) development
	5	Updated two point-to-point and networked-mode waveforms to align with final C2 MOPS
2	6	Reimplemented two point-to-point waveforms on low size, weight, and power (SWaP) C-band SDR, added features to get additional statistical performance data from the radio to enhance analysis
	7	Implemented and updated point-to-point waveforms and a networked-mode waveform to support MOPS Revision A

TABLE 2.—TYPES OF COMMUNICATION TRAFFIC IN UNMANNED AIRCRAFT SERVICE CLASSES

Service class	Telemetry	Voice	Navigational aids	Aircraft targets	Weather radar
1	X	----	----	----	----
2	X	X	----	----	----
3	X	X	X	X	----
4	X	X	X	X	X

TABLE 3.—GENERATION 7 (GEN 7) CONTROL AND NON-PAYLOAD COMMUNICATIONS WAVEFORM MODES  
[Only highlighted waveforms were implemented in the Gen 7 prototype radio.]

Waveforms	Mode	DO-362A <sup>a</sup> designation	Direction	-54dBc/kHz power spectral density (PSD) bandwidth, kHz	Channel width, C, kHz <sup>b</sup>	Physical data rate, kbps	User data rate, kbps <sup>c</sup>
Point-to-point	A	DC1	Uplink and downlink	51.6	90	34.5	7
	B	DC2	Uplink and downlink	94.1	130	69	16
	C	DC3	Uplink and downlink	131	170	103.5	25.6
	D	DC4	Uplink and downlink	170.8	210	138	34.6
Multiuser	6-slot	UL6	Uplink	247.3	285	207	7, 16, or 25.6
	9-slot	UL9	Uplink	361.3	400	310.5	7, 16, or 25.6
	12-slot	UL12	Uplink	473.4	510	414	7, 16, or 25.6
	15-slot	UL15	Uplink	583.3	620	517.5	7, 16, or 25.6
	18-slot	UL18	Uplink	692.1	730	621	7, 16, or 25.6
	21-slot	UL21	Uplink	800.2	840	724.5	7, 16, or 25.6
	24-slot	UL24	Uplink	907.3	945	828	7, 16, or 25.6

<sup>a</sup>Reference 5.

<sup>b</sup>Channel width C is equal to the -54 dBc/kHz PSD bandwidth plus a guard bandwidth of 35 kHz for transmit frequency inaccuracy and Doppler frequency error plus any remaining bandwidth necessary for C to equal a positive integer multiple of 5 kHz.

<sup>c</sup>User rates for multiuser modes shown per user using 1 to 3 slots.

To allow flexibility in the throughput needs for UA and to meet the data flow needs of the service classes, several waveforms were developed. Together NASA and Collins defined four point-to-point waveform modes to address the four data classes, offering user throughput rates from approximately 7 to 34 kbps. For the multiuser networked operation, in which one CNPC radio can uplink to as many as 24 separate UAs, several additional waveforms were added for demonstration purposes. UAs operating with the multiuser waveforms can utilize 1 to 3 slots in the uplink to support throughput rates from 7 to 25 kbps. The characteristics of the Gen 7 waveforms are shown in Table 3.

## 2.2 Radio Physical Platform

The Gen 7 C2 waveforms were implemented on a prototype, small form factor, C-band SDR prepared by Collins Aerospace (Figure 1). The radio was based on an L-band design (designated as the CNPC-1000) that had been previously developed for application in a UA by a commercial customer. For the NASA Gen 6 and 7 prototypes, Collins modified the RF design of the CNPC-1000 radio for C-band operation, designating it as model CNPC-5000E. All Gen 7 CNPC flight and ground testing was performed using the CNPC-5000E C-band radio. The radio was tunable from 5,030 to 5,091 MHz with a nominal RF output power level of 100 mW. The radio was intended to be paired with an external amplifier suitable for the specific flight application.



Figure 1.—Control and Non-Payload Communications (CNPC) C-band prototype radio (CNPC–5000E).

### 2.3 Radio Transmission Profile

The Gen 7 CNPC radios operated using Gaussian Minimum Shift Keying (GMSK) modulation to produce an output signal spectra similar to that shown in Figure 2. The output power versus frequency trace shown is for CNPC–5000E radio serial number E10 operating at the 5,035 MHz center frequency. The ordinate axis is for scale only. The radios were operated in point-to-point data class mode 3 with the 170-kHz channel width waveform, providing a symbol rate of 103,500 symbols per second.

For all validation flight tests, the MOPS CNPC radios were operated within their respective frequency authorizations at a center frequency of 5,035 MHz for both uplinks and downlinks. For the validation flight tests, the CNPC radios were operated with an external amplifier at an output power level of 10 W average envelope power.

### 2.4 Laboratory Radiofrequency Testing

The Gen 6 CNPC–5000E radios received early in the UAS Phase 2 project exhibited several technical problems that required investigation and correction. Glenn and Collins engineers collaborated to discover, identify, and resolve each of the performance problems, eventually producing the Gen 7 radios that had suitable performance for flight testing. Both physical and software modifications were incorporated into the radios for the UAS Phase 2 flight test campaign.

Spectral output power measurements were made in the laboratory on each radio. The nominal design was for a 100 mW output that could be adjusted internally to over 64 settings. At the maximum setting, the output power was considerably higher at 500 mW or more. The measured spectral noise floor for the output of this new design was considerably better than the military SDR radios used in the earlier Phase 1 Gen 5 flight tests. This was a key improvement for meeting the DO–362 spectral mask requirements, and essential for improved spectrum reuse in such a limited frequency band.

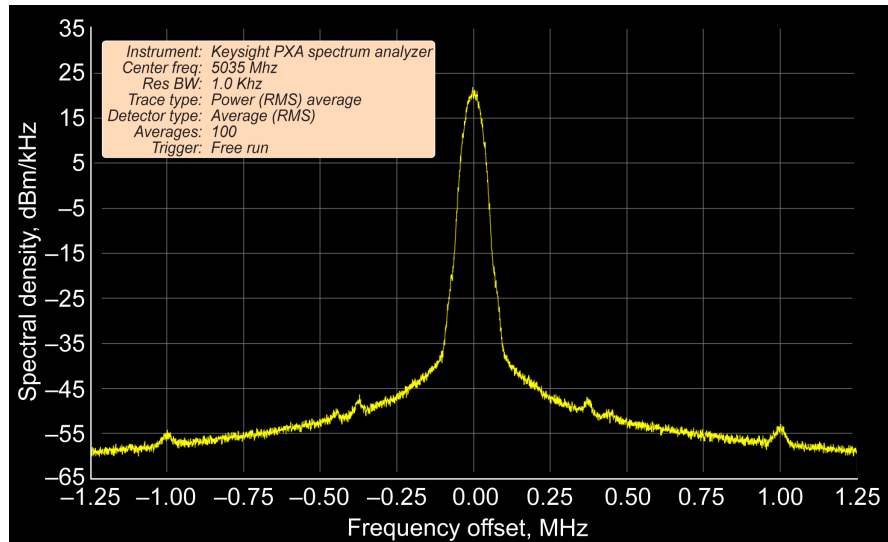


Figure 2.—Control and Non-Payload Communications (CNPC) radio output signal, 90-kHz mode. Root mean square (RMS).

The Gen 6 radios suffered from several problems that included (1) strong close-in spectral spurious signals that would vary as a function of output power; (2) strong local oscillator (LO) signal leakage and a LO frequency minus two times the intermediate frequency ( $LO - 2(IF)$ ) modulated spurious; (3) an abrupt pulse fall time resulting in excessive spectral peaks; (4) an unexplained, intermittent anomaly occurring during the pulse rise time related to output power; and (5) inaccurate received signal strength indicator (RSSI), which was a critical piece of information used for validating link performance during flight. All of these problems were mitigated before moving into the Gen 7 radio flight test campaign.

Figure 3 displays a comparison of spectral emissions from two separate radios. The blue line is the before trace, displaying the many unwanted spurious signals emitted by early Gen 6 radios delivered to Glenn. The black trace shows the signals emitted by radios in later deliveries. Still present were the LO leakage signal and the  $LO - 2(IF)$  spurious signal where IF is the intermediate frequency. These two signals were reduced to unmeasurable levels by the addition of an external 10 MHz wide bandpass filter at the radio output. The difference in the displayed noise floor between the two signals was due to differences in resolution bandwidth and other instrument settings.

For the Gen 7 radios, Collins placed RF absorbing material inside the radios to suppress the internal cavity resonances and isolate internal stray signal couplings from clocks, the IF, and the LOs. Firmware changes further reduced spurious output levels. The Gen 7 transmitters were spectrally very clean with the very minor exception of a very low LO leakage signal, which will be corrected in future units. This LO leakage signal was very close to the  $-60$  dBm/kHz design value.

For the Gen 6 and Gen 7 flight tests, a 20-MHz-wide filter was placed externally on the transmitter output between the radio and the power amplifier to eliminate the spurious signals and to allow operation over a modest range of adjacent channels. The filter characteristics are shown in Figure 4. The filter had approximately 0.5 dB insertion loss and was extremely flat (no ripple) over a 12-MHz bandwidth.

#### 2.4.1 High-Power Amplifiers

The small form factor CNPC-5000E radio was designed for a transmitter output power of 100 mW. The maximum permissible transmitter power specified in the MOPS is 10 W. For validation testing of the MOPS, an external amplifier was required to bring the radio output power up to the required MOPS level. Three different amplifier configurations were investigated over the course of the project.

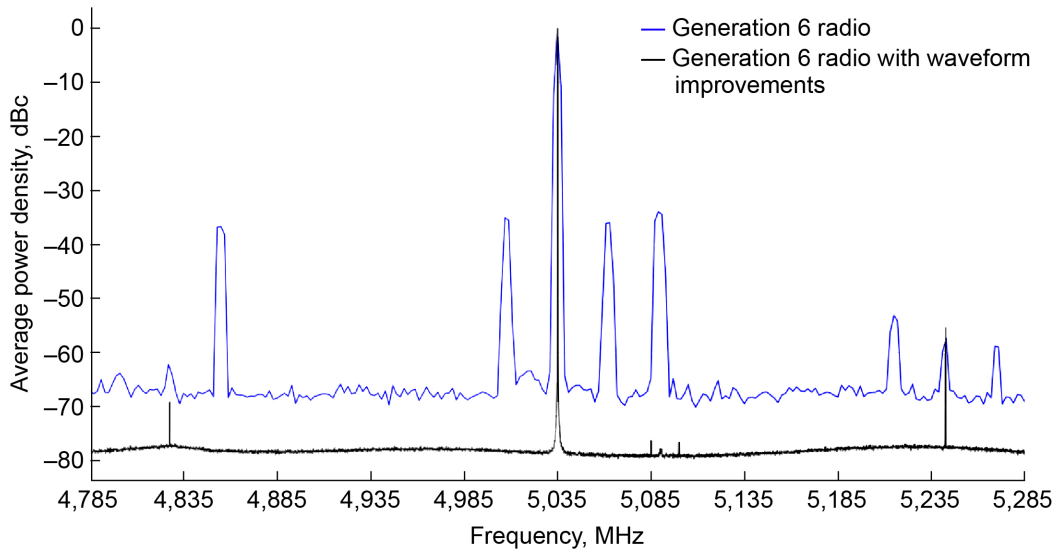


Figure 3.—Spurious radio emissions comparison before and after adjustments to Control and Non-Payload Communications (CNPC) radio (CNPC-5000E).

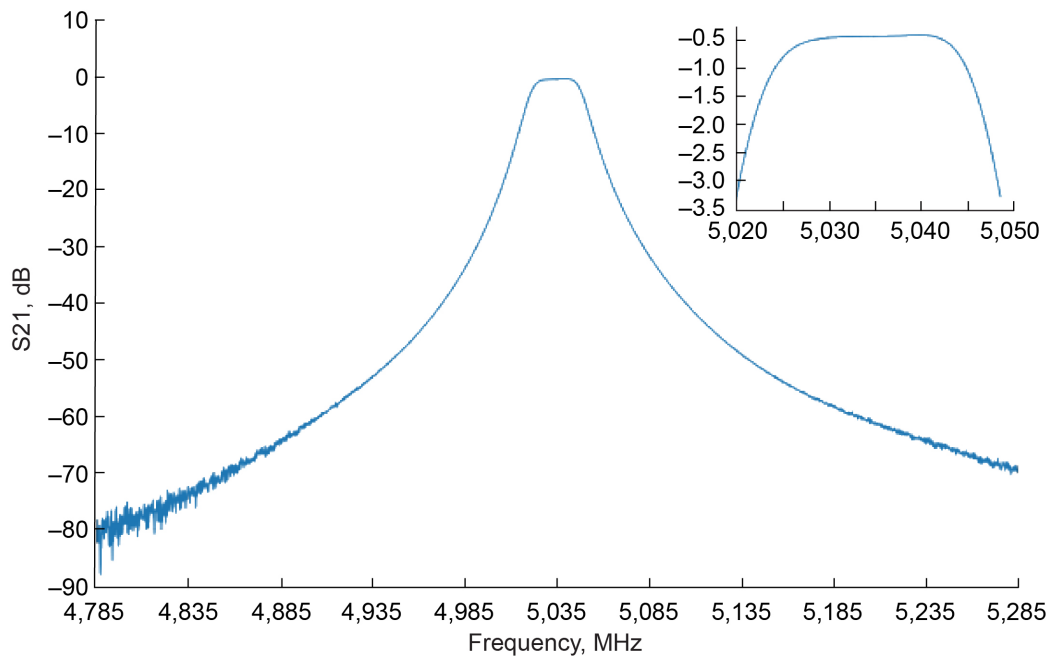


Figure 4.—Custom filter passband, center frequency 5,035 MHz.

To meet the 10-W transmit power requirement, an existing laboratory-grade, high-power rack-mounted amplifier was integrated into each of the ground stations using a Glenn-developed transmit and receive (T/R) plate. The SWaP consumption of these amplifiers makes them impractical for use on small aircraft, but they were well suited to the experimental environment of the NASA ground radio stations and S-3 research aircraft. The large amplifiers offered excellent performance, high power levels, and linear RF gain, and they could also support the multi-aircraft uplink modes where higher output levels are allowed.

At about the same time, a small form factor airborne power amplifier was identified from a commercial supplier. The published specifications appeared to be a close match with requirements, and the amplifier would also use the T/R plate designed for the rack-mounted amplifier. Laboratory testing

proved that this amplifier would fill the airborne requirement. The small amplifier was integrated into a second airborne radio system (ARS) and used as a backup test system and as a second interfering aircraft for adjacent channel and co-channel interference measurements.

A third amplifier configuration was a custom commercial development of a T/R module with integrated amplifier matched to the CNPC–5000E radio. This unit was designed to interface directly to the Collins CNPC–5000E radio and is of similar size and weight (Figure 5). The T/R module included all T/R switching, filtering, and amplification needed to support the radio. The T/R module was under evaluation at the conclusion of the UAS Phase 2 Subproject.

### 2.4.2 Spectral Mask

Much SC–228 discussion had surrounded the shape of the MOPS-defined GMSK CNPC spectral mask, which defines the allowable spectral power content in the transmitted signal. Figure 6 shows the transmit spectrum mask for a data class 3 signal and compares the shape to actual CNPC radio performance. The red line shows the power spectral density (PSD) mask requirement from the MOPS. Emissions from a radio must be below the red line. The green trace is the measured transmit output spectrum from the ARS in the S–3B Viking research aircraft. This green trace is nearly identical to the spectral emissions from the ground stations used in the flight tests, so all of the stations used in flight testing met the spectral mask. The Gen 5 radio, used in Phase 1 of the UAS C2 Subproject, was based upon a military SDR radio platform. Its power trace (orange) clearly showed excessive out-of-band emissions as the orange was above the red mask line. For final comparison, the blue trace was the output from a precision laboratory-grade vector signal generator after amplification produced a 10-W CNPC signal using the 10-W commercial solid-state power amplifier. The signal generator included a precision frequency reference to produce an extremely low-phase noise output. This blue trace was included in the figure to show what performance was possible.

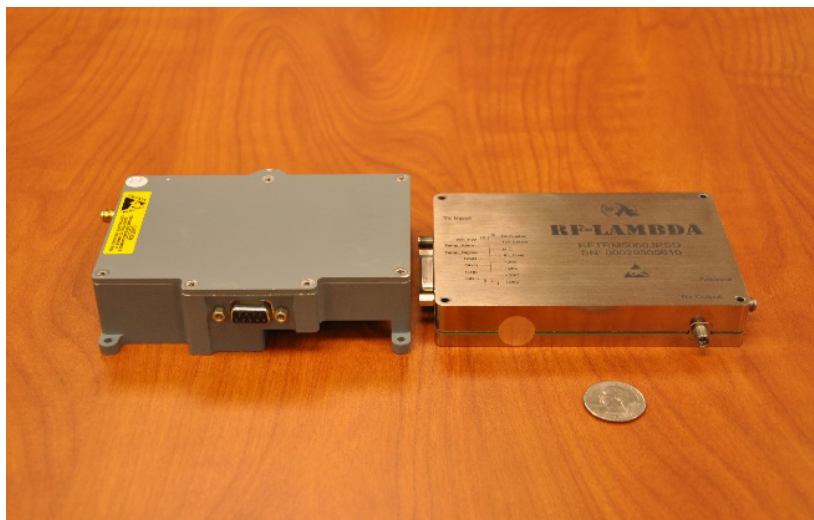


Figure 5.—Control and Non-Payload Communications (CNPC) radio (CNPC–5000E) (left) with custom transmit and receive module (right).

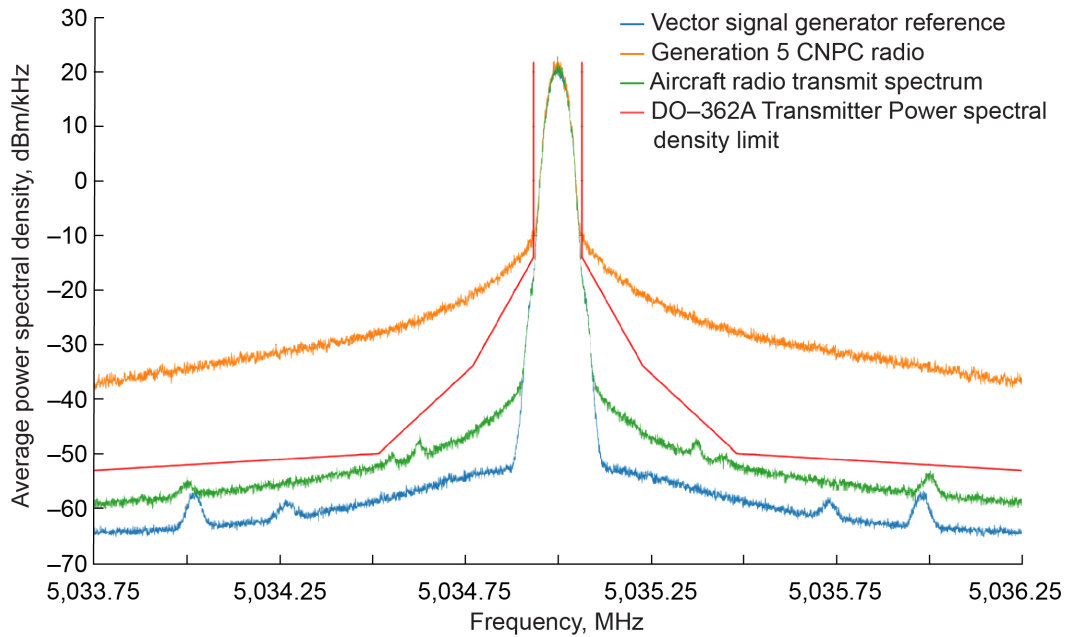


Figure 6.—Radio emissions mask and sample signal traces of the data class 3 power spectral density for 10 W average power. Control and Non-Payload Communications (CNPC).

### 2.4.3 Power Stability and Temperature Compensation

Laboratory testing showed radio output power level stability to be very good, and the decision was made not to instrument the stations to measure output power. Laboratory data showed the output power was within 0.2 dB of steady state 10 minutes after cold turn on and stabilized to 0.1 dB of its final value approximately 15 minutes after cold power on. Day-to-day commanding of the radio to a predefined power level was found to be highly repeatable. Active output power monitoring or corrections were not required for the flight tests. After a 10-minute warmup period, the radio was commanded to the setpoint for the target output power. Power stability was measured over time and with temperature. In a laboratory environment, the output power remained highly stable after a 30-minute warmup. During the final two flight tests, performed during very cold outdoor temperatures, minor variations in output power as a function of temperature were observed. Power versus temperature data was collected and used as the stations warmed up. The data collected was used to create formulas for postflight temperature corrections. Correction traces are displayed in all flight test data (Sections 4.3 to 4.5).

### 2.4.4 Power Adjustment

The radio's output power was controllable over a modest range, through a computer control command. The power control algorithm changed over the generations of radio. The first version included a large number of small power steps, but the step sizes varied, yielding an "S"-shaped curve of power level setting versus actual output power. The second version attempted to linearize the step size and provide temperature correction, but that resulted in a very coarse output power step size and lower transmitter power. The firmware version for Gen 7 removed the active temperature compensation, improved the number of steps (range), and made the step sizes more uniform. A plot of radio output power versus control setting is shown in Figure 7 for all CNPC waveforms.

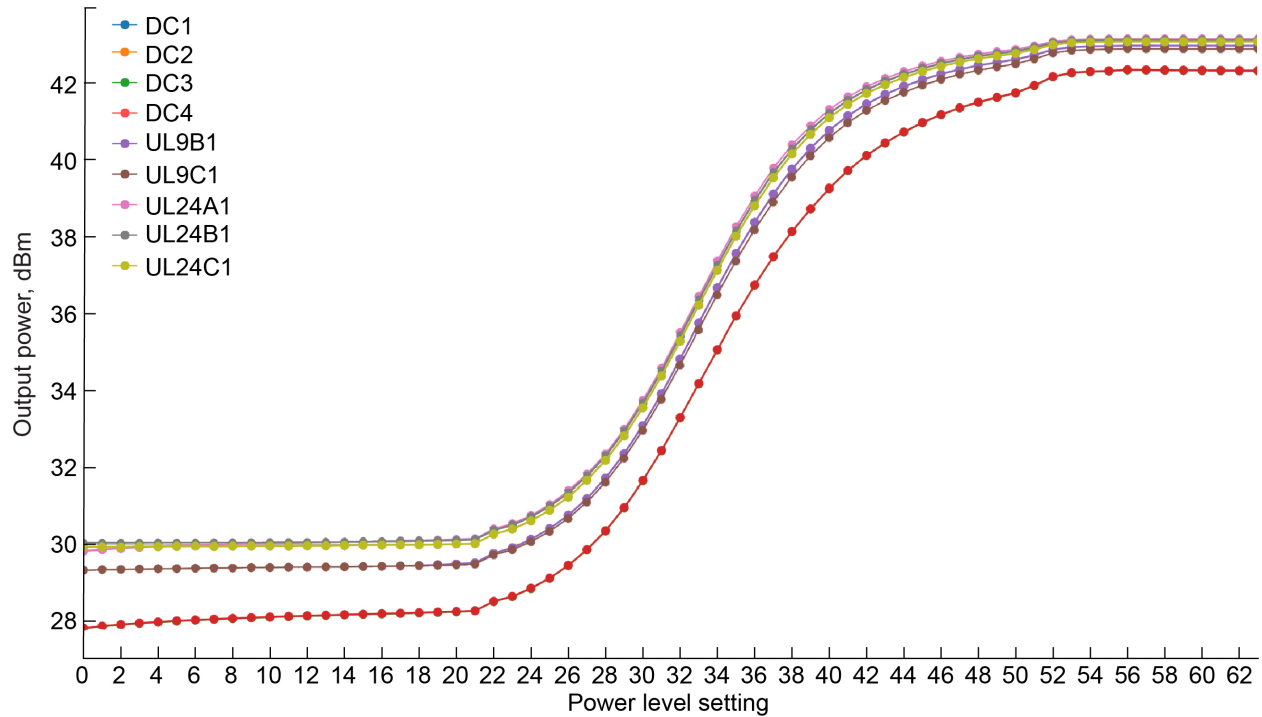


Figure 7.—Control and Non-Payload Communications (CNPC) radio (CNPC–5000E) output power control.

#### 2.4.5 Receiver Sensitivity Measurement Methodology

Receiver performance of the CNPC–5000E was measured both as a component (radio alone) and as an integrated system (station), which includes the high-power amplifier and T/R plate. Each receiver combination (component and system) was tested in every data class (symbol rate) mode. For each receiver and mode combination, the software stepped over a wide range of signal power levels in 1-dB steps while recording the receiver performance at each level. A wide range of performance metrics were collected for each receive subframe. For strong signal levels (with very low measurement noise), a minimum of 50 consecutive error-free subframes were collected. The performance metrics of all 50 subframes were averaged into individual scalar values for the current receive power level step. For low-level signals, dropped (due to uncorrectable errors) or lost (could not recognize) subframes began to occur and the measurement noise was much greater. For low signal levels, a different measurement technique was used to dynamically increase the number of collected subframes averaged into the results by at least an order of magnitude. At each power level step, subframes were collected until 500 subframes were recognized as being received (included: discarded due to excessive or uncorrectable errors, fully error corrected, and error-free subframes). Data collection times for the lowest receive powers increased when a subframe was present at the receiver input but lost. A lost subframe occurred when the receiver was unable to recognize its presence within the noise (could not recover timing). The last measurement point of the power sweep concluded when the receivers’ turbo decoder required more than 3.95 iterations to decode errors (an indication the turbo decoder was having extreme difficulty correcting errors), or the receive health metric reported 0.0 (no subframes were identified).

#### 2.4.6 Received Signal Strength Indicator Calibration, Sensitivity, and Linearization

The RSSI value reported by the radio was critical to analysis of flight test data as it was the only available source of received signal strength during flight testing. It was, therefore, critical that the

reported value be calibrated against the actual received power value. To calibrate the reported RSSI readings, sensitivity measurements were collected in the laboratory over a large signal level range. This resulted in a table for correction of RSSI values, as well as a custom static offset calibration value that could be entered directly into each radio.

Collins and NASA worked closely to linearize and calibrate the reported RSSI values for each receiver. The receive performance of every radio and for every mode was accurately measured and calibrated using a laboratory vector signal generator as the signal source and a laboratory power meter placed before the high-power attenuator feeding the receiver. The linearity curves were consistently within  $\pm 0.25$  dB over a wide range of power levels. The absolute error was corrected by averaging the curve over the  $-90$ - to  $-50$ -dB receive range and programming this average as a static calibration offset value into the radio to correct the reported RSSI for the selected mode. This calibration offset value yielded an absolute power accuracy of  $\pm 0.50$  dB over a very wide range of receive power levels.

As expected, the linearity curve breaks away sharply for signal levels near and above input compression point (corresponds to a transmitter located a few hundred feet away), but the compression did not impact reception as GMSK waveforms used signal phase and not amplitude to convey information. GMSK signals above the input compression were demodulated, essentially error-free, up until the signal strength neared the receiver’s RF input damage level.

Table 4 presents the receiver sensitivities for eight CNPC–5000E radios used in the Gen 7 flight test campaign, either in airborne or ground-based systems, for a range of six different data classes. The high sensitivity resulted in long flight range and low data subframe losses.

#### 2.4.7 Signal Threshold and Noise Floor Removal

Since the receiver measured the combination of signal power plus noise power, the RSSI linearity curves showed the expected upward trending curve for signal levels very close to the signal threshold. To determine the receiver noise power (noise floor), a least-squares curve fit of several extremely low reported RSSI values along with strong signal levels near  $-95$  dBm were curve fit against the signal plus noise to noise ratio  $((S+N)/N)$  to determine the receiver noise power and to remove it. This technique worked very well and removed the noise contribution for signal levels several dB above the noise floor. The accuracy of the correction diminished rapidly for barely recoverable signals. It is not uncommon to use this technique to remove 10 to 12 dB of noise from the measurement.

TABLE 4.—CNPC–5000E RADIO SENSITIVITY

Serial number	Receiver sensitivities, dBm					
	Data class					
	Downlink (air to ground)				Uplink (ground to air)	
	DC1	DC2	DC3	DC4	UL9	UL24
E23	-118.4	-115.7	-114.0	-112.7	-109.5	-105.2
E5	-117.2	-114.7	-113.0	-111.9	-108.6	-104.3
E6	-117.2	-114.6	-112.9	-111.7	-108.6	-104.4
E8	-116.1	-113.8	-112.2	-110.9	-107.7	-103.8
E4	-115.4	-113.0	-111.4	-110.3	-107.1	-102.6
E9	-115.3	-112.9	-111.2	-110.0	-106.8	-102.5
E10	-114.6	-112.1	-110.6	-109.0	-106.0	-101.7
E3	-114.3	-112.0	-110.4	-109.2	-105.9	-101.8

### 3.0 Flight Test System Description

A diagram of the CNPC flight test system operational scenario is presented in Figure 8. The primary elements of the system are the ARS carried on the S-3B Viking test aircraft, and the ground radio system (GRS), which is collocated with support equipment and instrumentation in a mobile ground station. Both the ARS and GRS are monitored and controlled by a centralized test operations center at Glenn. CNPC-5000E radios were installed in both the test aircraft and in the ground stations to establish bidirectional radio connectivity, allowing researchers to simultaneously monitor both air-to-ground and ground-to-air signal propagation characteristics and radio performance. Much of the support equipment used in these systems was selected for prototype testing purposes only; precise antenna types, placement, and transmit power levels are not necessarily those that will be used in a future deployed system. Instead, the test systems were developed and instrumented to provide flexibility in monitoring and recording a range of performance parameters of the air-to-ground radio links.

The ground station was equipped with an internet connection for control, monitoring, programming, and test operations at remote locations. The test system also includes a commercial, satellite-based communications link to carry some test data and to coordinate test operations between Glenn’s test operations center and the test aircraft.

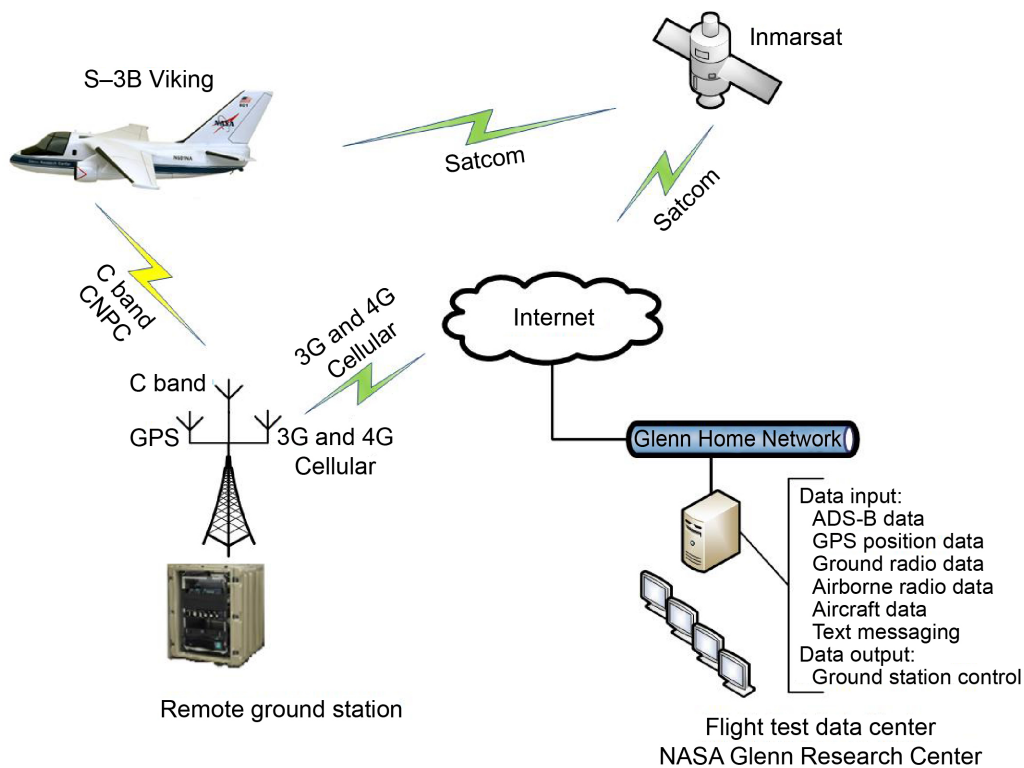


Figure 8.—Control and Non-Payload Communications (CNPC) radio test scenario. Yellow path is for research. Green path is for test support. Automatic Dependent Surveillance-Broadcast (ADS-B). Global Positioning System (GPS). Satellite communication (Satcom).

### 3.1 Airborne Radio System Description

The airborne research equipment consisted of one CNPC-5000E C-band radio, a solid-state RF high-power amplifier, attendant RF components, electrical power supply hardware, a research computer, a Global Positioning System (GPS) receiver for timing and position information, an avionics-bus interface system, and an unmanaged network switch. These components were mounted in 19-in.-wide equipment racks (Figure 9 and Figure 10) within the pressurized volume in the rear of the research aircraft.

A flight-certified, C-band, low-profile, omnidirectional, 1/4-wave monopole antenna was permanently mounted on the underside of the S-3B aircraft to support both the transmit and receive functions of the ARS. The antenna was connected through the pressure bulkhead to the radio by a single customized, aircraft-grade, fully shielded, low-insertion-loss coaxial cable. When the landing gear is stowed for level flight, the antenna field of view (in the downward or nadir direction) is a full hemisphere that is unobstructed by protuberances from the aircraft. The antenna is positioned slightly right of the aircraft centerline to reduce coupling to adjacent aircraft antennas. The antenna was certified for high-speed operations.

The aircraft antenna used in the CNPC flight tests is shown in Figure 11. The antenna mounting location is shown in Figure 12.

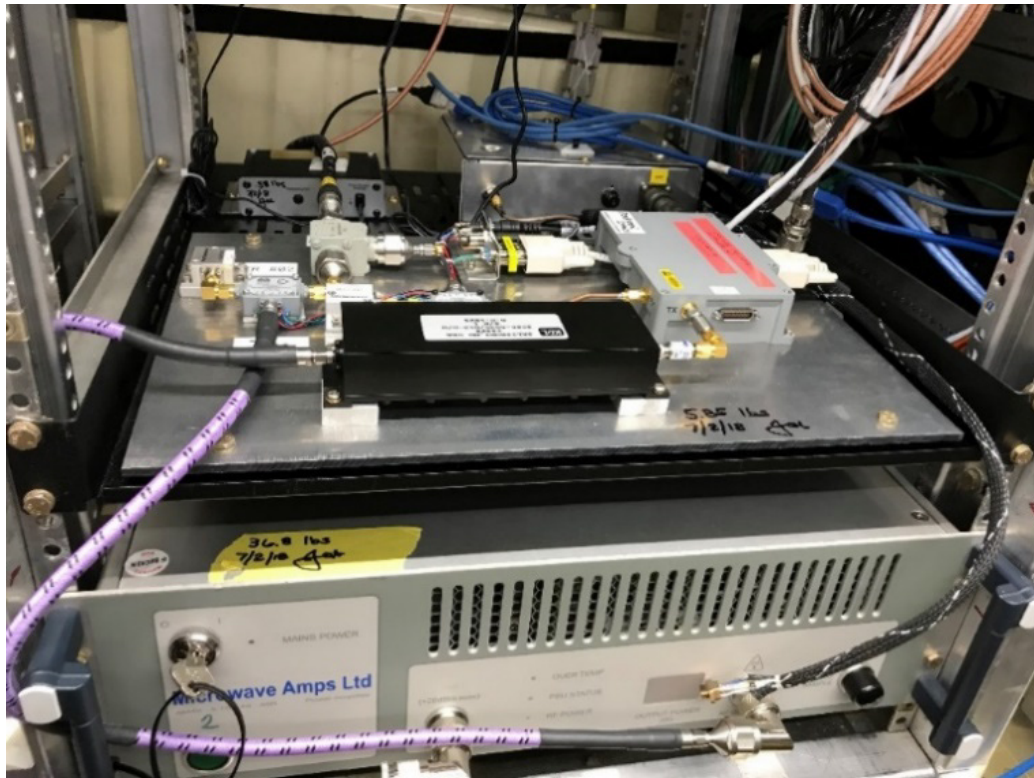


Figure 9.—CNPC-5000E radio on transmit and receive plate with high-power amplifier below.



Figure 10.—Research computer, switch, and time server.



Figure 11.—C-band aircraft antenna.



Figure 12.—NASA S-3B Viking test aircraft showing antenna mounting location.

Gain patterns for the aircraft radio antenna are provided in Figure 13. The patterns were measured at Glenn in an anechoically treated, far-field antenna range under laboratory conditions. The antenna was mounted in the center of a 3-ft-diameter ground plane to simulate the aircraft fuselage, and to demonstrate its impact on the antenna radiation pattern. The manufacturer’s performance data was included for comparison, which is listed as a 5-dBi nominal antenna gain. The measured pattern, when imposed on the image of the aircraft, shows a regular series of gain nulls. The overall gain value of 5 dBi is similar to the manufacturer’s data near the horizon, where most CNPC communication occurs.

A three-dimensional (3D) visualization of the antenna pattern, shown in Figure 14, was created from antenna range measurements with the azimuth plane rotated in 1° increments. Note that the 3D visualization is rotated 180° (inverted) as if the antenna was mounted on the top of the aircraft. The antenna gain value used in simulating and predicting the in-flight experimental results was dependent on the precise line-of-sight path between the aircraft and ground station, so the antenna gain value at those specific azimuth and elevation angles was used.

Accurate knowledge of the aircraft position, airspeed, and attitude were vital to experiment monitoring and test data analysis. Aircraft telemetry data was captured from the S-3B’s MIL-STD-1553 and ARINC 429 data buses using an Astronics Corporation, Ballard Technology OmniBusBox (Figure 15) and recorded to the local research computer for postflight data analysis. An onboard GPS receiver provided the timing for the CNPC radio and was also connected to the research computer to record accurate timestamps, aircraft position, and altitude data. A subset of that aircraft telemetry, including roll, pitch, heading, speed, altitude, latitude, and longitude was relayed twice per second through a secure air-to-ground virtual private network (VPN) connection via the onboard satellite communication (Satcom) link to allow the ground-based test controllers to monitor and display the real-time location of the aircraft during flight testing.

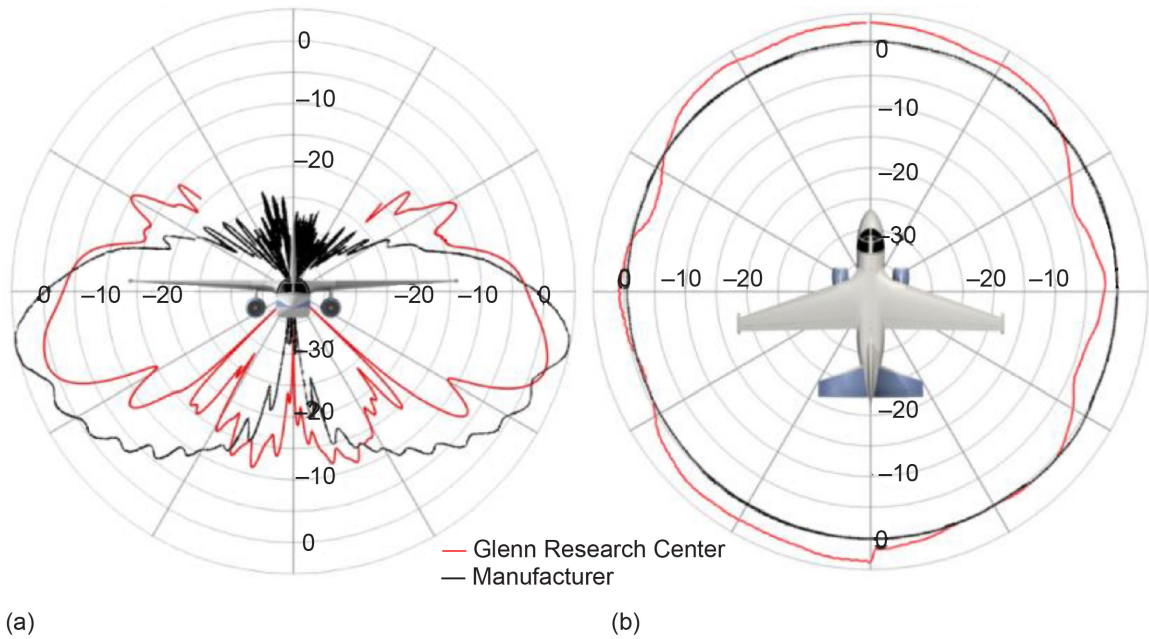


Figure 13.—C-band aircraft antenna gain patterns in dBi. (a) Vertical plane. (b) Horizontal plane.

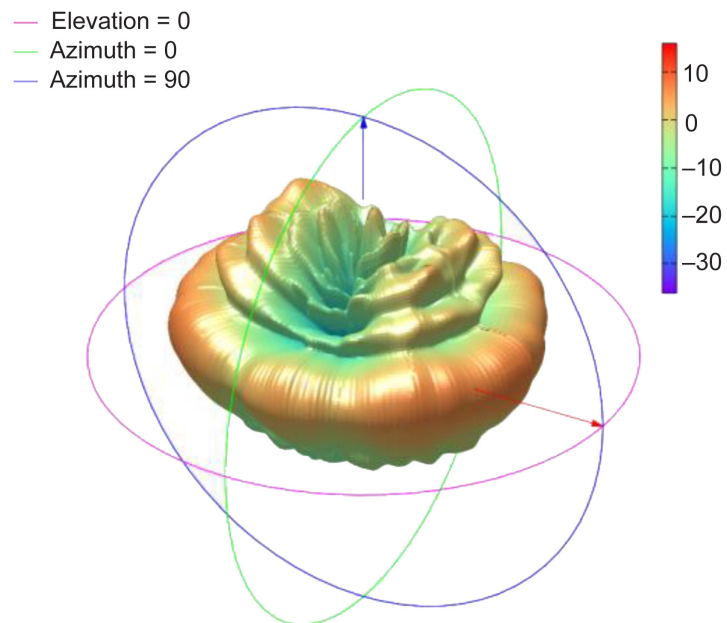


Figure 14.—Three-dimensional visualization of aircraft antenna gain based on measured data in dBi.



Figure 15.—Aircraft telemetry interface.

The ARS support equipment used in the Gen 7 CNPC radio flight testing is the same as that used in the Gen 6 tests. A single ruggedized computer was used to manage the ARS and airborne research instruments from an onboard researcher station. The computer offered features of small size, high processing speeds, large and fast memory, and a large number of modern interfaces, all available in a lightweight, lower-power computer package. An unmanaged, multiport, network switch offering high initialization speed was used to interconnect the airborne equipment.

In addition to collecting telemetry about the aircraft's operational status, the onboard research computer was used to monitor and record the RF and per-packet statistics from the CNPC-5000E C-band radio using custom scripts. During the flight test, the onboard flight researcher used a set of the scripts to configure the radio and monitor its status in realtime. Once the test flight was concluded, the flight researcher offloaded all of the collected data into portable memory for postflight data analysis.

### 3.2 Ground Radio System Description

The ground equipment used in the validation testing was also prepared and operated by Glenn. Like the ARS test system, the ground system consisted of one C-band MOPS CNPC radio with attendant RF, high-power amplifier (HPA), networking, and time base equipment. The ground equipment was connected to the internet through either a hardwired host-site network or a 3G and 4G cellular network, allowing full control and monitoring of the GRS from the Glenn test operations center in Cleveland, Ohio.

Figure 16 shows a block diagram of the main elements of the ground station and GRS. The blue boxes represent the prototype CNPC radio and attendant devices. These components are grouped inside a broken-line box to indicate all the functions that would typically reside internally to a CNPC radio. The green components are interface and support equipment specific to the NASA test system. The orange boxes are power supply equipment and power lines have been omitted for clarity.

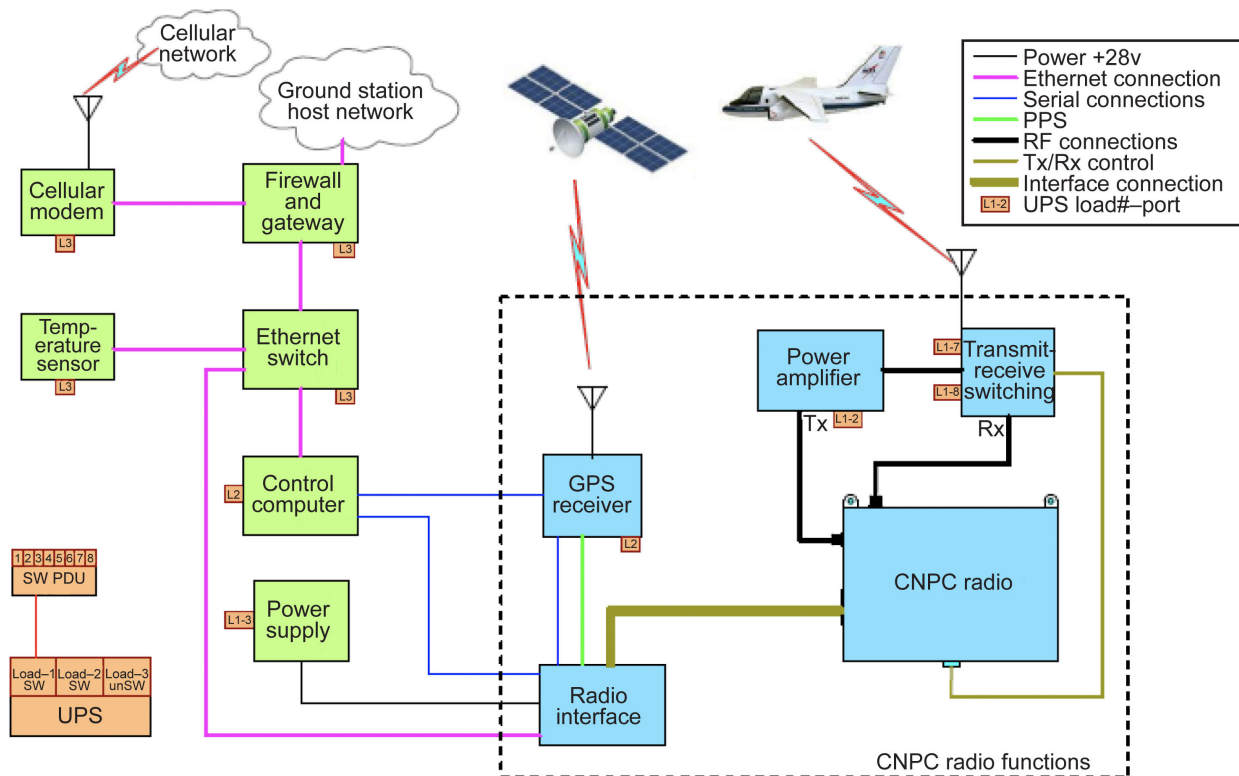


Figure 16.—NASA ground equipment. Control and Non-Payload Communications (CNPC). Global Positioning System (GPS). Pulse per second (PPS). Power distribution unit (PDU). Radiofrequency (RF). Receive (Rx). Switched (SW). Transmit (Tx). Uninterruptible power supply (UPS).

### 3.2.1 Transmit and Receive Switching

The small form factor, prototype CNPC radio used in the flight tests did not contain an internal T/R antenna switch or transmit amplifier. To provide these functions, Glenn designed and assembled a T/R circuit (Figure 17) that contained components to merge the radio transmit (Tx) and receive (Rx) signal connections into a single antenna port connection. The T/R circuit also provided a bandpass filter to prohibit out-of-band emissions. High-speed electronic switches controlled the transmitted and received RF signal flow paths to synchronize with the 20-Hz time-division duplex (TDD) rate of the CNPC radio (configured to accommodate 0.23 seconds transmit and 0.23 seconds receive subframes, with necessary guard times for switching). The circuit diagram of the T/R system is shown in Figure 18. One T/R switching circuit was used with each CNPC radio in each ARS and GRS.

### 3.2.2 Ground Radio System Support Systems

A commercially available, solid-state, rack-mounted, 120-W HPA was included in the GRS to compensate for insertion losses of the RF components and cabling. The HPA was operated in its linear amplification region well below its saturation level, where it produced nominally 10 W of signal power at the radio tray antenna port, appropriate for flight testing.

A GPS receiver delivered a coded signal to the ground radio, which was used as a time server for the computer and cellular modem. This allowed all ground equipment to be time synchronized with the aircraft and Flight Test Operations Center. This synchronization was necessary for accurately recording the precise spatial and geometric relationship of the ARS to the GRS, as well as measuring data flow latency throughout the network.

A CNPC radio interface box was fabricated that provides all electrical connections and signals between the CNPC-5000E radio and the ground station (or aircraft system). These include signals from the control computer, GPS receiver, networking, and power. The interface box was used instead of a direct wiring harness to provide electrical test points for troubleshooting.

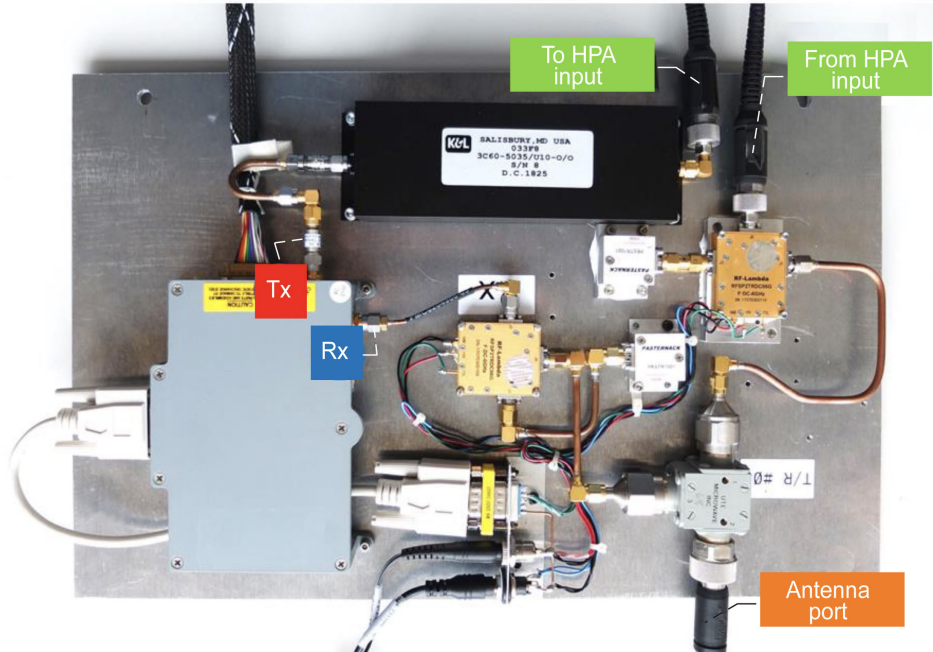


Figure 17.—Transmit (Tx) and receive (Rx) switching, bandpass filter, and radio. High-power amplifier (HPA).

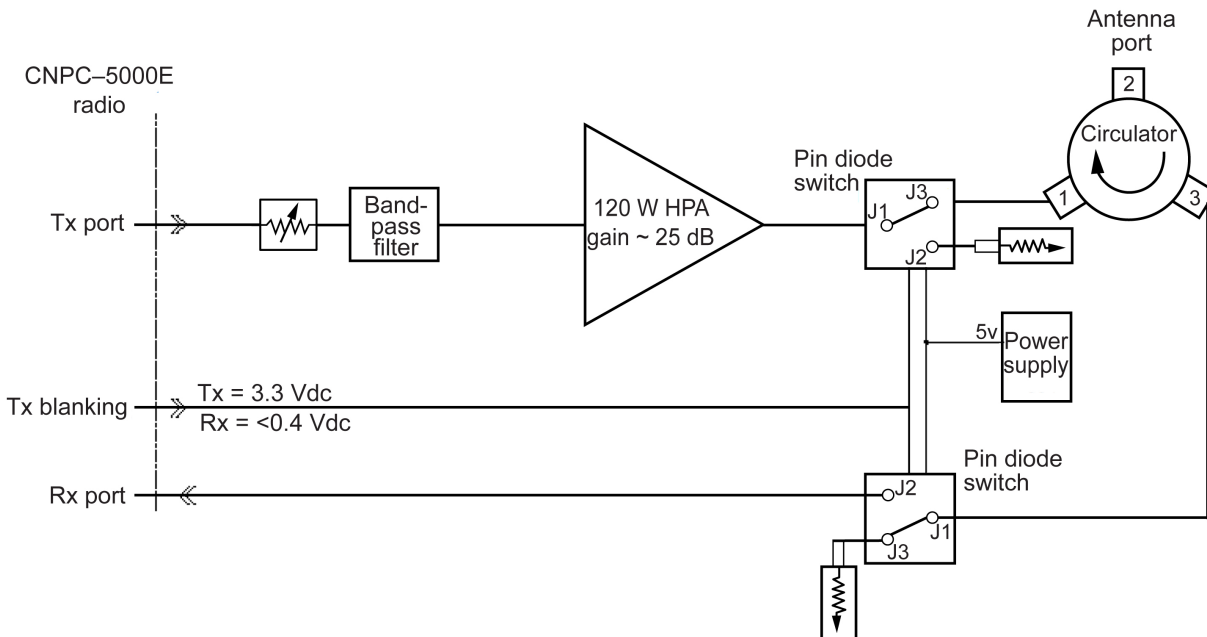


Figure 18.—Control and Non-Payload Communications (CNPC) radio transmit (Tx) and receive (Rx) circuit diagram. High-power amplifier (HPA).



Figure 19.—Transportable ground radio system equipment.

Figure 19 shows the ground equipment installed into a ruggedized transport case. Antenna coaxial cables, main power cable, and a network cable exit the case to external locations. Multiple GRS were fabricated to facilitate specific tests, such as the switchover test described in later sections of this report.

### 3.2.3 Ground Station Antennas

The C-band antenna used at the ground station for the CNPC flight tests is shown in Figure 20. The antenna was a commercially available, linearly polarized, lensed horn fed through a rectangular waveguide section from a right angle coaxial launcher. The antenna has an H-plane 3-dB beamwidth of nominally 30°, resulting in the ability to achieve a directional beam to improve directivity and reduce multipath reception. The antenna was mounted to a pan and tilt mechanism at the top of a mobile tower mast for precise azimuth and elevation alignment at each test location.

Gain patterns for the ground radio antenna are provided in Figure 21. The patterns were measured at Glenn in an anechoically treated antenna range under laboratory conditions. When available, the manufacturer's performance data was included for comparison. Figure 22 presents a 3D model of the ground antenna pattern. This pattern was based on relatively few antenna range azimuth measurements, or cuts, so the pattern had to be heavily interpolated to obtain the 3D pattern shown. Because of this, the antenna pattern could not be considered accurate over most of the pattern. However, over the main beam of the antenna, the pattern was more easily interpolated (confirmed by a third measured cut at a 45° angle through the main beam).



Figure 20.—Installed ground station directional antenna.

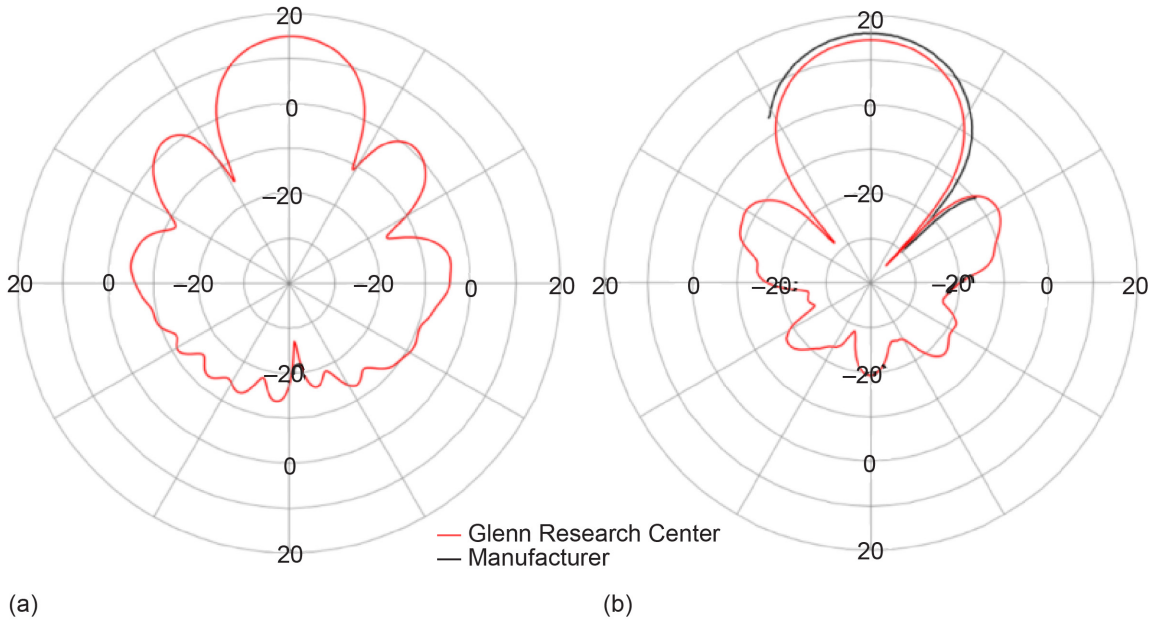


Figure 21.—C-band ground directional antenna gain patterns in dBi. (a) Vertical plane. (b) Horizontal plane.

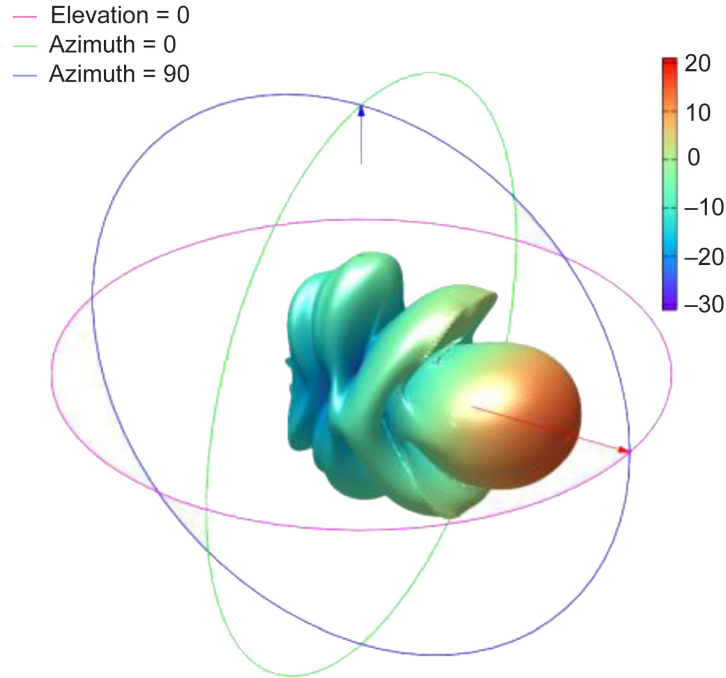


Figure 22.—Three-dimensional visualization of ground station antenna gain based on measured data in dBi.



Figure 23.—Ground station C-band omnidirectional antenna.

For the airport surface operations testing described in Section 4.7 of this report, Glenn used a commercially available C-band, full-wave dipole, omnidirectional, ground station antenna shown in Figure 23. Due to the close proximity of the ground station to the airport property, the antenna was required to have a wide azimuthal coverage, thereby eliminating the use of the directional antenna. The dipole antenna was positioned vertically and elevated to a height of 15 ft above ground level for the taxi tests.

The vertical plane of the antenna was measured in NASA Glenn’s Far-Field Antenna Range, as shown in Figure 24. A gain of 3.76 dBi was measured, similar to, but slightly less than, the manufacturer’s specification of 4.15 dBi.

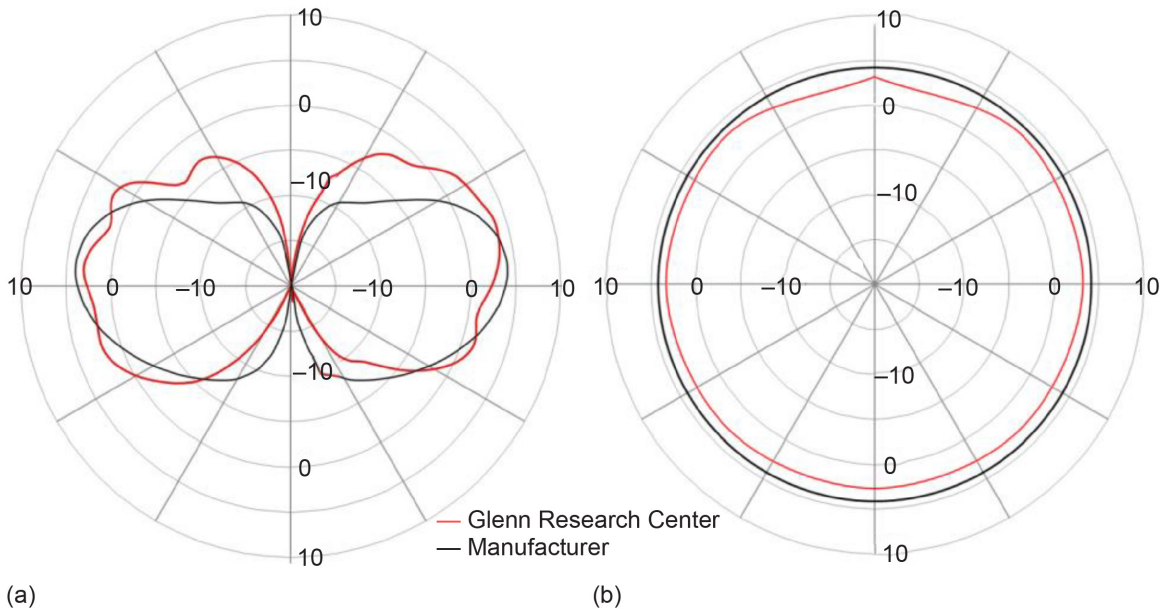


Figure 24.—C-band ground station omnidirectional antenna gain patterns in dBi. (a) Vertical plane. (b) Horizontal plane.

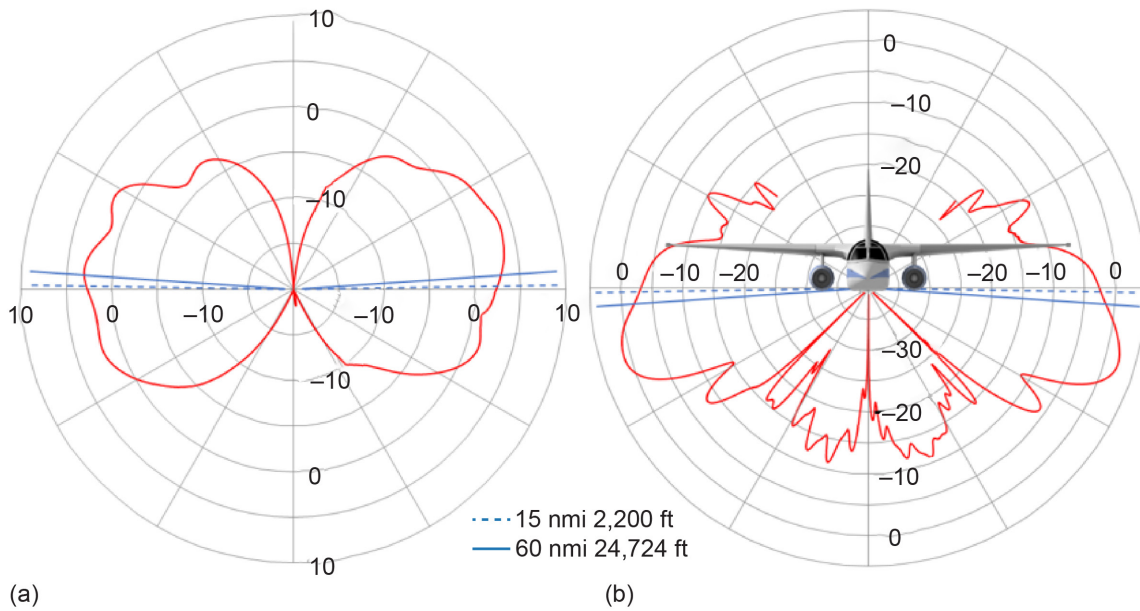


Figure 25.—Typical portion of ground and airborne measured C-band antenna gain pattern in dBi used in Generation 7 flight tests. (a) Ground radio system. (b) Airborne radio system.

### 3.3 Flight Test Planning

#### 3.3.1 Flight Range

NASA flight tests planned for radio operation at slant range distance of up to 60 nmi, allowing data collection in excess of the 35 nmi range planned in Reference 5. This way, the CNPC signal was tested beyond its nominal operating range and then to the point where the communications link is lost. Figure 25 shows the approximate portion of each antenna pattern that was used to communicate at altitudes of 2,200 and 24,724 ft above mean sea level for the 15- and 60-nmi distances, respectively. As the figure shows,

the flight tests typically utilized high-gain portions of the antenna radiation patterns and were not to be operating near any of the primary antenna nulls at these distances.

### 3.3.2 Ground Station Networking Equipment

Each ground station and GRS connected to the internet through either a hardwired host-site network or a 3G and 4G cellular network, allowing full control and monitoring from the NASA Glenn test operations center. A firewall and gateway were responsible for securing and managing the networks provided by the 3G and 4G connection and host network at the installation site. In situations where both the physical internet and cellular connections exist, the gateway utilized the cellular network as a backup. If the host network experienced an outage or other disruption, the gateway would automatically switch to the cellular connection. The cellular modem was selected to provide data access using one of several cellular service providers, depending on service available at the specific ground site location.

The computer had an Intelligent Platform Management Interface (IPMI) that permitted remote monitoring and control of the computer without the use of the operating system. In the event of a computer failure, the ground equipment could be powered down and rebooted and have errors logged via IPMI.

### 3.4 Flight Test Operations Center

Flight test activities for the CNPC radios were managed from the UAS Flight Test Operations Center located in Building 54 at Glenn Research Center. The Flight Test Operations Center was an audio and videocentric collaborative facility that collected relevant data from the airborne RF testing and displayed that data for real-time analysis and adjustments to the test in progress. The facility housed the test conductor and three operations and research personnel for the entirety of the test and served as the control point for remotely located GRS assets and test equipment (Figure 26).



Figure 26.—Unmanned Aircraft Systems Integration Flight Test Operations Center.

The facility featured three 84-in. high-resolution wall-mounted displays placed forward of the flight operations crew stations. During flight tests, these displays generally hosted the CNPC radio statistics, the aircraft position map (APM), and a flight information display. The two smaller, secondary displays mounted on the adjacent wall hosted any required ancillary information, such as atmospheric conditions, specialized aircraft control information flow, flight track mappings, or radio engineering data.

The Flight Test Operations Center was utilized whenever the test aircraft communicated through the fixed ground station located at Glenn. When flight testing was managed from offsite locations, a mobile mission operations center was utilized. The mobile operations center was set up in a support vehicle and was a scaled-down version of the Glenn facility, devoid of any large screen displays or video switching utilized for group viewing and collaboration. The mobile facility was functionally identical with regards to the information presented to the test conductor. All information not derived directly at the GRS site was obtained through a commercial cellular-connected VPN between the mobile operations center and the main Glenn facility.

A flight test operations team consisting of a test conductor, radio engineer, network engineer, and data visualization personnel managed all elements of the airborne test activities. The test conductor planned, monitored, controlled, and coordinated the activities of the CNPC test aircraft. The radio engineer controlled and monitored the performance of both ground-based and airborne radios. The network engineer managed all ground, Satcom, and very high frequency (VHF) communications, and supported data visualization personnel to ensure test performance and situational awareness data was obtained, processed, and presented in realtime from multiple data sources. All real-time data displayed within the facility was recorded and stored as data for future detailed analysis and playback. A flight research engineer onboard the test aircraft communicated directly with the test conductor throughout each flight test. The flight engineer managed the operation of all airborne research equipment and served as the real-time interface between the test conductor and the aircraft pilot to execute the flight test plans.

Aircraft situational awareness elements included geoposition, speed, heading, and aircraft attitude (roll, pitch, and yaw). Situational elements generated onboard the aircraft were logged to an onboard computer and sent over the test aircrafts' geosynchronous satellite communications system, then relayed over a secure internet connection to the facility in realtime. In order to ensure awareness of the test in progress, the facility also received Automatic Dependent Surveillance-Broadcast (ADS-B) data (position, speed, and heading) over the wide-area network (internet) from a third party ADS-B surveillance vendor. All situational awareness elements were plotted on the aircraft position map, located on the center 92-in. display.

Test system performance data elements were dependent upon the RF technology under test. These elements often included RSSI, recovered (corrected) frames, and frames lost. The elements could be conveyed over the RF link of the system under test or via the aircraft's onboard satellite link. Performance elements were logged at both ends of the RF test path to ensure critical performance metrics were being recorded even when external RF connections were nonexistent or insufficient to transport the data. Within the facility, the performance elements were displayed using terminal sessions to the ground station and on aircraft CNPC radios and viewed on the left-mounted 92-in. display. Graphical representations of performance data could also be viewed on the right-mounted 92-in. display.

#### **4.0 Generation 7 Control and Non-Payload Communications Radio Propagation Flight Test Results**

Frequency authorizations were obtained for NASA flight test operations in areas covering most of the Ohio region. All propagation and validation testing occurred in these flight zones, indicated by the 140-

km-radius circles shown in Figure 27. Both the transportable GRS and flight ARS operated within these authorized areas.

Three distinct ground site locations were selected within the authorized operating areas. Each ground site selection was influenced by many factors but was primarily driven by local terrain features and the ability to establish the point-to-point, line-of-sight CNPC connection between the airborne radio and the ground radio in that particular terrestrial setting. Unique propagation and dispersive signal propagation conditions were desired in each location. Special attention was given to man-made obstructions and terrain surface roughness in the areas extending to 1 km immediately in front of the ground antenna where primary RF signal reflections would occur. Table 5 lists location details for the ground sites used in the validation testing.



Figure 27.—U.S. map identifying two authorized 140-km-radius Control and Non-Payload Communications (CNPC) operating areas. Image ©2018 GoogleEarth.

TABLE 5.—FLIGHT TEST GROUND SITE (GS) LOCATIONS

Test date	GS location	Latitude, longitude	Setting	Ground elevation above mean sea level, ft	Antenna height above ground level, ft
10/8/2019	NASA Plum Brook Station <sup>a</sup> Perkins Township, Ohio	41° 20' 22.50" N 82° 38' 59.60" W	Flat terrain (smooth plain)	623	51.3
12/3/2019	Cedar Point Sandusky, Ohio	41° 28' 41.89" N 82° 40' 35.59" W	Open, freshwater	569	51.3
12/5/2019					
12/6/2019					
12/11/2019	Ohio University Airport Albany, Ohio	39° 12' 44.40" N 82° 13' 23.40" W	Hilly terrain (slightly rolling plains)	763	51.3
12/12/2019					

<sup>a</sup>Now the Neil A. Armstrong Test Facility.

## 4.1 Flightpath General Description

The planned flightpath was purposely the same for each of the three test settings to allow direct comparison of electromagnetic propagation over the diverse terrain conditions. Flight altitudes required slight tailoring in land areas to account for ground elevation changes. The azimuthal direction of the flightpath and GRS antenna pointing direction were adjusted to achieve desired ground obstruction and surface roughness conditions. Careful planning ultimately allowed the flight to be executed above the desired terrain, avoid ground obstructions, observe frequency authorization restrictions, and meet limitations imposed by FAA and local air traffic control authorities. Flight pattern areas are shown in Figure 28.

For each test flight, the NASA research aircraft was piloted between pairs of preselected waypoints at fixed range from the ground station. Aircraft altitude, attitude, and airspeed were held constant between waypoints to create a one-way flight segment or crosstrack, ranging from approximately 1.5 to 4.0 minutes in duration. After completing a flight segment, the aircraft reversed direction and traveled the same flightpath between waypoints, but in the opposite direction. This technique intended to determine the impact of asymmetrical installation of the antenna on the aircraft. During these flight segments, the aircraft traveled transverse to the direction of RF radiation from the ground station, thereby presenting the port and starboard sides of the aircraft to the ground station antenna.

The test aircraft flew the path between each pair of waypoints not only in two directions, but also at multiple altitudes to capture the effects of terrain obstruction, multipath reflections, and signal dispersion. Flight segments were arranged at the 15-, 30-, 45-, and 60-nmi range from the ground station at altitudes that would achieve 1.0°, 1.5°, 2.0°, and 3.0° elevation angles of above ground level.

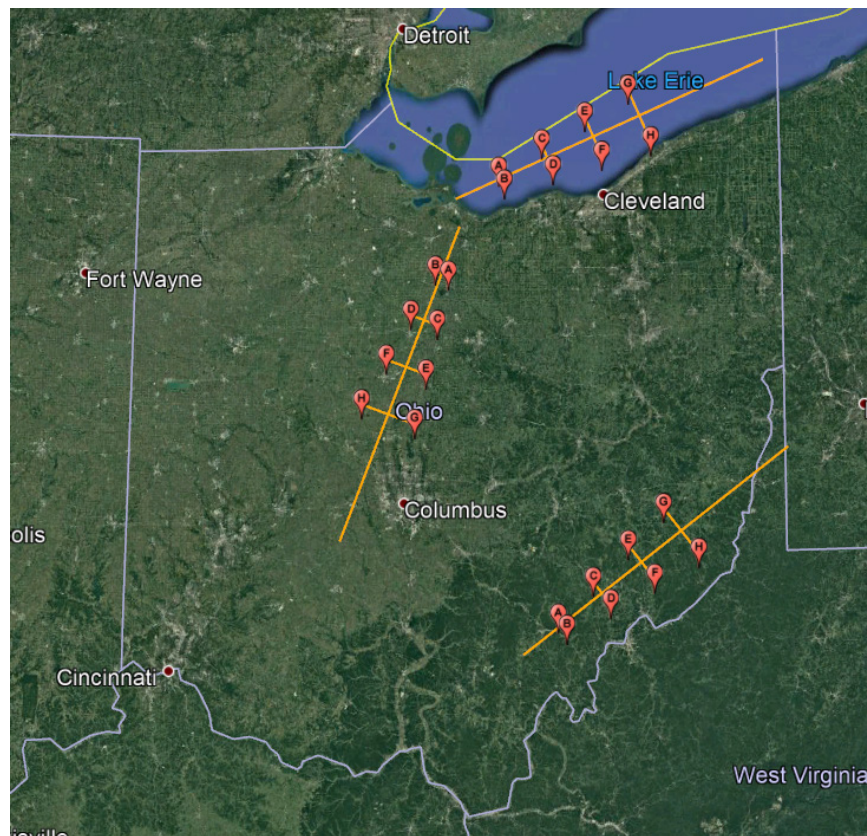


Figure 28.—Ohio flight test areas. Image ©2018 GoogleEarth.

TABLE 6.—VALIDATION FLIGHT TEST SUMMARY

Waypoints	A, B	C, D	E, F	G, H	Inbound track (descending)	Outbound track (ascending)
Range, nmi	15	30	45	60		
Elevation angle	Altitude over terrain, above mean sea level, ft				Maximum range from GRS, nmi	
Flat terrain						
1.0°	2,500	5,000	7,500	10,500	60	60
1.5°	3,500	6,500	10,000	14,000	60	60
2.0°	4,000	8,000	12,500	17,500	55	60
3.0°	Not performed (NP)					
Hilly terrain						
1.0°	3,000	5,500	8,000	11,500	75	75
1.5°	3,500	7,000	10,500	15,000	70	60
2.0°	4,500	8,500	13,500	18,500	60	60
3.0°	6,000	11,500	17,500	NP	70	60
Open freshwater						
1.0°	2,000	4,000	6,500	9,000	75	75
1.5°	3,000	5,500	8,500	12,000	65	65
2.0°	3,500	7,000	11,000	15,500	70	60
3.0°	5,000	10,500	15,500	NP	65	60

In addition to transverse flightpaths, inbound (descent) and outbound (ascent) segments were flown at each test location along the GRS antenna centerline on 1.0°, 1.5°, 2.0°, and 3.0° elevation angles. When weather and air traffic conditions allowed, the ascent or descent path was flown in a single run. A summary of as-flown flight altitudes, ranges, and flightpaths is presented in Table 6. The altitudes flown during the test were adjusted to the nearest 500 ft to meet FAA flight rules.

#### 4.2 Validation Flight Test Data Format Description

CNPC radio performance data from over 120 flight segments were recorded during the validation test campaign, covering the three terrain settings. A complete data package was delivered to the SC-228 C2 Working Group for analysis in January 2020. The data package was too extensive to include in this report, so sample plots were included to illustrate performance features or to highlight specific technical issues. Section O.3.2 in Reference 5 presents and discusses data collected over generally flat terrain (referred to as “smooth plains” in Ref. 6) on October 8, 2019. Section O.3.3 in Reference 5 presents and discusses data collected over hilly terrain (referred to as “slightly rolling plains” in Ref. 6) on December 11 and 12, 2019. Section O.3.4 in Reference 5 presents and discusses data collected over open freshwater on December 3, 5, and 6, 2019.

Each flight segment highlighted in a flight track plot corresponds directly to data plots for both ground-to-air and air-to-ground radio links. Separate data plots are presented for each direction of aircraft travel between the waypoints, for each test altitude, and for the 15-, 30-, 45-, and 60-nmi range from the ground station. A sample plot is shown in Figure 29.

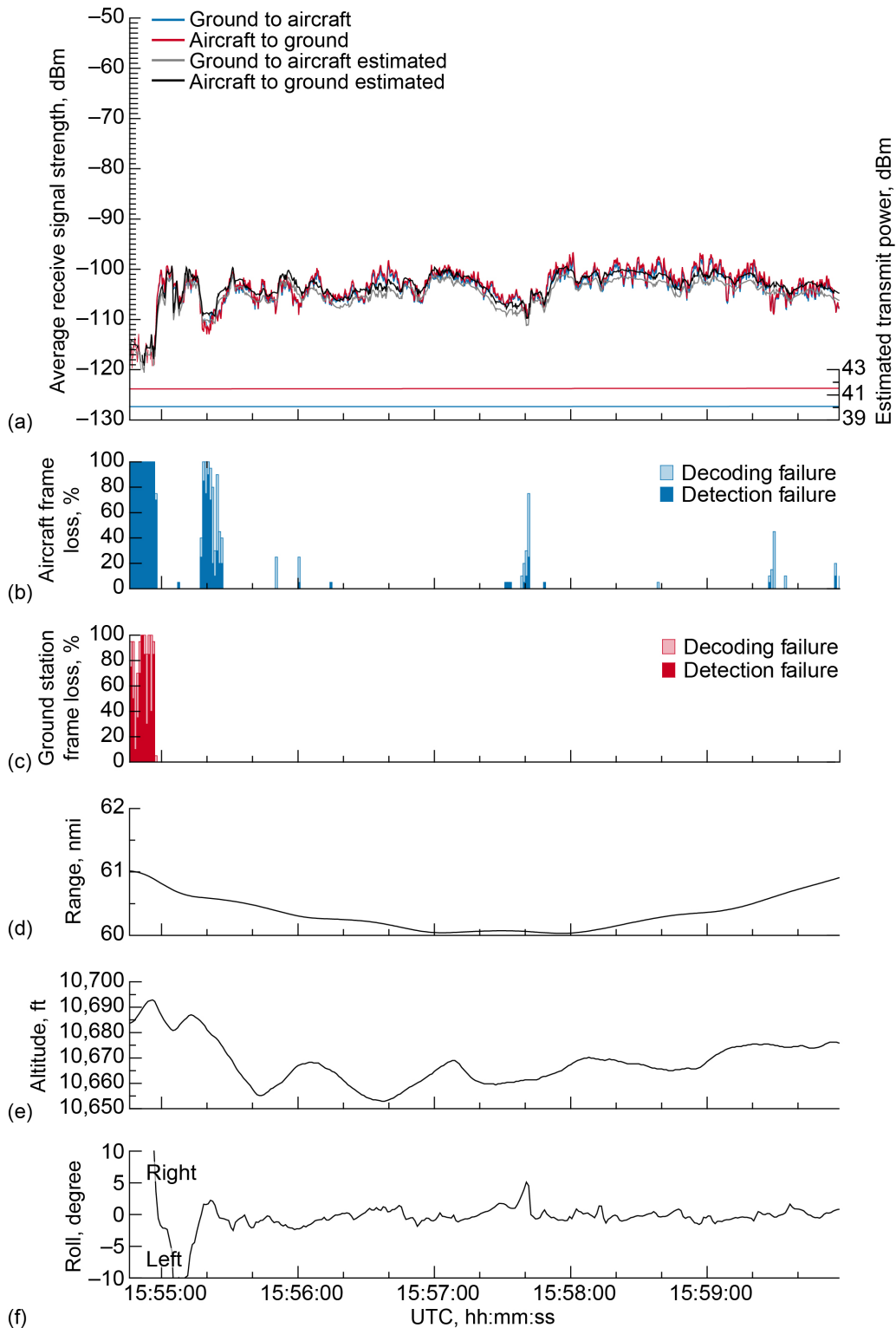


Figure 29.—Example data plot for one flight segment. NASA flight test on October 8, 2019, at 60 nmi at 10,500 ft, 1.0° on an east to west pass. Coordinated universal time (UTC). (a) Average receive signal strength. (b) Aircraft frame loss. (c) Ground station frame loss. (d) Range. (e) Altitude. (f) Roll.

Received signal strength values were measured at the radio receivers and are plotted in blue and red traces at the top of the figure for both the ground-to-air uplink and air-to-ground downlink path. The signal strength data are measured for each data frame (at a rate of 20 times per second, or every 50 ms), then plotted as an average value every 200 ms as necessary for the excess path loss (EPL) analysis in Section 4.6 of this report. Signal strength values are time synchronized and plotted with the aircraft flight position and attitude data, which is presented once per second. The CNPC radios were operated with the Data Class 3 waveform for a point-to-point, 170-kHz wide data channel at the 103,500 symbol rate.

Estimated signal strength values for the uplink and downlink paths are plotted with the empirical flight data as gray and black traces. These estimates are calculated using the temperature-compensated power levels, ground station and aircraft antenna gains, cable losses, and free space path loss. The aircraft and ground station antenna gains are computed from measurement-enhanced, 3D antenna models at the specific phi and theta angles determined from the ground station and aircraft locations, ground station antenna orientation, and the aircraft heading, pitch, and roll. The free space path loss was based on the slant range distance between the aircraft and ground station. The difference between the measured received signal strength and estimated received signal strength forms the basis of the EPL analysis.

Directly below the signal strength traces are the percentages of data frame losses averaged over 1 second at the ground and aircraft receivers. Where the CNPC link system was transferring all data to the receiving radio with zero decoding errors, the performance is presented as a 0-percent loss and no trace is visible on the grid. Where errors occurred, the lost frame data results in a visible vertical line ranging from 0 to 100 percent, where the latter represents a total loss of the link. The second trace on each loss graticule is detection failure, which indicates when the received signal is sufficiently corrupted or of such low signal power that it cannot be viably detected by the radio.

Aircraft parameters are plotted in the lowest portion of each figure. The range plot is the slant range between the ground station and aircraft, calculated from the GPS data of the aircraft and the ground station. Because each path between waypoints was flown as a line segment rather than as an arc segment, the range plot predictably shows small variation across the test period. Aircraft altitude and roll angle are acquired from aircraft onboard instrumentation. All data in all traces is time synchronized using GPS-based timing information.

In a brief examination of the example plot shown in Figure 29, the reader will see that for the nominal 60-nmi slant range separation between aircraft and ground station over open flat land, the received signal strength at each radio varies in the range of  $-100$  to  $-110$  dBm (red and blue upper traces). These measured values track very well with predictions (gray and black traces). Below the signal strength traces, the CNPC data losses are shown to occur briefly in both uplink and downlink paths as signal power decreases during periods of high aircraft roll. These airframe obstruction losses were expected as the aircraft was stabilizing its flight attitude near the eastern waypoint for the flight segment.

### **4.3 Validation Flight Test Data for Flat Terrain Setting, October 8, 2019**

Figure 30 presents the flight track of the NASA aircraft over flat terrain in north-central Ohio. The orange trace is the complete flightpath of the aircraft, including all reversals, ascent and descent maneuvers, and range changes. Figure 31 is the same flight track viewed from an oblique perspective to show the flightpath at various test altitudes. Waypoints are identified with alphabet characters A to H. The flight segments between waypoints are highlighted in yellow, which precisely represents the locations where RF data was captured for evaluation. For this location, the GRS was positioned at the southern

perimeter of NASA's Plum Brook Station facility<sup>1</sup> in Perkins Township, Ohio. The ground station antenna was overlooking open agricultural land with no natural or man-made obstructions for over 1 nmi.

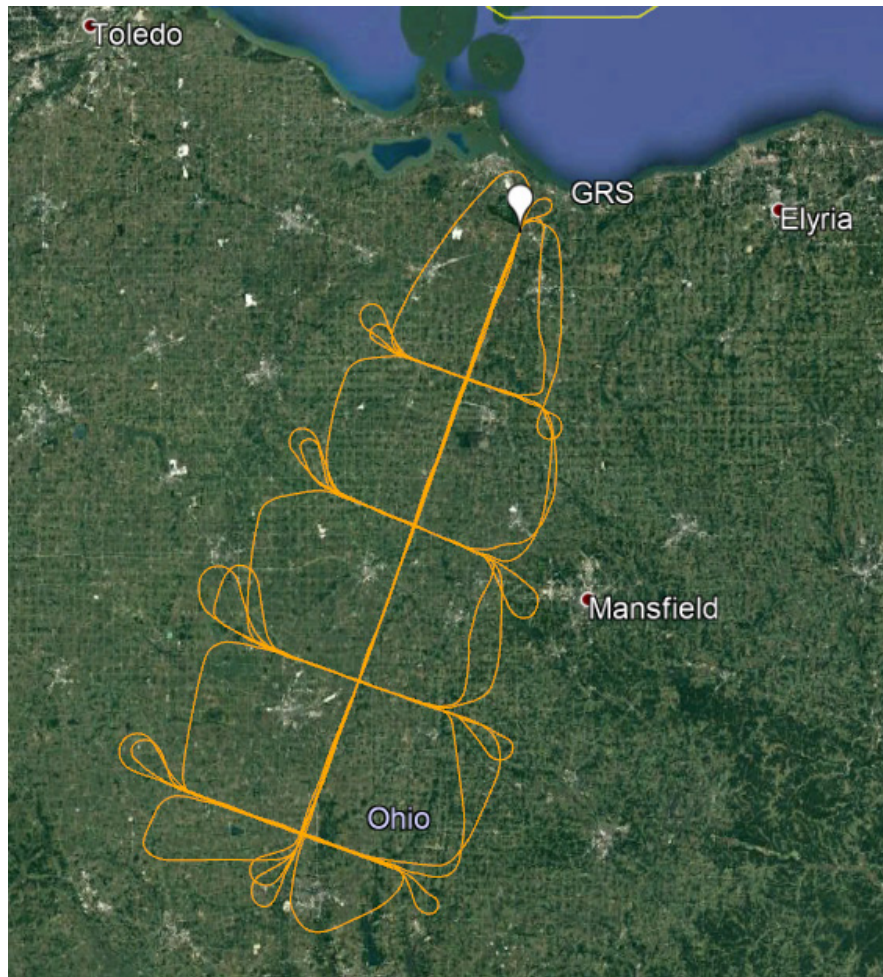


Figure 30.—Flightpath over flat terrain October 8, 2019. Image ©2018 GoogleEarth.

---

<sup>1</sup>Now the Neil A. Armstrong Test Facility.



Figure 31.—Perspective view of flightpath over flat terrain highlighting data capture segments, October 8, 2019.  
Image ©2018 GoogleEarth.

Figure 32 and Figure 33 present data for  $1.0^\circ$  inbound descending and  $1.0^\circ$  outbound ascending flight test segments. The range trace and lack of any radio data frame loss indicate that the CNPC link is successfully maintained to over 60 nmi in both the inbound and outbound directions. This range is well in excess of the planned 35 nmi required flight range, even at the antenna low,  $1.0^\circ$  elevation angle.

Sample crosstrack data plots are presented in Figure 34 and Figure 35 for the  $1.0^\circ$  elevation angle and 60 nmi line-of-sight range. The plots show that the CNPC radio link still transfers data even at the extended range, although some received data packets experienced errors due to low received signal strength. The two figures are the same flight segment flown in opposite directions, highlighting the effects of asymmetrical mounting location of the aircraft antenna.

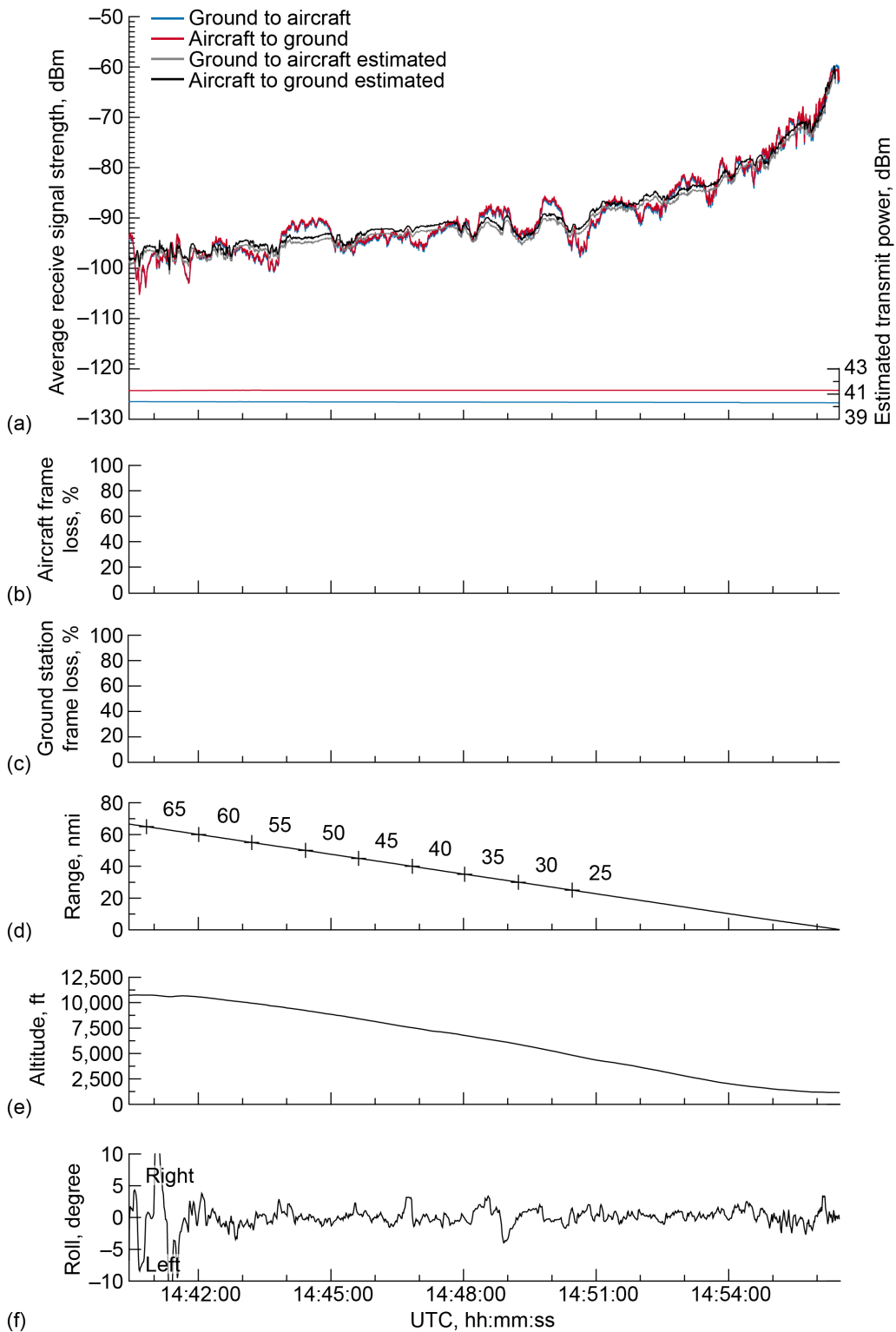


Figure 32.—Signal strength and frame loss over smooth plain terrain during inbound, descending track on 1.0° glide slope, traveling toward ground station. Coordinated universal time (UTC). (a) Average receive signal strength. (b) Aircraft frame loss. (c) Ground station frame loss. (d) Range. (e) Altitude. (f) Roll.

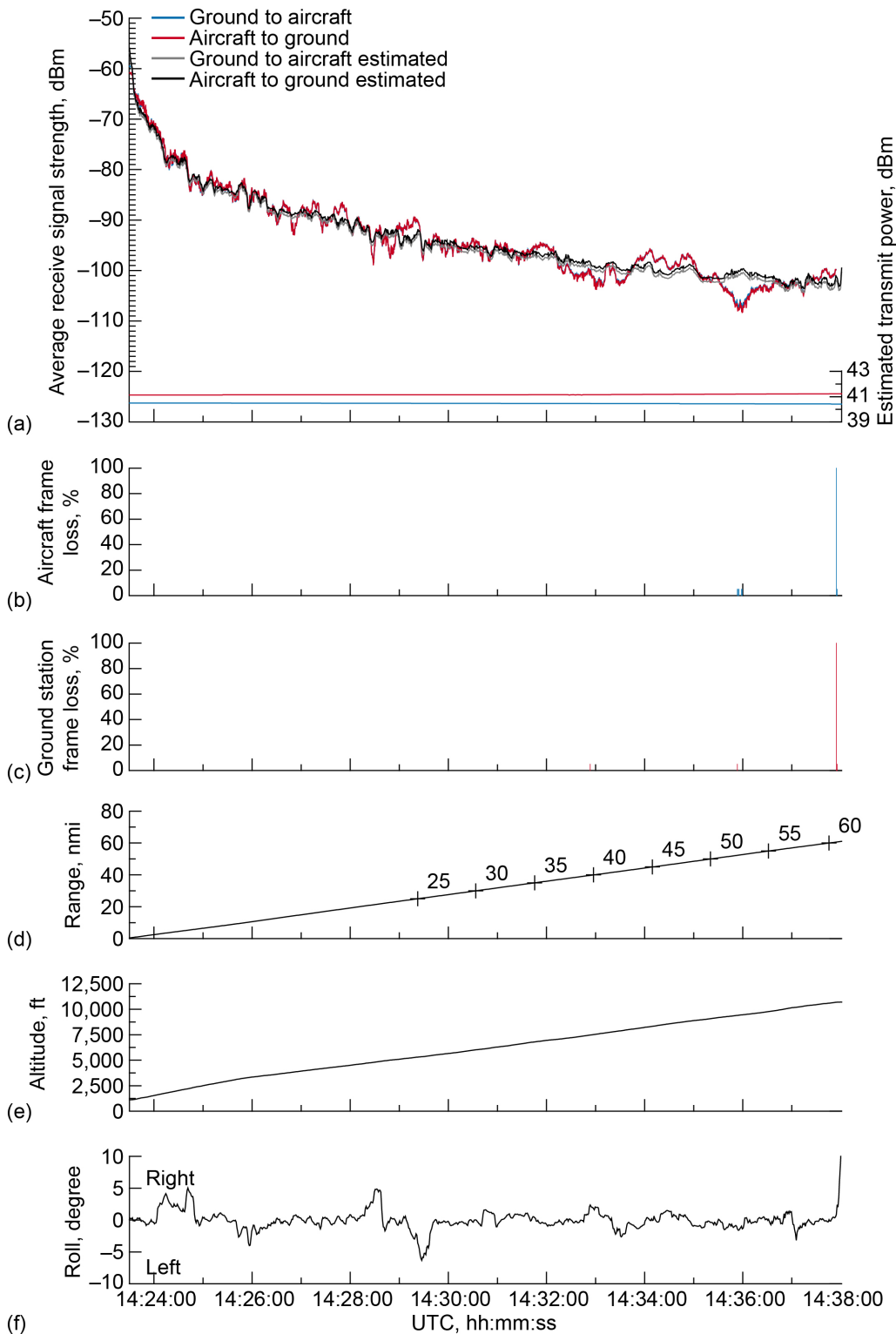


Figure 33.—Signal strength and frame loss over smooth plain terrain during outbound, ascending track on 1.0° glide slope, traveling away from ground station. Coordinated universal time (UTC). (a) Average receive signal strength. (b) Aircraft frame loss. (c) Ground station frame loss. (d) Range. (e) Altitude. (f) Roll.

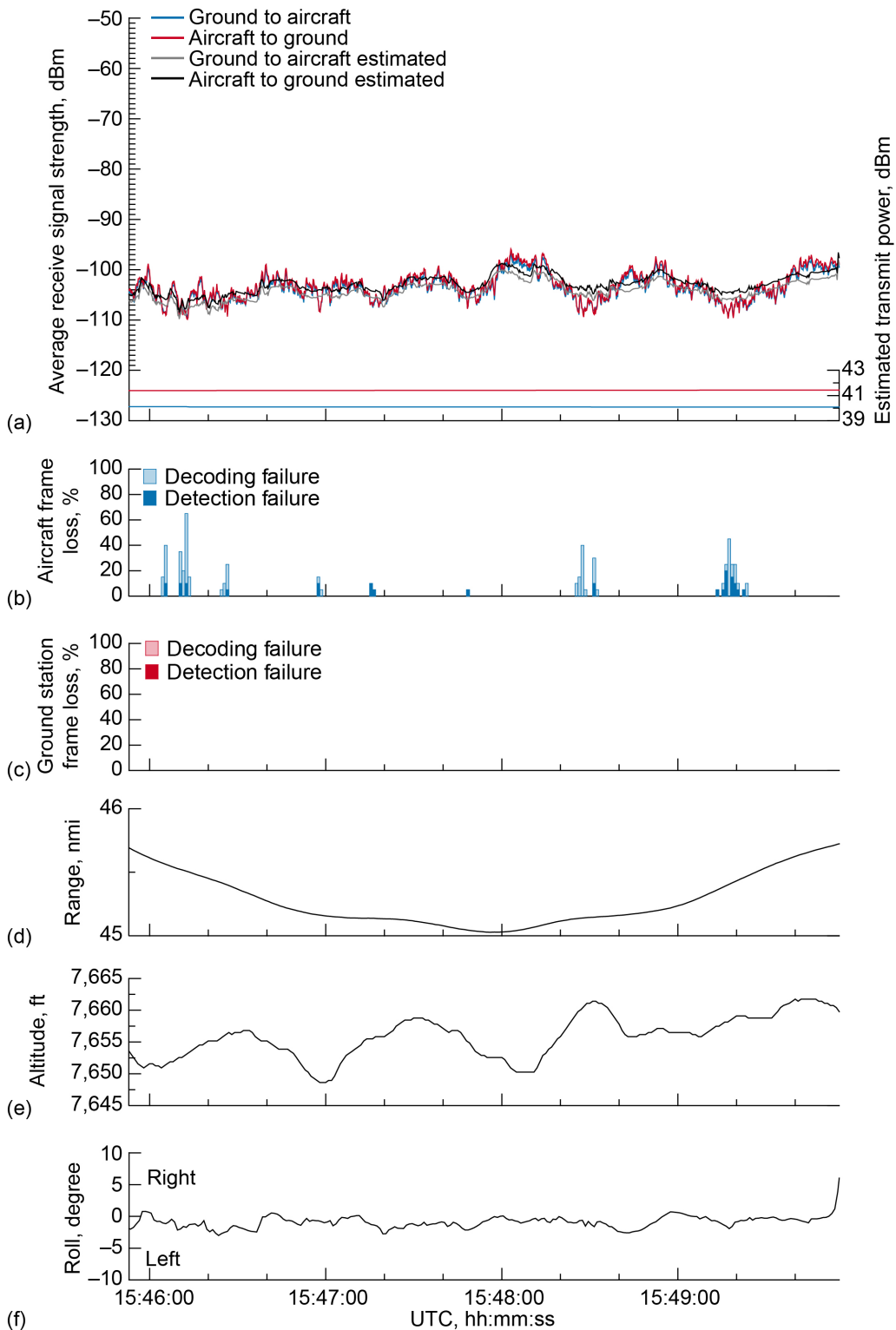


Figure 34.—Signal strength and frame loss over smooth plain terrain at 45-nmi range and 7,500-ft altitude, 1.0° antenna elevation, traveling from waypoint E to waypoint F. Coordinated universal time (UTC). (a) Average receive signal strength. (b) Aircraft frame loss. (c) Ground station frame loss. (d) Range. (e) Altitude. (f) Roll.

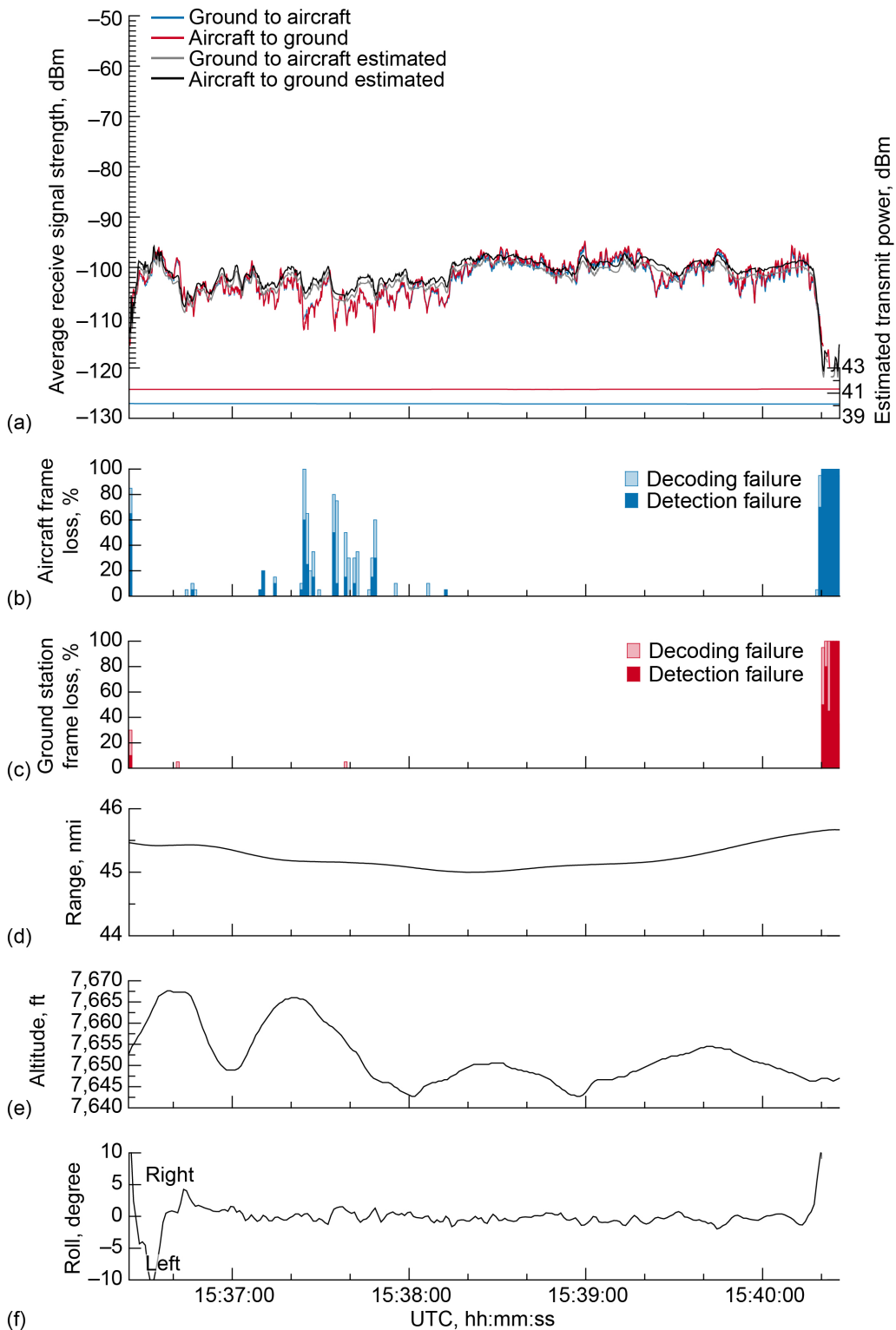


Figure 35.—Signal strength and frame loss over smooth plain terrain at 45 nmi range and 7,500 ft altitude, 1.0° antenna elevation, traveling from waypoint F to waypoint E. Coordinated universal time (UTC). (a) Average receive signal strength. (b) Aircraft frame loss. (c) Ground station frame loss. (d) Range. (e) Altitude. (f) Roll.

#### 4.4 Validation Flight Test Data for Hilly Terrain Setting, December 11 and 12, 2019

Figure 36 presents the flight track of the NASA aircraft over hilly terrain in the airspace east of Athens, Ohio. The orange trace is the complete flightpath of the aircraft, including all reversals, ascent and descent maneuvers, and range changes. Figure 37 is the same flight track viewed from an oblique perspective to show the flightpath at various test altitudes. Waypoints are identified with alphabet characters A to H. The flight segments between waypoints are highlighted in yellow, which precisely represents the locations where RF data was captured for evaluation. For this terrain setting, the GRS was positioned on the open tarmac of the Ohio University Airport in Albany, Ohio.

The propagation performance of the CNPC signals over hilly terrain in southern Ohio was generally quite similar to performance over the smooth plains in northern Ohio. Figure 38 presents data for the  $1.0^\circ$  outbound ascent flight segment in the hilly terrain setting. In this plot, a short period of data packet losses were observed in the ground-to-air (uplink) path at approximately 35 nmi range from the ground station. These losses were not observed in measurement over flat terrain (Figure 32), implying that ground reflections or obstructions may have caused the packet losses. It was often observed that the ground-to-air link regularly suffered greater losses than the air-to-ground link, due to reflection geometry. At the  $1.5^\circ$  ascent angle, the reflection geometry to the aircraft was different, resulting in less destructive multipath interference and fewer data packet losses, as shown in Figure 39.

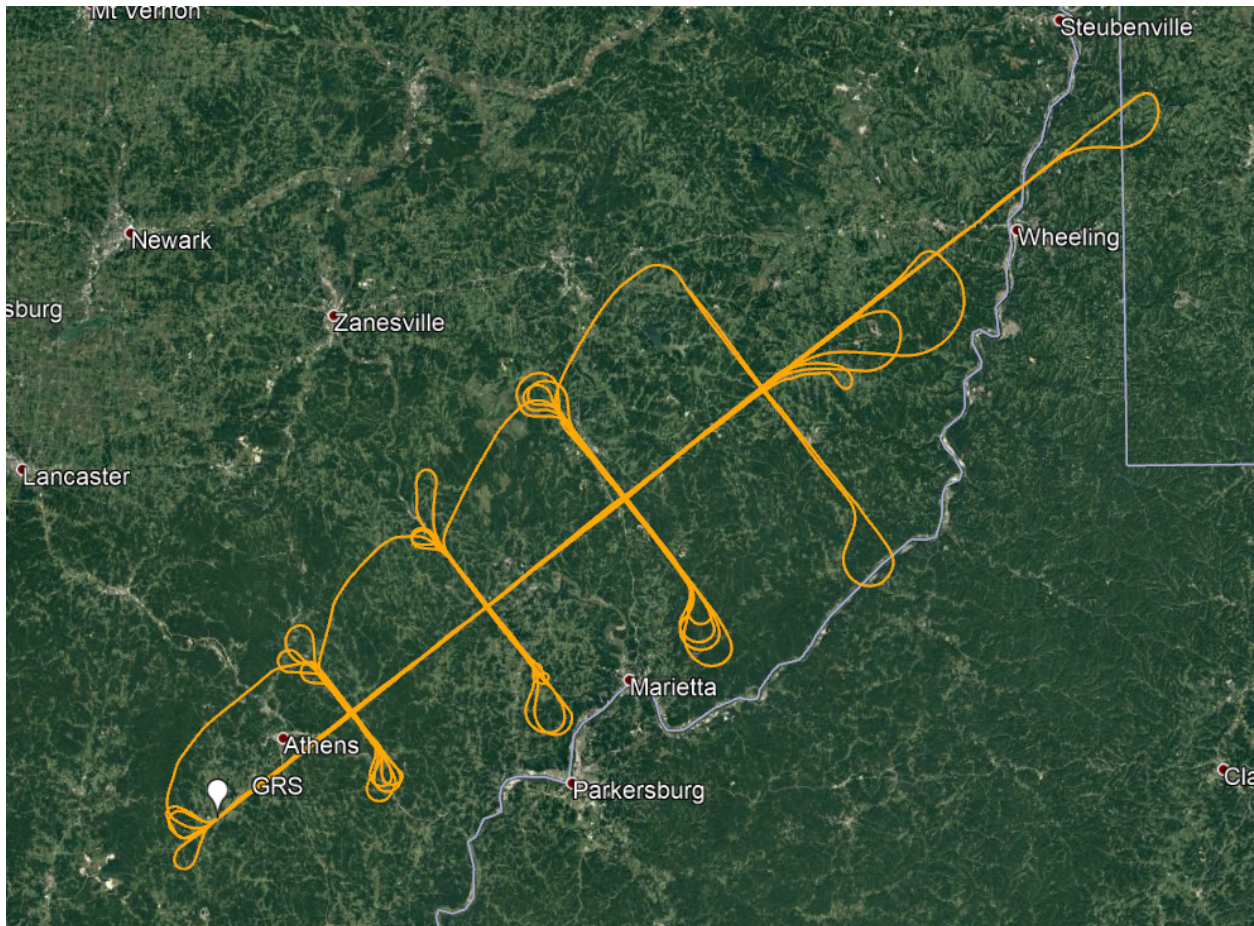


Figure 36.—Flightpath over hilly terrain December 11, 2019. Image ©2018 GoogleEarth.

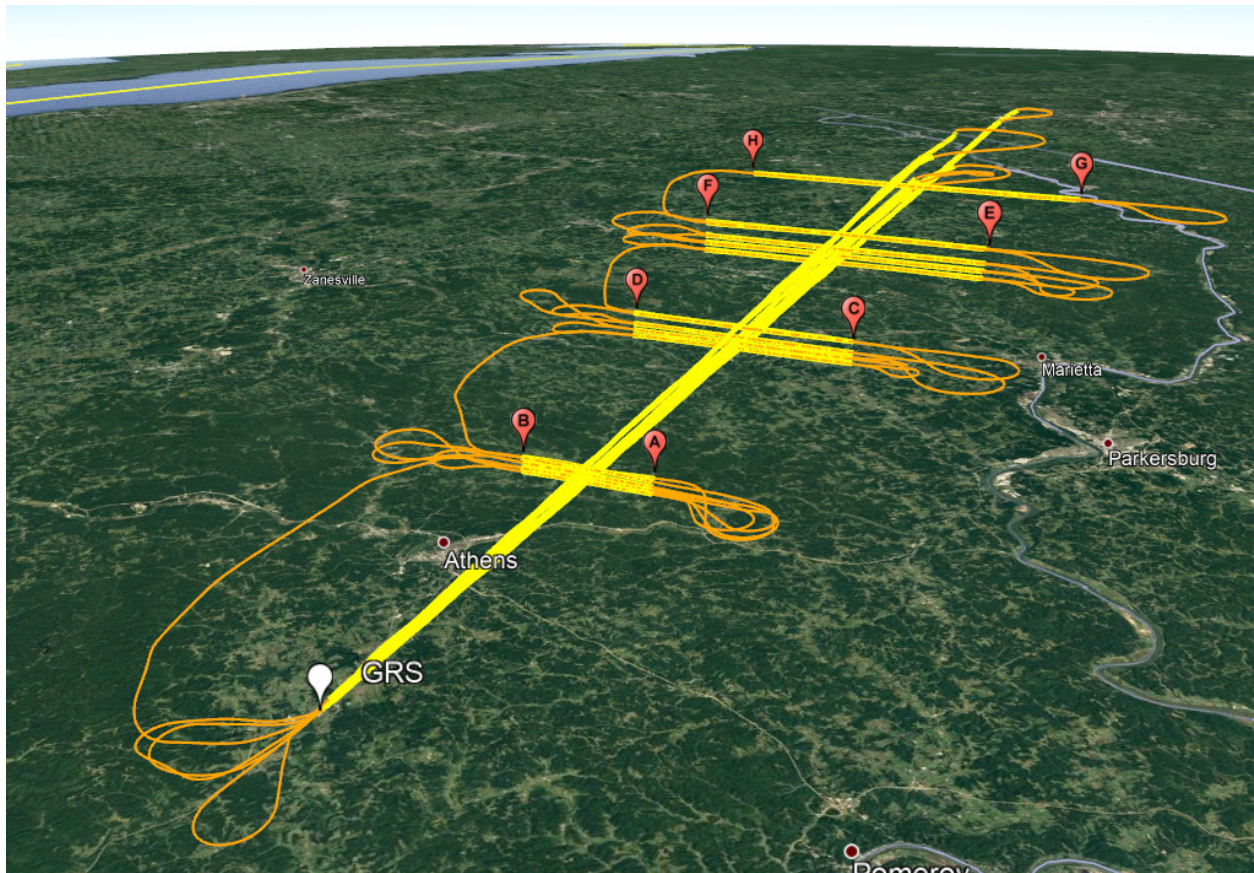


Figure 37.—Perspective view of flightpath over hilly terrain highlighting data capture segments for December 11, 2019. Image ©2018 GoogleEarth.

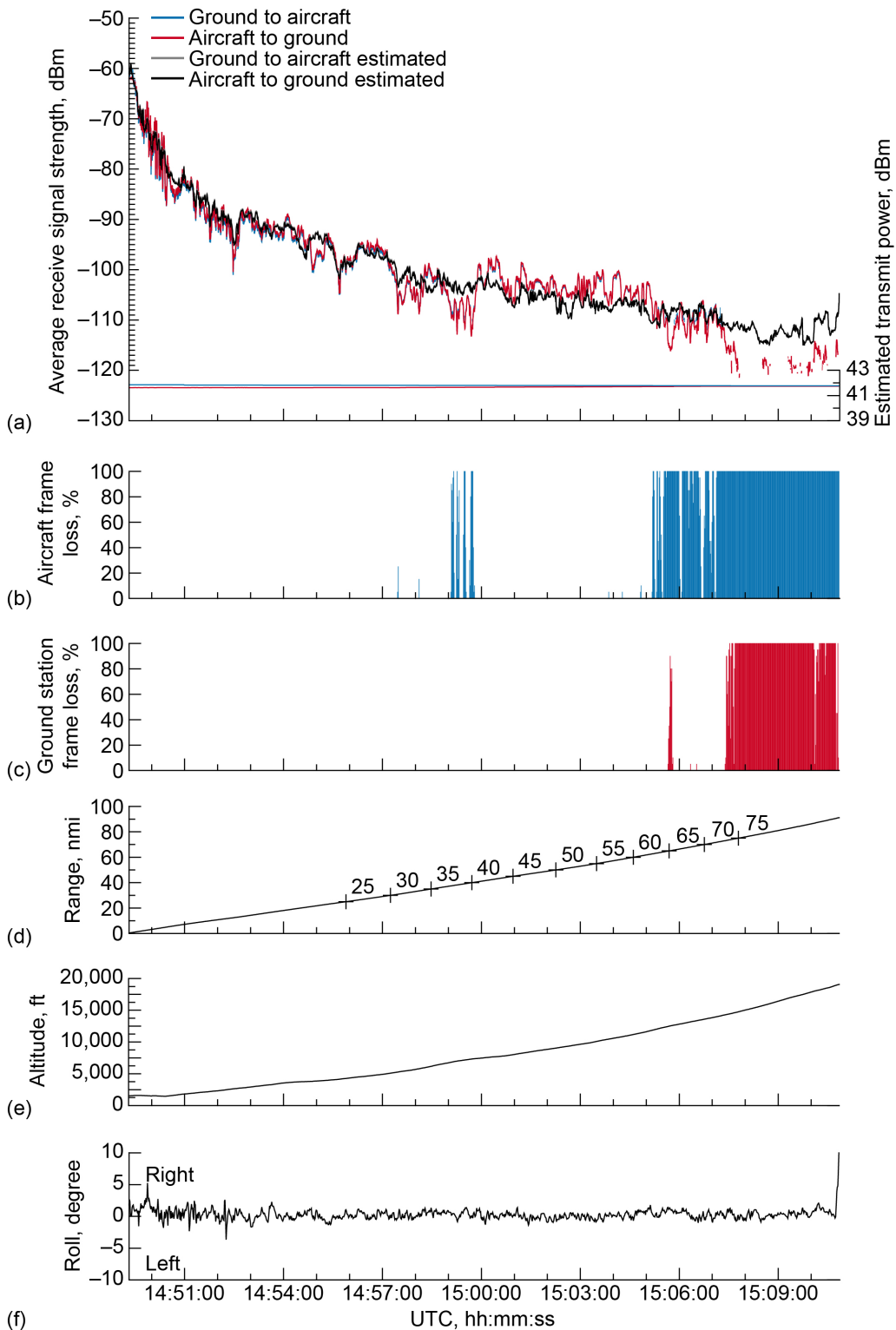


Figure 38.—Signal strength and frame loss over slightly rolling terrain during outbound, ascending track on 1.0° glide slope, traveling away from ground station. Coordinated universal time (UTC). (a) Average receive signal strength. (b) Aircraft frame loss. (c) Ground station frame loss. (d) Range. (e) Altitude. (f) Roll.

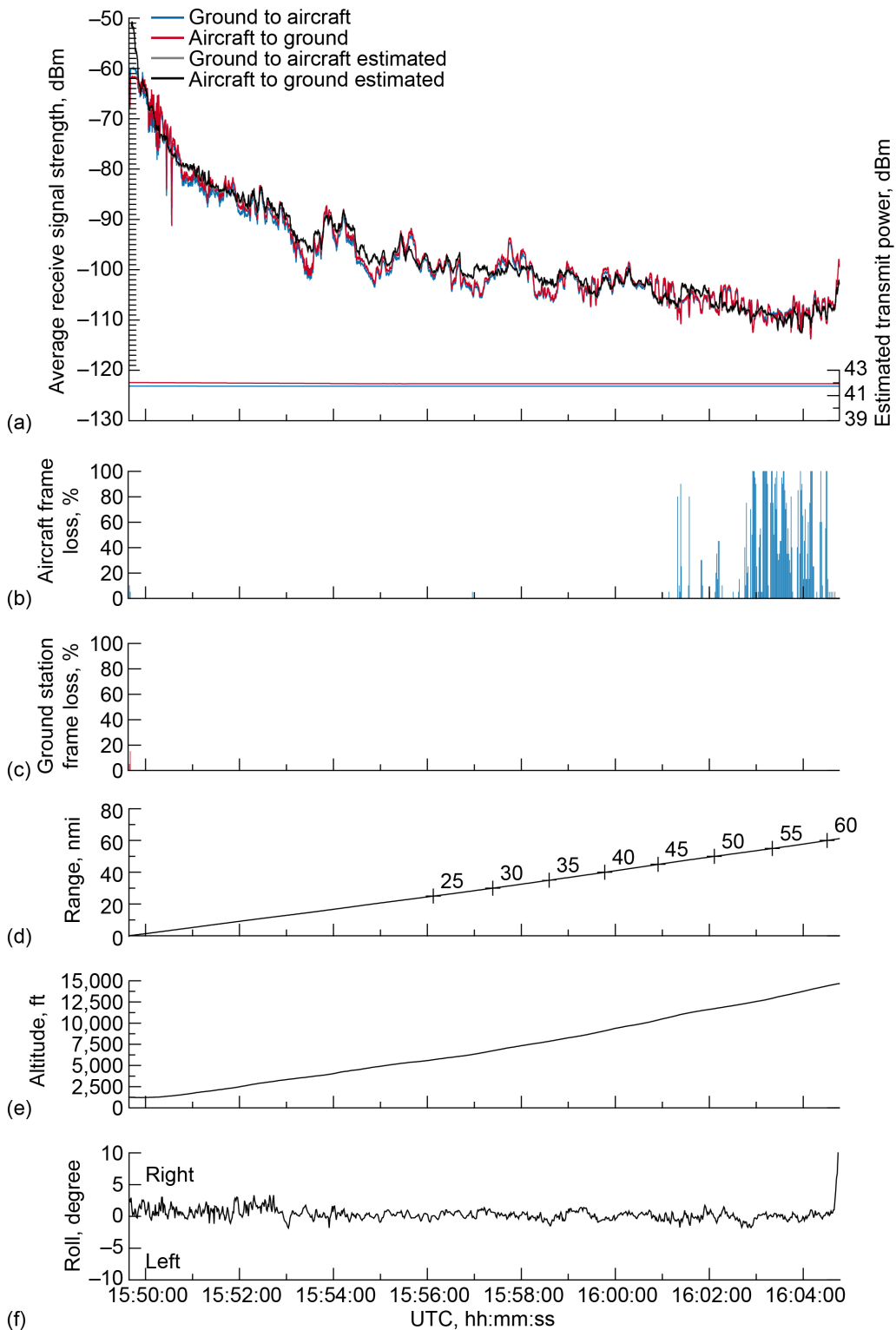


Figure 39.—Signal strength and frame loss over slightly rolling terrain during outbound, ascending track on 1.5° glide slope, traveling away from ground station. Coordinated universal time (UTC). (a) Average receive signal strength. (b) Aircraft frame loss. (c) Ground station frame loss. (d) Range. (e) Altitude. (f) Roll.

#### 4.5 Validation Flight Test Data for Open Water Setting, December 3, 5, and 6, 2019

Figure 40 presents the flight track of the NASA aircraft over the open water airspace above Lake Erie, North Cleveland, Ohio. The orange trace is the complete flightpath of the aircraft, including all reversals, ascent and descent maneuvers, and range changes. Figure 41 is the same flight track viewed from an oblique perspective to show the flightpath at various test altitudes. Waypoints are identified with alphabet characters A to H. The flight segments between waypoints are highlighted in yellow, which precisely represents the locations where RF data was captured for evaluation. For this setting, the GRS was positioned at the shoreline along the western edge of Lake Erie. The surface of the open water carried 1- to 3-ft waves as the result of the east-northeast breeze.

The northern end of each crosstrack flightpath shows a heavily folded reversal made by the aircraft. This was due to the limits imposed by the frequency authorization for this test campaign, which prohibits the aircraft radio from transmitting in Canadian airspace.

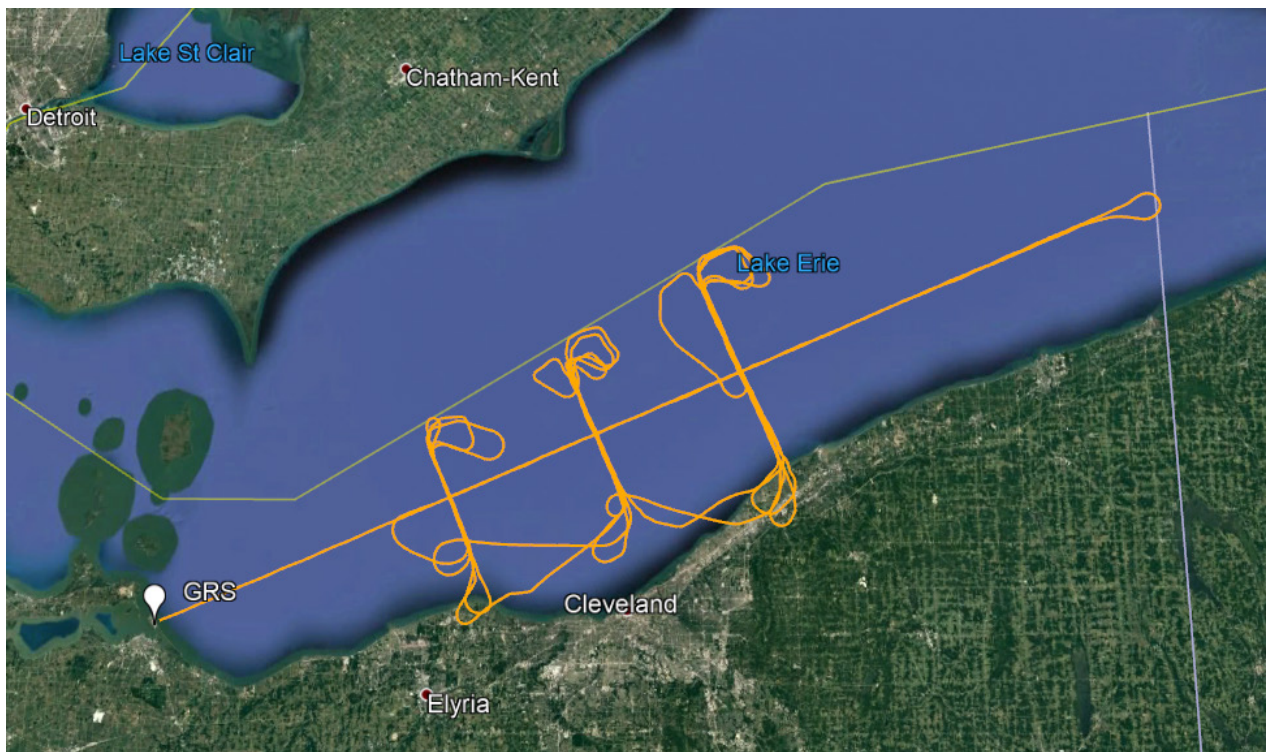


Figure 40.—Flightpath over freshwater December 3, 2019 (orange trace). International boundary indicated by yellow line. Image ©2018 GoogleEarth.



Figure 41.—Perspective view of flightpath over freshwater highlighting data capture segments December 3 and 5, 2019. Image ©2018 GoogleEarth.

Water is well known to produce a highly reflective surface for electromagnetic energy and is often used as a worst-case propagation situation. Figure 42 presents data for the outbound flight segment at a  $1.5^\circ$  ascent angle over a freshwater surface. The received signal strength traces clearly show cyclical variations and nulls caused by multipath reflections at both air and ground radio receivers. The received signal strength traces (red and blue) both deviate greatly from the predicted signal strength traces (black and gray) as the aircraft moves away from the ground station. This effect was observed in both inbound and outbound directions at all the low elevation angles.

Crosstrack flight segments, when flown at a range geometry not prone to destructive interference, observed little signal impairment, as shown in Figure 43. By raising the aircraft altitude from the  $1.5^\circ$  elevation angle to the  $2.0^\circ$  elevation angle, the aircraft moved from an area of clear radio contact into a region with multipath signal degradation. Packet decoding errors and detection errors can be seen in the C2 ground-to-air data, as shown in Figure 44. Notably, the air-to-ground data was not impacted because of the different multipath reflection geometry.

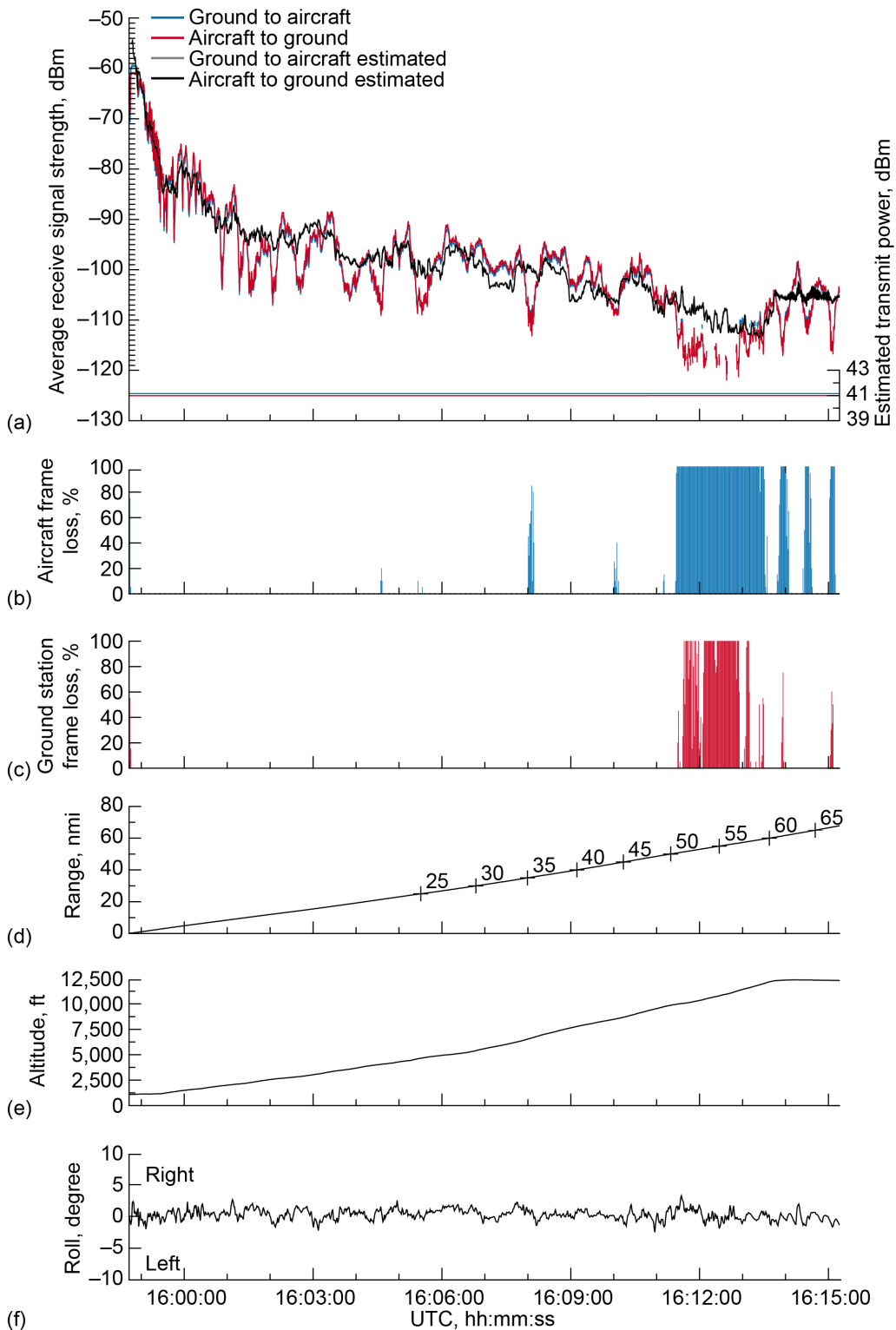


Figure 42.—Signal strength and frame loss over open freshwater during outbound, ascending track on 1.5° glide slope, traveling away from ground station. Coordinated universal time (UTC). (a) Average receive signal strength. (b) Aircraft frame loss. (c) Ground station frame loss. (d) Range. (e) Altitude. (f) Roll.

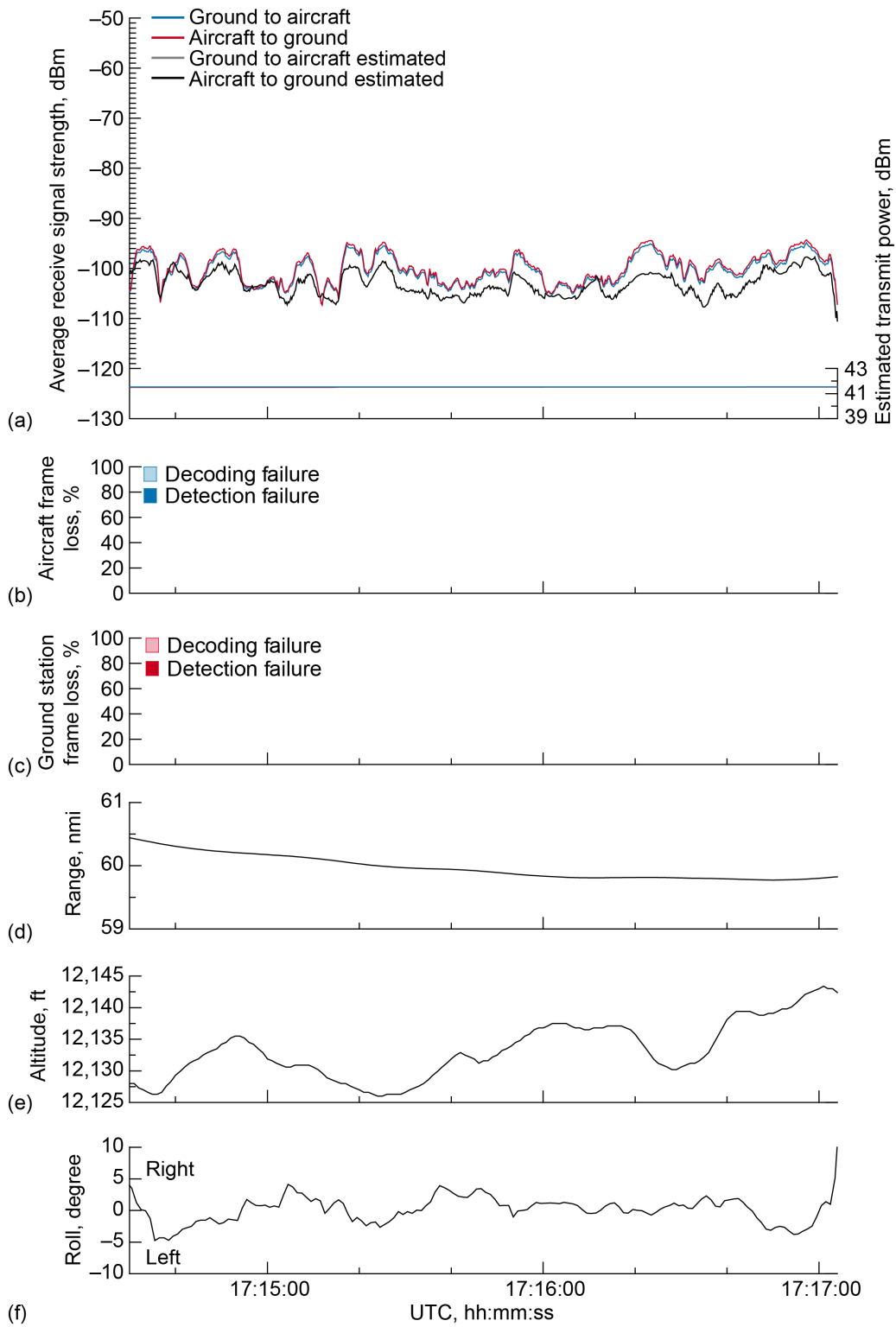


Figure 43.—Signal strength and frame loss over open freshwater at 60-nmi range and 12,000-ft altitude, 1.5° antenna elevation, traveling from waypoint H to waypoint G. Coordinated universal time (UTC). (a) Average receive signal strength. (b) Aircraft frame loss. (c) Ground station frame loss. (d) Range. (e) Altitude. (f) Roll.

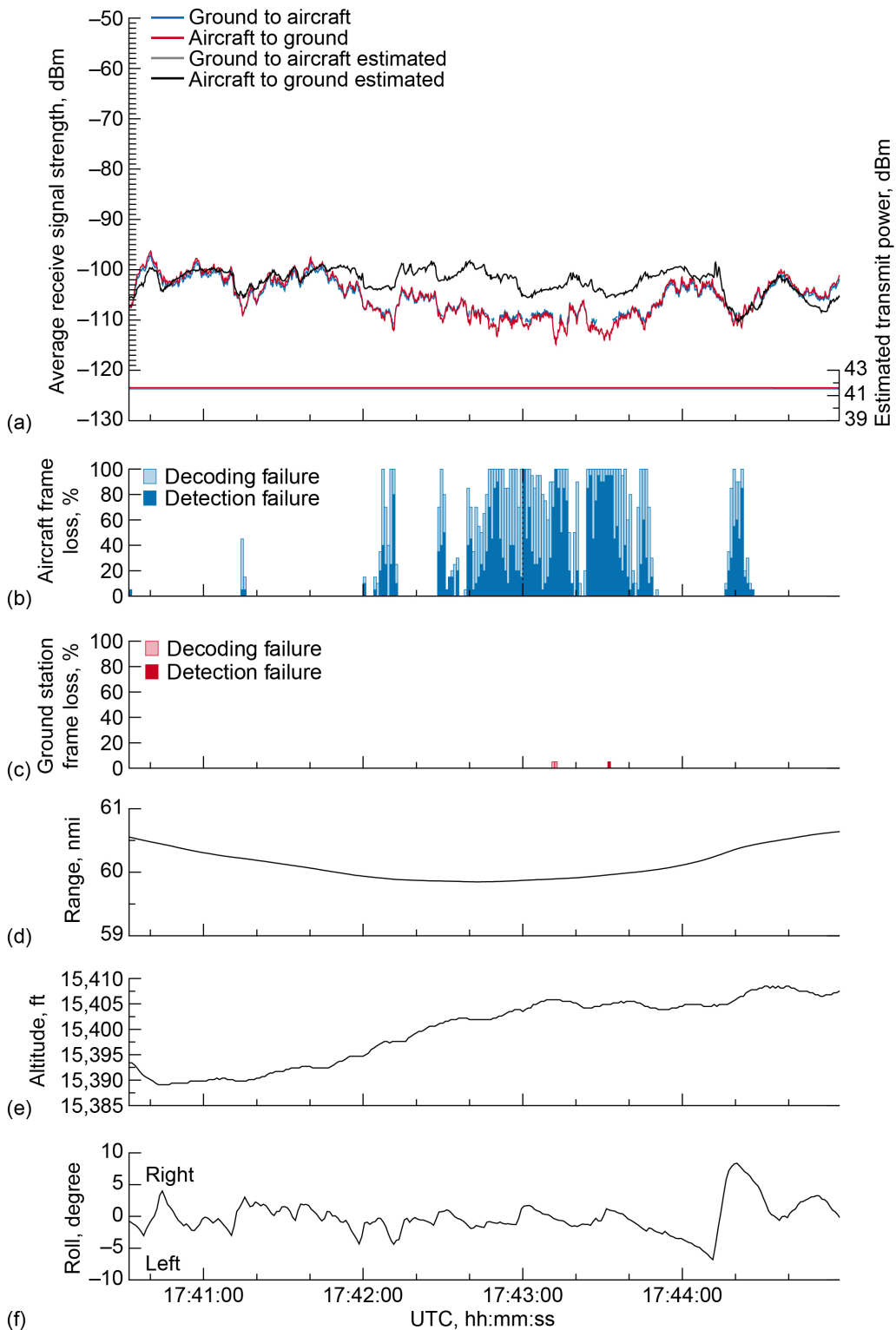


Figure 44.—Signal strength and frame loss over open freshwater at 60 nmi range and 15,500 ft altitude, 2.0° antenna elevation, traveling from waypoint H to waypoint G. Coordinated universal time (UTC). (a) Average receive signal strength. (b) Aircraft frame loss. (c) Ground station frame loss. (d) Range. (e) Altitude. (f) Roll.

## 4.6 Excess Path Loss Data Processing and Fade Analysis

In addition to collecting the data to verify the overall performance of the CNPC radios for the RTCA standards, the flight test data was used to determine the EPL that would be experienced by any link operating under similar conditions, frequencies, and waveforms. The EPLs were needed in a variety of locations in Reference 5 to support the CNPC link budget considerations, to provide data for radio designers in the signal-to-noise analysis for both airborne and surface operations, and to ensure that the appropriate amount of excess link margin is included in the system design.

The CNPC C-band EPLs were also used in a signal fade analysis to provide crucial fade information to system designers and operators to ensure that the C2 link will support the mission. By understanding the fade depths and durations, designers can ensure that sufficient link margin is provided for a robust link. The basis of this analysis is comparing how often and how long RF fades, determined by the EPL, exist in excess of a series of reference levels. These reference levels would be considered the amount of link margin that would be required for the system.

The three main statistics calculated in this data are

- Availability—The percentage of time the average EPL is less than the reference level.
- Average fade duration (AFD)—The average length of time that the average EPL exceeded the reference level, expressed in seconds.
- Level crossing rate (LCR)—The rate at which the average EPL crossed the reference level in an increasing direction. This is also equivalent to the fade rate expressed in number of fades per minute.

The EPLs were determined by subtracting the measured path loss (between the two antennas) captured during the flight tests from the calculated free space RF transmission loss based on the known exact location of the aircraft and ground antenna (slant range). A positive value of EPL indicates that the measured path loss was greater than the calculated path loss. EPLs ranging from  $-6$  dB (i.e., 6 dB of signal enhancement) down to over 30 dB (i.e., 30 dB of fading) were measured. The measured path loss between the two antennas was calculated from the precisely measured transmitter power, aircraft, and ground antenna cable losses and received signal strength indicator in the receiver.

Both ground and aircraft antenna gains needed to be considered when calculating the measured path loss. For the ground antenna, this was done by “looking up” the gain that had been previously measured in an antenna test range for the exact azimuth and elevation of the aircraft at each sample point. For the aircraft antenna, this was not possible as its gain is significantly impacted by the presence of the aircraft’s airframe.

To overcome this difficulty, the installed aircraft antenna pattern was estimated based on gain estimates measured across all of the UAS CNPC flight test datasets. As can be seen from Figure 45, there was a significant difference between the estimate of the antenna gain when installed on the aircraft (black line) and the gain of the antenna when measured on an antenna test range (red line). The gray data points indicate the raw (unfiltered) data. The pattern shown is for all azimuths at an elevation angle  $5^\circ$  below horizontal relative to the aircraft’s airframe, which is close to the angle used during the flight tests.

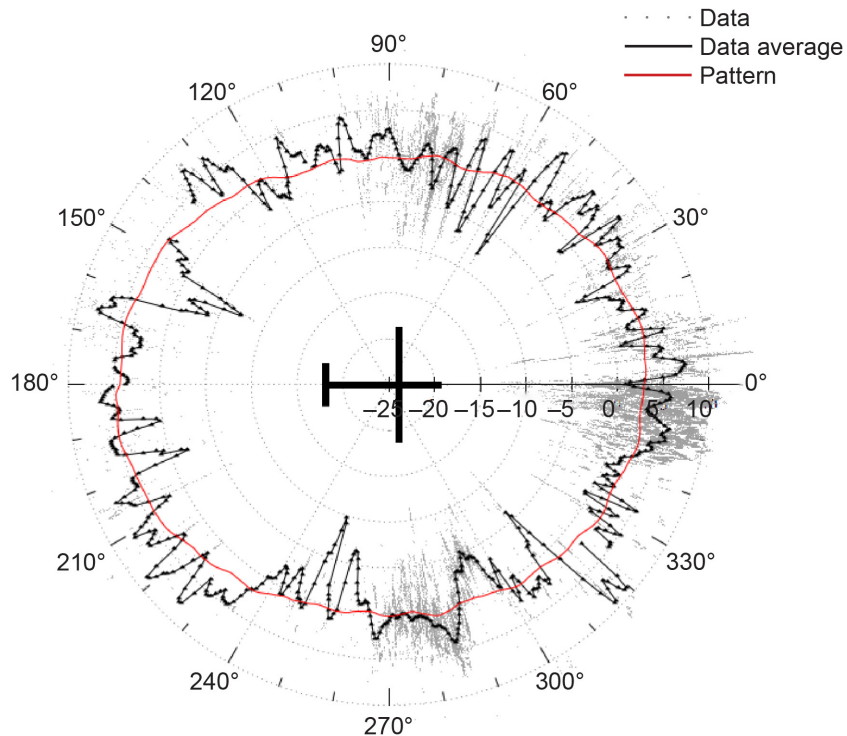


Figure 45.—Installed antenna gain estimate.  $\theta = 85^\circ$ .

The flight test received power data was first averaged to 200 ms. This averaging, which includes four samples taken 50 ms apart, smooths out measurement noise but can also mask very short fades. The flight test data reports received power in both the uplink and downlink direction, allowing the EPL to be calculated separately for both directions. Since the link should be symmetric, the uplink and downlink EPL values were then averaged when both were available.

The data was then split into the appropriate segments. For the crosstracks, a segment is limited to the approximately straight and level flight at constant range and in the main beam of the ground antenna, excluding the initial maneuvering for alignment and direction reversal at the end. For the inbound segments, data within  $\pm 10$  nmi of the selected slant ranges were included as part of that corresponding range group. The complete analysis incorporated data from 109 inbound and crosstrack flight segments.

Within each category, the EPL data for each flight segment was compared to a series of reference levels from  $-6$  to  $30$  dB. For each reference level, a flight segment is divided into periods of fades (where the EPL exceeds the reference level) and nonfades (where the EPL is less than the reference level). The number and length of the faded and unfaded periods are recorded for further use.

Figure 46 shows faded periods (red highlighting) and unfaded periods (green highlighting) occurring during a typical crosstrack flight, for a reference level that is  $0$  dB.

Figure 47 shows the same EPL data but using a reference level of  $5$  dB. It is readily visible how the change in the reference level affects both the number of faded and unfaded periods, along with the duration of those periods. In general, increasing the reference level would increase the average unfaded period length and decrease the average faded period length.

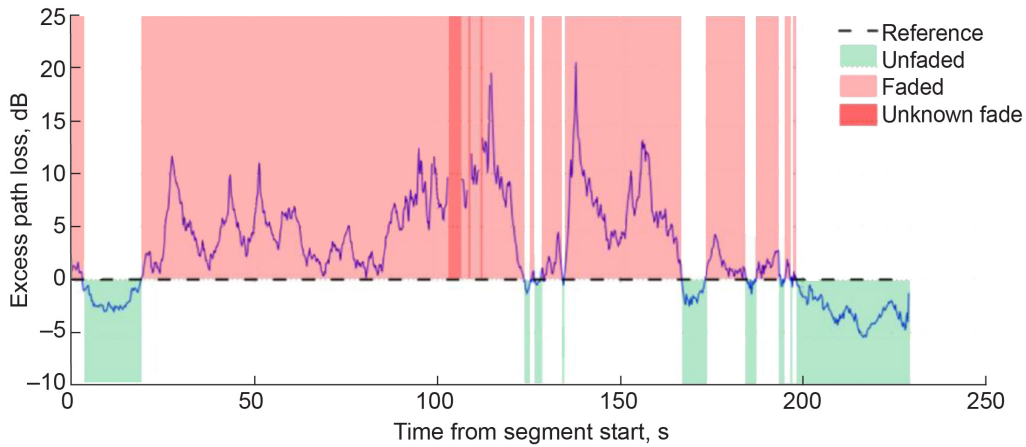


Figure 46.—Example fades and nonfades (0 dB reference level).

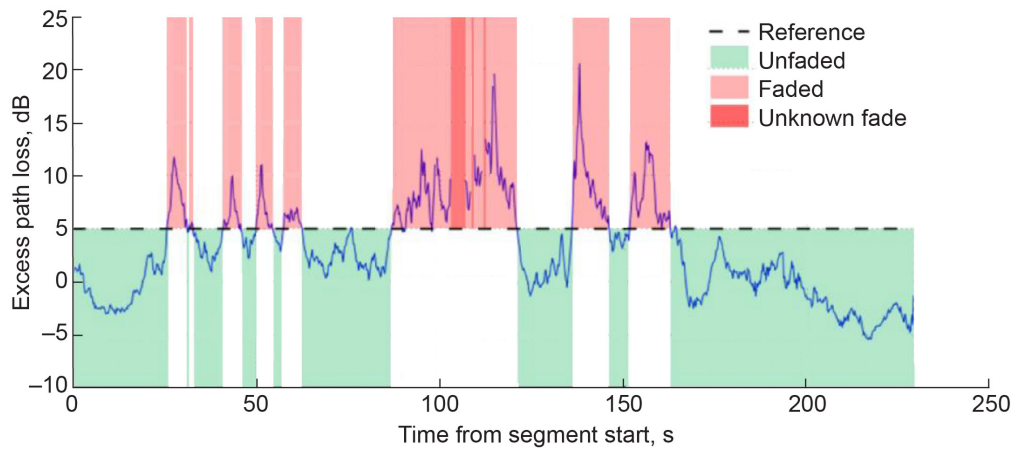


Figure 47.—Example fades and nonfades (5 dB reference level).

The flight segments are then categorized by underlying terrain type (smooth plains, slightly rolling plains, open water), range (15, 30, 45, and 60 nmi), and elevation angle (1°, 1.5°, 2°, and 3°). For each combination of terrain setting, range, and elevation angle, the corresponding segments (both crosstracks and inbound) are processed at reference levels ranging from –6 to 30 dB. The airport surface segment is similarly processed. At each reference level, all of the faded and unfaded periods are collected and used to calculate the overall statistics. The partial fades are included if the length of the partial fade is greater than the average nonpartial fade duration and excluded otherwise. From this data, several basic quantities were calculated:

- Total number of fades ( $N_{\text{faded}}$ ). The count of faded periods across all flight segments of a category at the reference level.
- Total faded duration ( $T_{\text{faded}}$ ). The sum length of all faded periods across all flight segments of a category at the reference level.
- Total unfaded duration ( $T_{\text{unfaded}}$ ). The sum length of all unfaded periods across all segments of a category at the reference level.

From these quantities, the three parameters characterizing the EPL were computed.

- Availability: 
$$A\% = \frac{T_{\text{unfaded}}}{T_{\text{faded}} + T_{\text{unfaded}}}$$

- Average fade duration:  $AFD = \frac{T_{\text{faded}}}{N_{\text{faded}}}$

- Level crossing rate:  $LCR = \frac{N_{\text{faded}}}{T_{\text{faded}} + T_{\text{unfaded}}}$

#### 4.6.1 Fade Analysis Results

The results from the analysis were presented to SC-228 analysts and included in Appendix O of Reference 5. The complete set of tables and plots providing the availability, AFD, and LCR versus the reference EPL level for the flat terrain, hilly terrain, and open water settings for each of the elevation angles and ranges were included in that appendix.

A sample dataset, showing the availability, AFD, and LCR results for the flat terrain setting are presented in Table 7. In the tests, fades of up to 10 dB were experienced. The availability was limited at the 45- and 60-nmi ranges at 1° elevation due to loss of measurements during the segment, resulting in fades of unknown depth. These were not necessarily very deep fades; at long ranges and low elevation angle, the received RF power was expected to be low and a moderate fade could drop the signal power below radio sensitivity.

The fade margins required for 99.9 percent availability (based only on EPL; not considering antenna nulls) were also prepared and delivered to RTCA. Table 8 to Table 10 show the required fade margin for each terrain setting based on the elevation angle and range from the ground station. In some cases, 99.9 percent availability was not achieved during the test due to the packet loss resulting in unknown fade depths. In those instances, the maximum reference level at which fades could be determined was provided, along with the resulting availability in parentheses.

TABLE 7.—FLAT TERRAIN RESULT AT 1° ELEVATION

Reference EPL, <sup>a</sup> dB	Range, nmi											
	15			30			45			60		
	A%, <sup>b</sup> %	AFD, <sup>c</sup> s	LCR, <sup>d</sup> ft/min	A%, <sup>b</sup> %	AFD, <sup>c</sup> s	LCR, <sup>d</sup> ft/min	A%, <sup>b</sup> %	AFD, <sup>c</sup> s	LCR, <sup>d</sup> ft/min	A%, <sup>b</sup> %	AFD, <sup>c</sup> s	LCR, <sup>d</sup> ft/min
-3	0.8	58.5	0.8	2.7	20.9	2.5	4.6	31.1	1.9	6.0	13.3	4.2
-2	4.5	19.1	2.6	12.9	6.4	8.0	10.5	10.4	5.2	15.1	5.8	8.8
-1	17.5	5.4	9.2	31.2	2.8	14.5	19.4	5.7	8.5	30.6	3.3	12.6
0	38.9	2.1	17.3	56.2	1.7	15.1	32.7	2.8	14.4	49.1	2.1	14.8
1	59.3	1.6	15.6	74.1	1.4	11.3	54.2	1.7	16.7	69.3	1.5	12.1
2	77.1	1.2	11.5	85.5	1.3	6.7	75.4	1.3	11.6	82.2	1.4	7.9
3	90.5	1.0	6.4	93.3	1.1	3.8	87.8	0.9	8.1	91.4	1.1	4.9
4	96.7	0.8	2.9	97.8	0.7	2.1	95.3	0.7	4.3	96.4	0.8	3.0
5	99.3	0.7	1.0	99.4	0.5	0.9	97.8	0.7	2.1	98.4	0.8	1.4
6	>99.9	0.2	0.5	>99.9	0.2	0.4	99.0	0.6	1.2	99.0	0.7	1.0
7	-----	-----	-----	-----	-----	-----	99.3	0.8	0.7	99.5	0.8	0.6
8	-----	-----	-----	-----	-----	-----	99.4	1.2	0.5	99.5	1.0	0.5
9	-----	-----	-----	-----	-----	-----	99.4	1.5	0.4	-----	-----	-----

<sup>a</sup>Excess path loss (EPL).

<sup>b</sup>Availability (A%).

<sup>c</sup>Average fade duration (AFD).

<sup>d</sup>Level crossing rate (LCR).

TABLE 8.—REQUIRED FADE MARGIN FOR 99.9 PERCENT AVAILABILITY—FLAT TERRAIN

Elevation angle, degree	Range, nmi			
	15	30	45	60
1.0	5.5	5.5	9.0 (99.4%)	7.2 (99.5%)
1.5	5.3	4.4	8.3	9.1
2.0	4.4	6.0	6.6	7.0

TABLE 9.—REQUIRED FADE MARGINS FOR 99.9 PERCENT AVAILABILITY—HILLY TERRAIN

Elevation angle, degree	Range, nmi			
	15.0	30.0	45.0	60.0
1.0	6.4	6.5 (99.8%)	7.0	7.3
1.5	13.7	12.8	7.2	7.6
2.0	10.0	8.7	9.3	14.0 (99.8%)
3.0	8.2	13.2	6.6	6.5 (99.8%)

TABLE 10.—REQUIRED FADE MARGINS FOR 99.9 PERCENT AVAILABILITY—OPEN WATER

Elevation angle, degree	Range, nmi			
	15.0	30.0	45.0	60.0
1.0	19.4	19.0	24.9 (98.2%)	21.5 (99.4%)
1.5	14.6	14.5	21.3 (99.8%)	19.6
2.0	10.5	11.9	14.5 (99.4%)	15.0 (98.5%)
3.0	6.6	7.2	7.2	7.2

#### 4.7 Validation Test Data for Airport Surface Operations, February 19, 2020

Subsequent to the in-flight propagation measurements, the NASA GMSK CNPC test system was used to collect data during aircraft operations (taxiing) on a representative airport surface. Data from the test was processed and included in the EPL analysis delivered to RTCA. This was a very preliminary test performed without the engineering rigor used in the previously described tests. Still, it did validate concerns about aircraft antenna placement, it solidly confirmed the need for further tests to investigate ground-specific multipath propagation issues, and it provided RTCA with important data enabling a C-band CNPC channel model for airport surface operations.

For this test, the CNPC GRS was positioned at the northwest edge of the Cleveland Hopkins International Airport property (designation KCLE) in Cleveland, Ohio. The mobile tower mast supporting the GRS test antenna was elevated to 15 ft above ground level and remained stationary for the test. A full-wave dipole omnidirectional antenna providing 4.1 dBi gain was used to achieve the wide azimuthal coverage needed for the test. The NASA-owned S-3B Viking aircraft again served as the ARS using the same systems and C-band omnidirectional blade antenna as used in all previous tests. The aircraft was operated under its own power and was moved at a constant rate of speed along KCLE’s 6,000- and 10,000-ft runways in both directions while CNPC radios were operated. Dwell periods were required between taxi and backtaxi runs to allow airport traffic to clear. The full path of the aircraft is displayed in Figure 48, with the blue trace indicating the aircraft taxi and backtaxi travel segments.

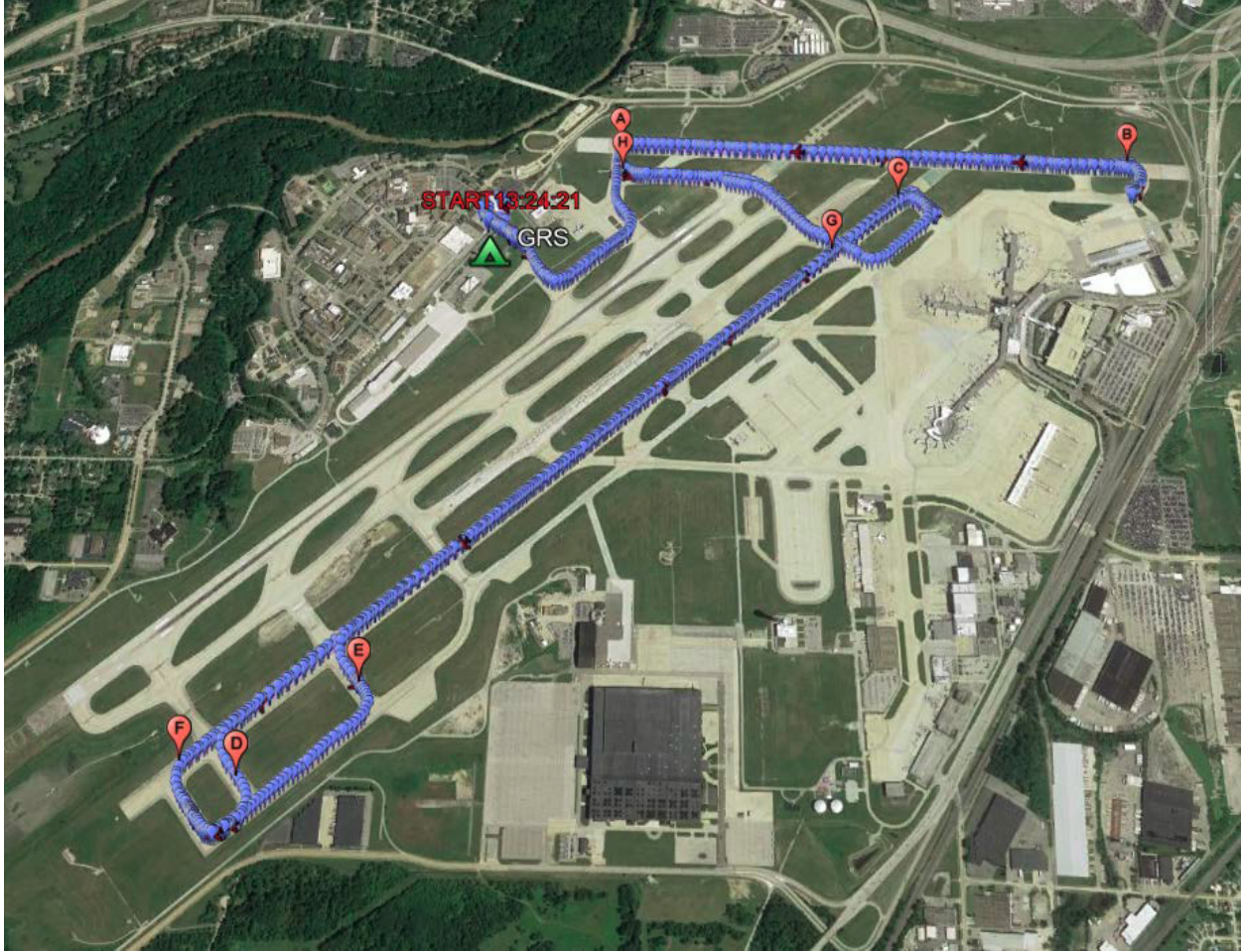


Figure 48.—View of taxiing path during surface operations test at Cleveland Hopkins Airport, February 19, 2020. Image ©2018 GoogleEarth.

Received signal strength and frame loss data from the surface operations test using GMSK CNPC waveform mode C are shown in Figure 49. Vertical gray bands highlight periods of aircraft movement. Frame loss traces indicated a clear correlation to periods of aircraft movement. When stationary, the aircraft uplink and downlink both exhibited zero data frame errors and stable signal strength readings. When moving, however, the radios both recorded significant frame errors. Although the radios had difficulty decoding the CNPC signals during movement, the average received signal power levels were still detectable and, therefore, suitable for the EPL analysis.

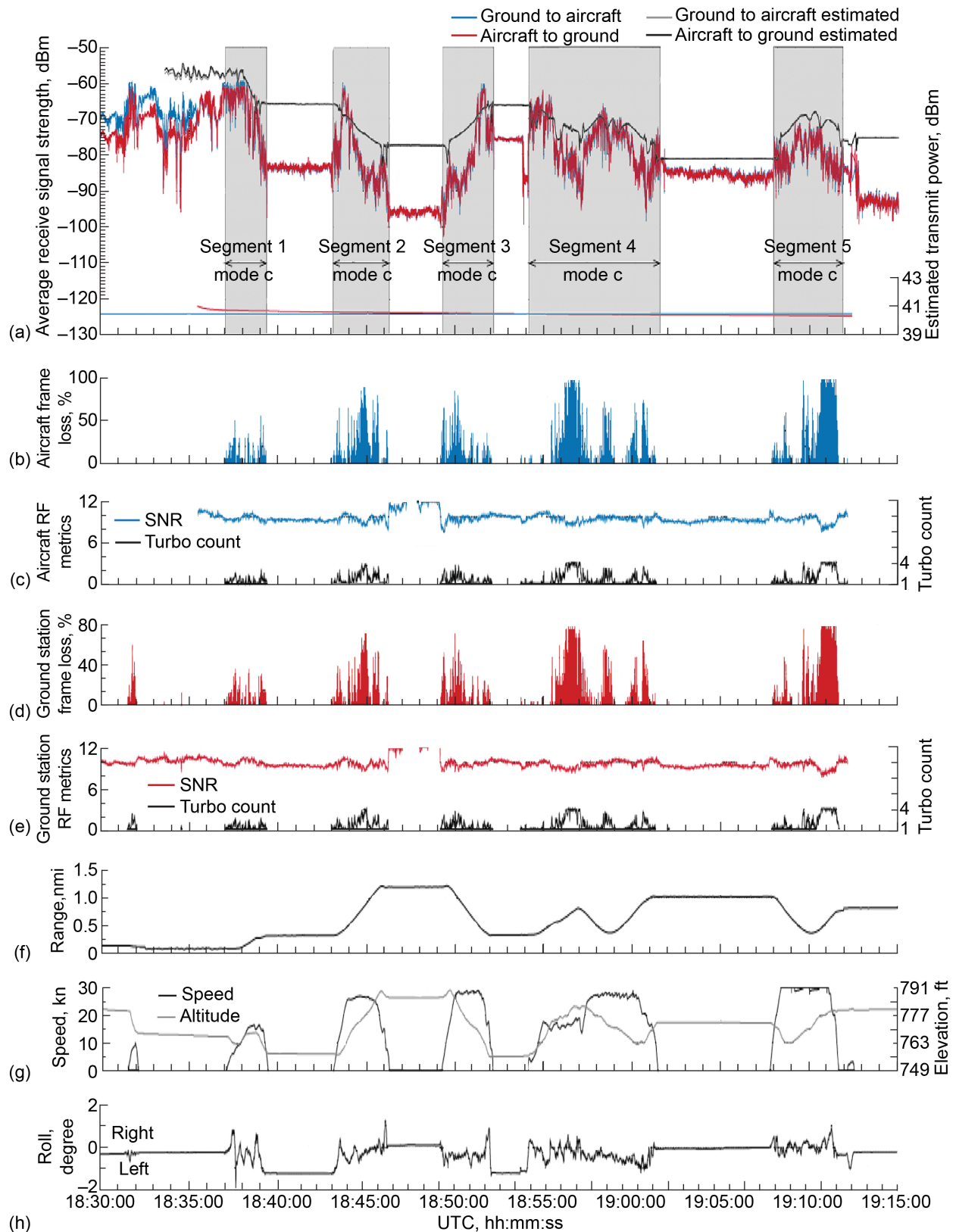


Figure 49.—Signal strength data from surface operations test, February 19, 2020. Signal-to-noise ratio (SNR). Coordinated universal time (UTC). (a) Average receive signal strength. (b) Aircraft frame loss. (c) Ground station frame loss. (d) Range. (e) Altitude. (f) Roll.

Investigations into the causes of the signal errors immediately converged on multipath fading, channel delay dispersion, and the need for more frequent Doppler estimation. While these radio corrections were all achievable, the schedule to complete the UAS C2 Subproject would not permit the execution of that effort. Guidance for addressing the surface operations propagation issues was planned for inclusion in Reference 5.

#### **4.8 Generation 7 Control and Non-Payload Communications Radio Data Latency Test Results**

Two flight tests were performed to measure time required for transmission of user data over the network architecture detailed in Section 3.0. This architecture provided a scalable and secure solution that allowed the aircraft to remain directly addressable and the contents of messages encrypted. The latency tests were configured to mimic the actual data message formats being sent over both the air-to-ground (downlink) and ground-to-air (uplink) links.

For proper replication of the data flow, a software application was created to generate IPv6 User Datagram Protocol (UDP) packets at the precise intervals for each of the different modes and phases of flight (Ref. 1). The software program generated messages at the correct size and rate but did not fill the messages with real user data. Instead, the messages all contained sequence and time stamp information, which aided in calculating performance metrics when they were received. A data collector program was also created that would receive these messages and log the results. All of the packets were UDP except for the Air Traffic Controller (ATC) voice traffic, which is expected to use Real-time Transport Protocol (RTP). Because the traffic generator program was not designed to process RTP, the software compensated for the missing RTP header by adding 12 bytes to the 60 bytes of application data, bringing the total for each voice packet to 72 bytes. A copy of the traffic generator program was run on the aircraft system to generate downlink traffic, while another copy of the generator program was run on a ground-based system acting as the pilot station to simulate uplink traffic. It was important to note that in this network architecture, the ground station was not a data endpoint, but rather data were routed through the ground station to a control computer.

Each of the message groups was also classified at one of seven available priorities. Table 11 shows the priority mappings used for the different message types. In addition to setting the priority, IPv6 flow labels were enabled in order to preserve each flow through the header compressor. A separate traffic generator program was activated for each type of data to reflect the behavior of a real system. In this example, transmission of C2 and other message types were initiated simultaneously, which imposes heavy data loading at the beginning of each 1-second transmission interval. Staggering the start times for the message types would distribute the data load over time, possibly improving the data latency and efficiency for lower priority messages over the CNPC radio link.

Because ranging was not the focus of this test, the flightpaths were a simple 20-nmi orbit around the ground station at Glenn in Cleveland, Ohio (Figure 50).

Sample results from the latency testing are shown in Figure 51 and Figure 52 for both uplink and downlink paths, for Service Classes 2 and 4, and for the arrival, departure, and en route phases of UA flight. The results are presented as a cumulative distribution function (CDF) of one-way delays for each message type present. Not all configurations generated the same amount or types of data. The CDFs show the percentage of messages that arrived at or before a given amount of time. Each plot also has statistics for each data type, including the number of messages that arrived within the test period. Table 12 shows a breakdown of the metrics for each data type.

TABLE 11.—PRIORITY MAPPINGS, HIGHEST (7) TO LOWEST (0)

Priority	Traffic class	Message type
7	0x7c	Key updates, mobility binding messages, and header compressor feedback
6	0x6c	Command and control messages <sup>a</sup>
5	0x5c	Air traffic control voice data
4	0x4c	Target data
3	0x3c	Weather data
2	0x2c	Reserved
1	0x1c	Reserved
0	0x00 or 0x0c	Unclassified, routing advertisements, pings, etc.

<sup>a</sup>NATO Standardization Agreement and Navigational aids (if applicable).

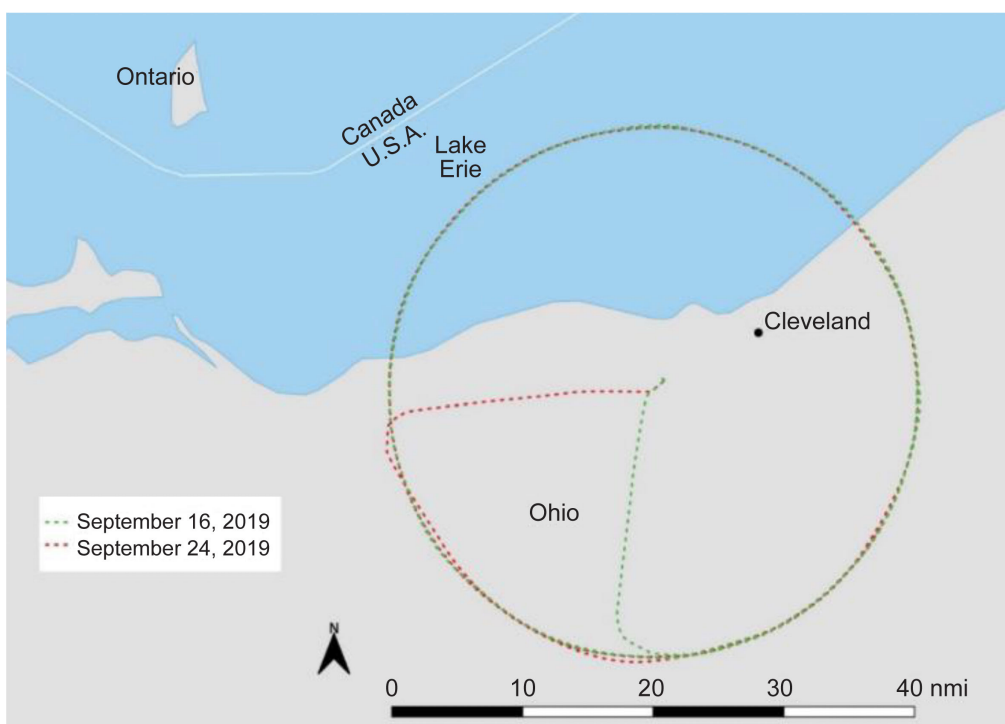


Figure 50.—Flightpath for data flow tests.

TABLE 12.—DATA LATENCY METRICS

Metric	Description
Samples	Number of messages that were successfully received
Minimum	Minimum latency observed
Maximum	Maximum latency observed
Mean ± standard deviation	Mean or average of all samples and their standard deviation
Median ± median absolute deviation	Median or midpoint of all samples and their median absolute deviation

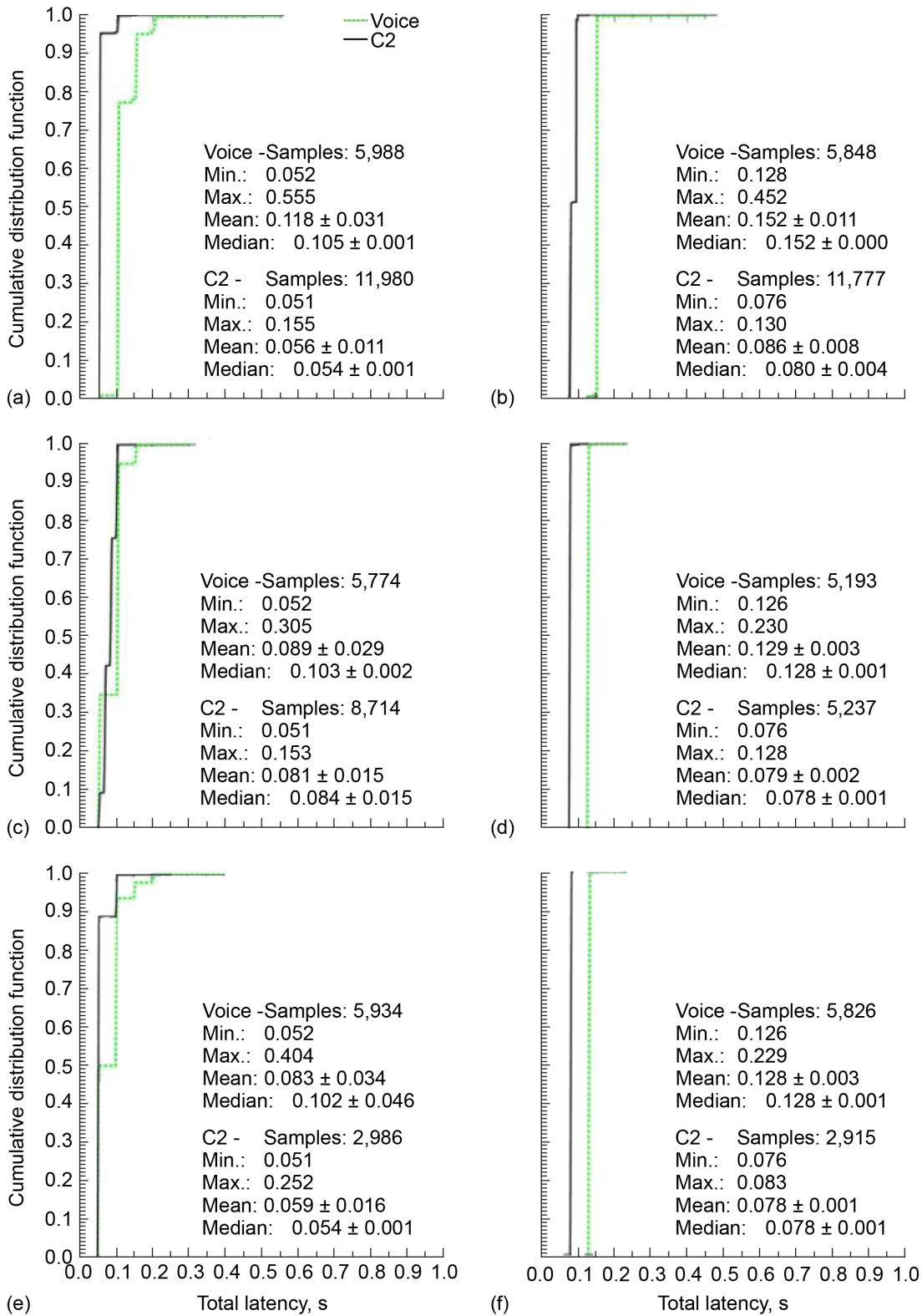


Figure 51.—Total latency distribution for Service Class 2 traffic on September 16, 2019. Command and control (C2). (a) Arrival downlink. (b) Arrival uplink. (c) Departure downlink. (d) Departure uplink. (e) En route downlink. (f) En route uplink.

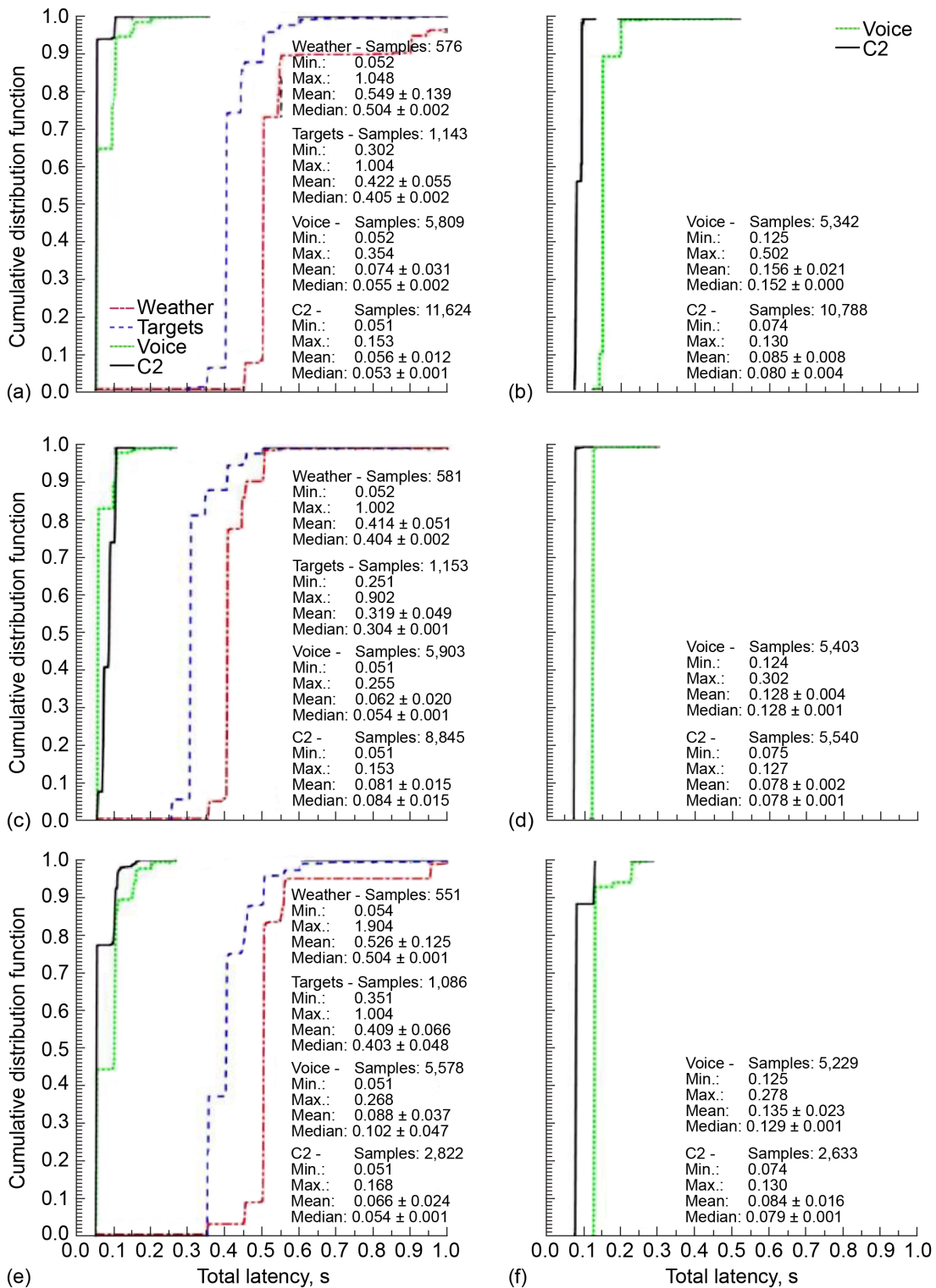


Figure 52.—Total latency distribution for Service Class 4 traffic on September 16, 2019. Command and control (C2). (a) Arrival downlink. (b) Arrival uplink. (c) Departure downlink. (d) Departure uplink. (e) En route downlink. (f) En route uplink.

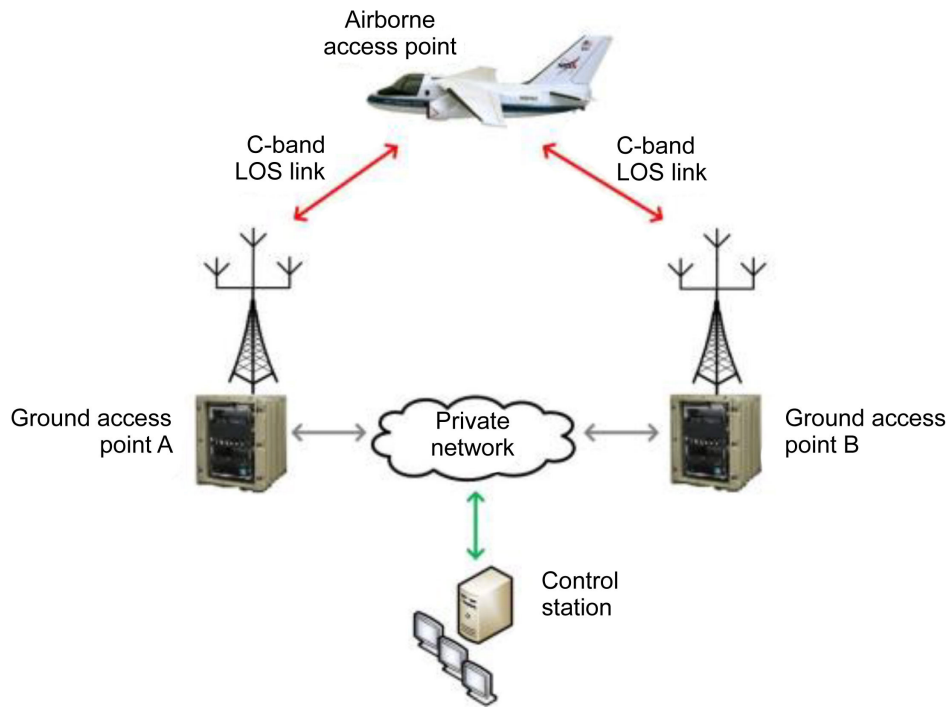


Figure 53.—Network switchover test scenario. Line of sight (LOS).

## 5.0 Generation 7 Control and Non-Payload Communications Network Switchover Test Results

Network switchover testing was performed to measure the impact of communication path changes during en route conditions of flight. A switchover should have low impact on key metrics such as latency and loss. In addition, security associations should be maintained during switchovers. The switchover scenario shown in Figure 53 was applicable to both line-of-sight and beyond-line-of-sight links.

Figure 54 shows the system of components used to emulate network layer switchover events, in a laboratory, between a ground-based pilot control station and an UA. The setup duplicated the configuration used in flight conditions and utilized three CNPC radios, one configured as the NASA S-3B aircraft and two configured as ground stations. RF power splitters, combiners, cables, and attenuators connected the radio transmit and receive ports at appropriate power levels. Flight tests were conducted with two, spatially separated ground stations to validate the laboratory results, and will be discussed in a subsequent report.

The emulation did not include manipulation of RF conditions, such as link fading or Doppler shift. Rather, attenuation was fixed to emulate a portion of flight where both ground stations would be equidistant. Thus, the focus of this test was purely on the impact of the network switchover.

The use of Mobile IPv6 allowed for seamless communication between the control station and UA as the communication path alternates between the ground stations. Figure 54 shows the path the encrypted uplink data (shown in green) would take when ground station A was active (solid red line). The figure also shows how the Mobile IPv6 tunnel changes when ground station B was used (dashed red line), making the change in paths transparent to the pilot in control.

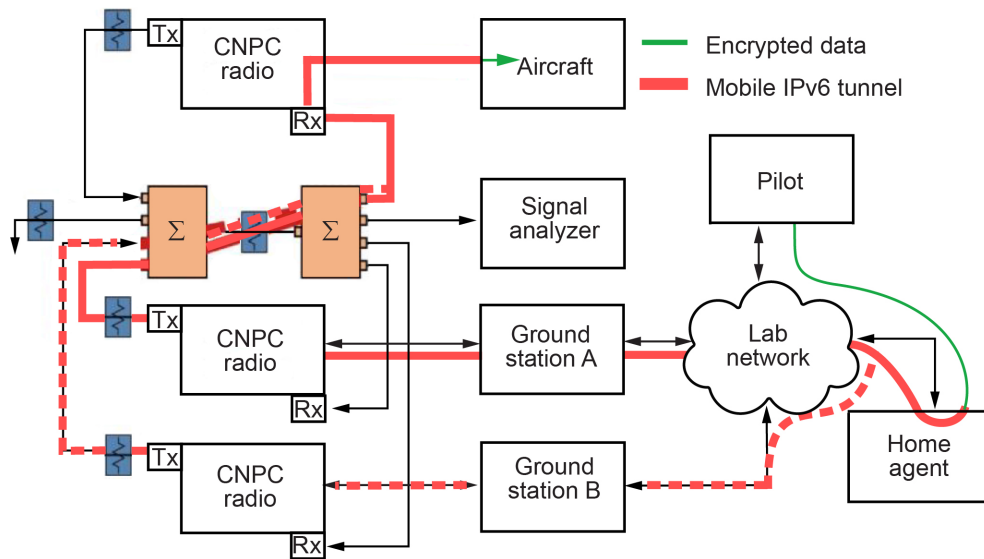


Figure 54.—Laboratory switchover test setup highlighting data flow using Mobile IPv6. Control and Non-Payload Communications (CNPC). Receive (Rx). Transmit (Tx).

Each experiment automatically performed switchovers once per minute over a 10-hour period, resulting in 600 1-minute data runs with 599 switchover events. Artificial traffic was generated to mimic Service Class 4 during the manual flight control, en route phase of flight. Service Class 4 was a traffic-heavy class that includes command and control messages and ATC voice in both directions, and additional weather and target data transmitted from the aircraft. Traffic flow from the generator was not altered or adjusted once it was started. The traffic emulator generated data at the highest possible data rates simulating a worst-case scenario. This, in addition to the high frequency of switches, was done in order to stress test switchover conditions.

Switchovers were triggered at the beginning of every minute and consisted of a series of automated changes performed by scripts intended to mimic the process of requesting a change to an already established alternate ground station. In this way, all switchovers would classify as “make-before-break” (MbB). The scripts would trigger reconfiguration of all three CNPC radios simultaneously. Figure 55 shows the frequency and subframe division used for these tests. The active link would carry data using 15 subframes. The secondary link would be established over the remaining five subframes. Note that only the even subframes switch between the two different configurations.

Two types of automated timing were tested. Figure 56 shows the timing of the system where disconnection of the active link was not tightly correlated with the change to the RF systems. Figure 57 shows the timing for a tightly tuned system that can clearly communicate the time of RF changes. In both cases, switchovers are initiated at the minute mark, beginning with a process that obtains the current radio configuration, a process that takes seconds to complete. The script then issues the appropriate reconfiguration commands that the CNPC radio will accept and implement at the next second mark. Thus, the RF configuration changes will occur exactly 3 seconds into each minute.

In the untuned case, the request to disconnect was triggered up to 1 second after the request to reconfigure the radio completes. The random wait was based on a uniform distribution and intended to mimic a system that only loosely communicates the upcoming transition. After the request to disconnect, Mobile IPv6 would wait an additional second to issue the binding update as per the standard configuration. In the tuned case, the request to disconnect was synchronized with the RF change.

Furthermore, the defaults for Mobile IPv6 were reduced, resulting in the binding update being sent shortly after the disconnection. Thus, the entire transition transaction completed much sooner. For reference, both Figure 56 and Figure 57 showed the arrival and spacing of Service Class 4 messages to help visualize the impact in the two different modes of operation. Finally, while not shown in the figures, the aircraft would initiate a reconnection to the ground station that was just disconnected (now acting as the secondary), 3 seconds after the network switchover was complete allowing for the next cycle of MbB switchover to occur.

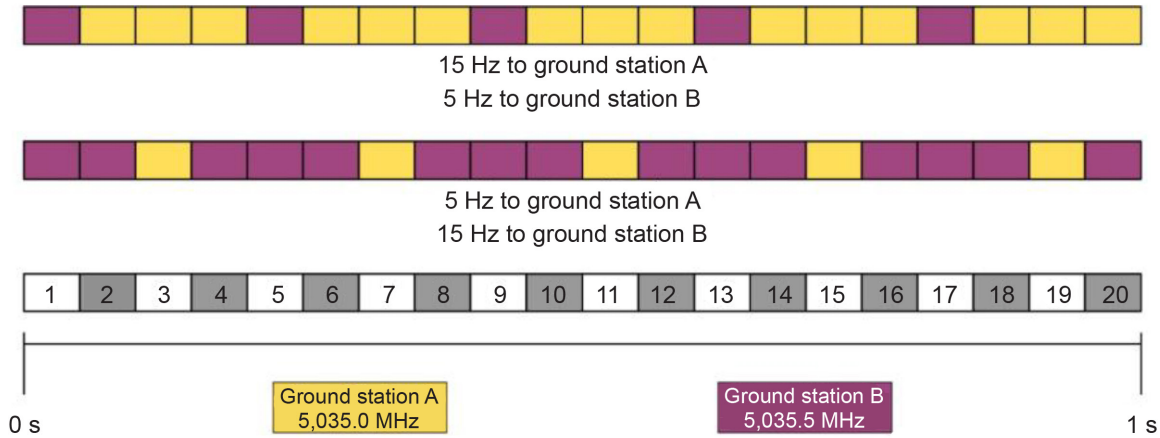


Figure 55.—Frequency and subframe division between ground stations.

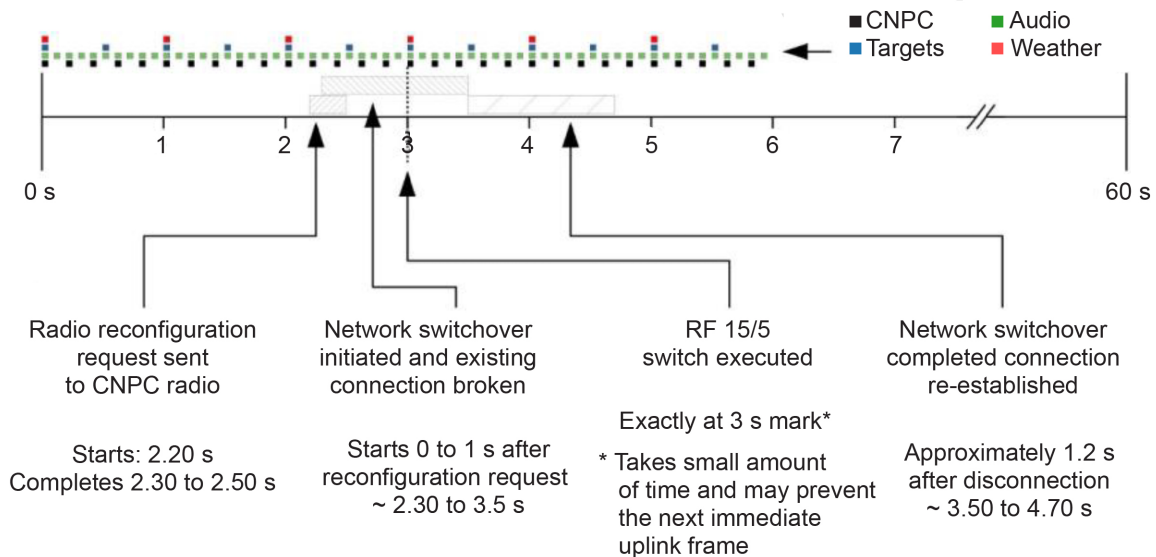


Figure 56.—Switchover timing events in an environment without fine tuning. Control and Non-Payload Communications (CNPC). Radiofrequency (RF).

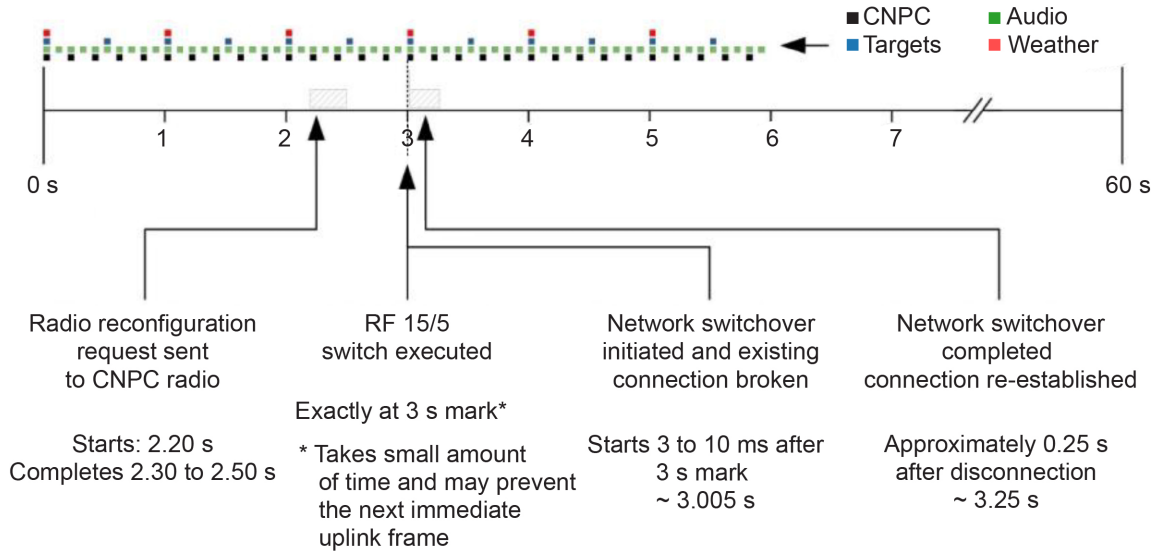


Figure 57.—Switchover timing events in an environment tuned to radiofrequency (RF) transitions. Control and Non-Payload Communications (CNPC).

The one-way latency or delay of messages between the aircraft and the pilot control station was measured during the test. Figure 58 presents the delays as a CDF for downlink and uplink traffic in both the untuned and tuned tests. The CDFs show the percentage of messages that arrived at or before a given amount of time. For example, in Figure 58(a), approximately 50 percent of the downlink C2 messages arrived at the pilot control station within 0.05 seconds and greater than 99 percent arrived by 0.1 seconds. The message priorities detailed in Section 4.8 of this report were utilized for these tests resulting in lower priority traffic having longer delays. Notably, low-priority flows have a significant increase in delays when compared to the data flow results in Section 4.8. This was due to the short 1-minute duration of each test, as the brief period of longer delays immediately after a switchover constituted a much larger portion of the data. The once-per-minute switchover rate used in this experiment exacerbated and highlighted the types of delay spikes one may expect, while the earlier data flow tests showed the more typical delays after the data flow had stabilized. Furthermore, under more common flight situations or more relaxed data rates, it was observed that delays would decrease towards a set minimum value needed to transmit a given message type. Lastly, the tuning did not significantly alter the stabilization of the data flow. However, the tuning does have a significant impact on metrics regarding the switchover directly.

Figure 59 illustrates the two types of switchover metrics captured for these tests. The first was the amount of time between reception events when one or more losses are present. While this metric was dependent on the message generation rate and size, it provided a good real use indicator of how long communication would go silent. The second metric was the total number of messages that were lost due to the switchover. If no loss occurred for a switchover event, both the time between reception events and the total number of lost messages would be zero.

Figure 60 and Figure 61 show additional CDF distribution plots for the two switchover metrics. The CDF shows the percentage of 599 switchover events that meet the metric. For example, Figure 61(c) shows the impact of tuning the switchover events, as roughly 50 percent of switchovers do not drop any messages as opposed to the untuned case in Figure 61(a) that shows the minimum number of four dropped C2 messages per switchover. Tuning the system also showed benefits for the switchover disruption duration, as the tuned system had significantly fewer delays and better adhered to the priority scheme and expected gaps, as shown in the examples in Figure 59.

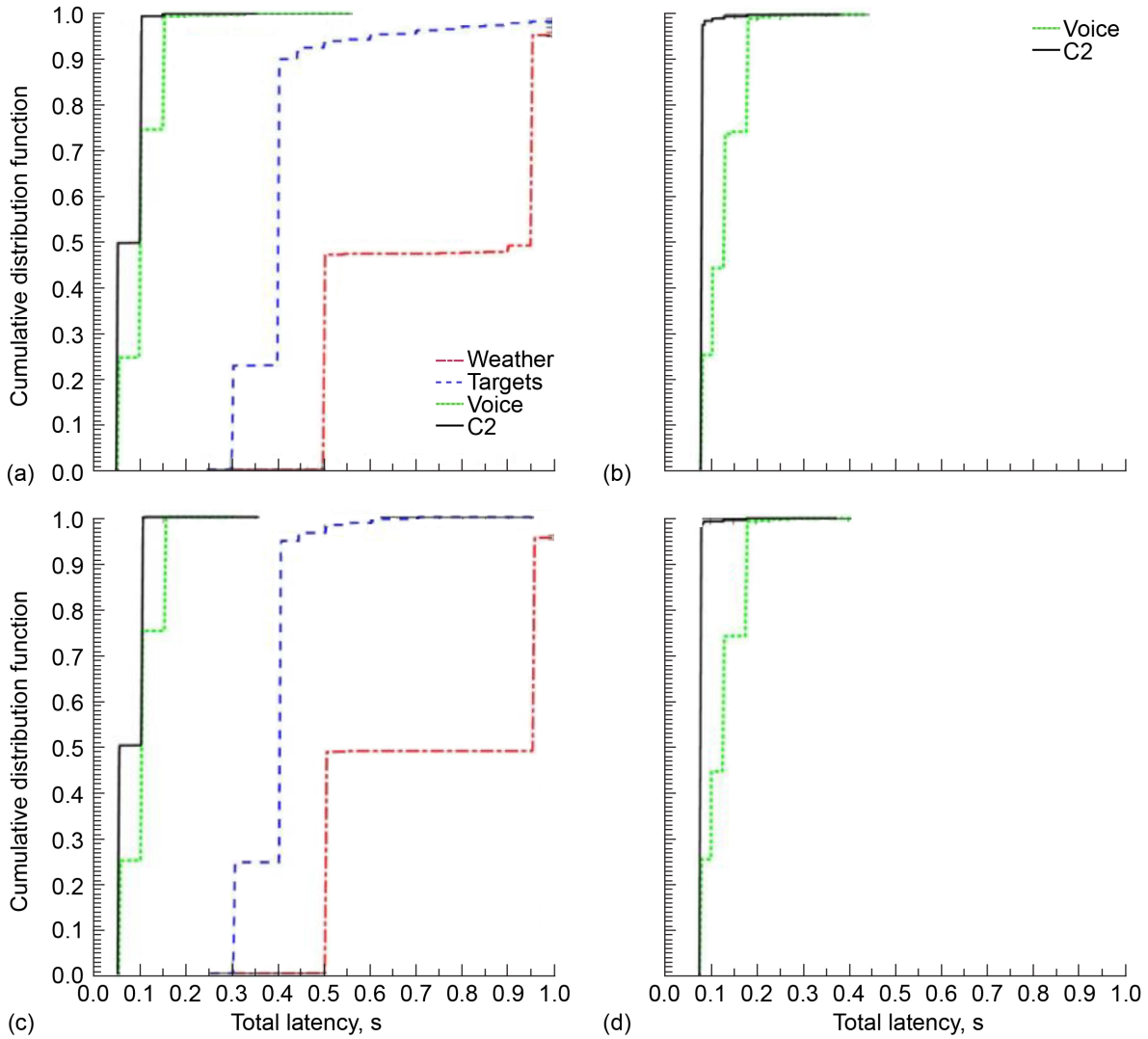


Figure 58.—Total latencies for the 10-hour switchover tests. Command and control (C2). (a) Untuned downlink. (b) Untuned uplink. (c) Tuned downlink. (d) Tuned uplink.

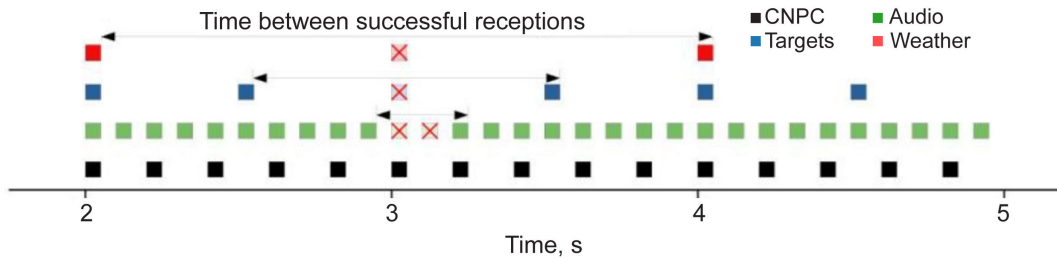


Figure 59.—Switchover metrics. Control and Non-Payload Communications (CNPC).

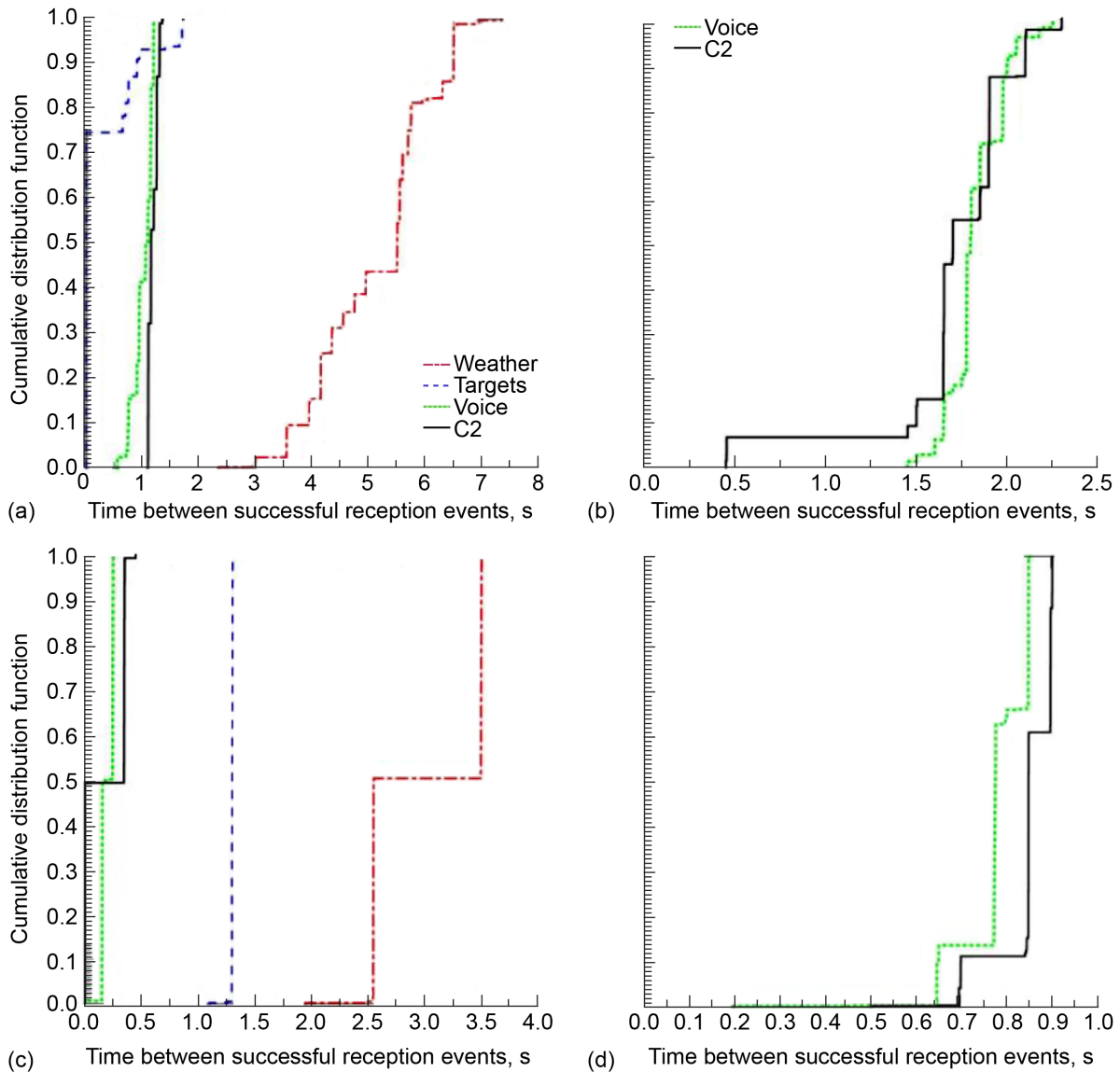


Figure 60.—Switchover disruption duration for the 10-hour switchover tests. Command and control (C2).  
 (a) Untuned downlink. (b) Untuned uplink. (c) Tuned downlink. (d) Tuned uplink.

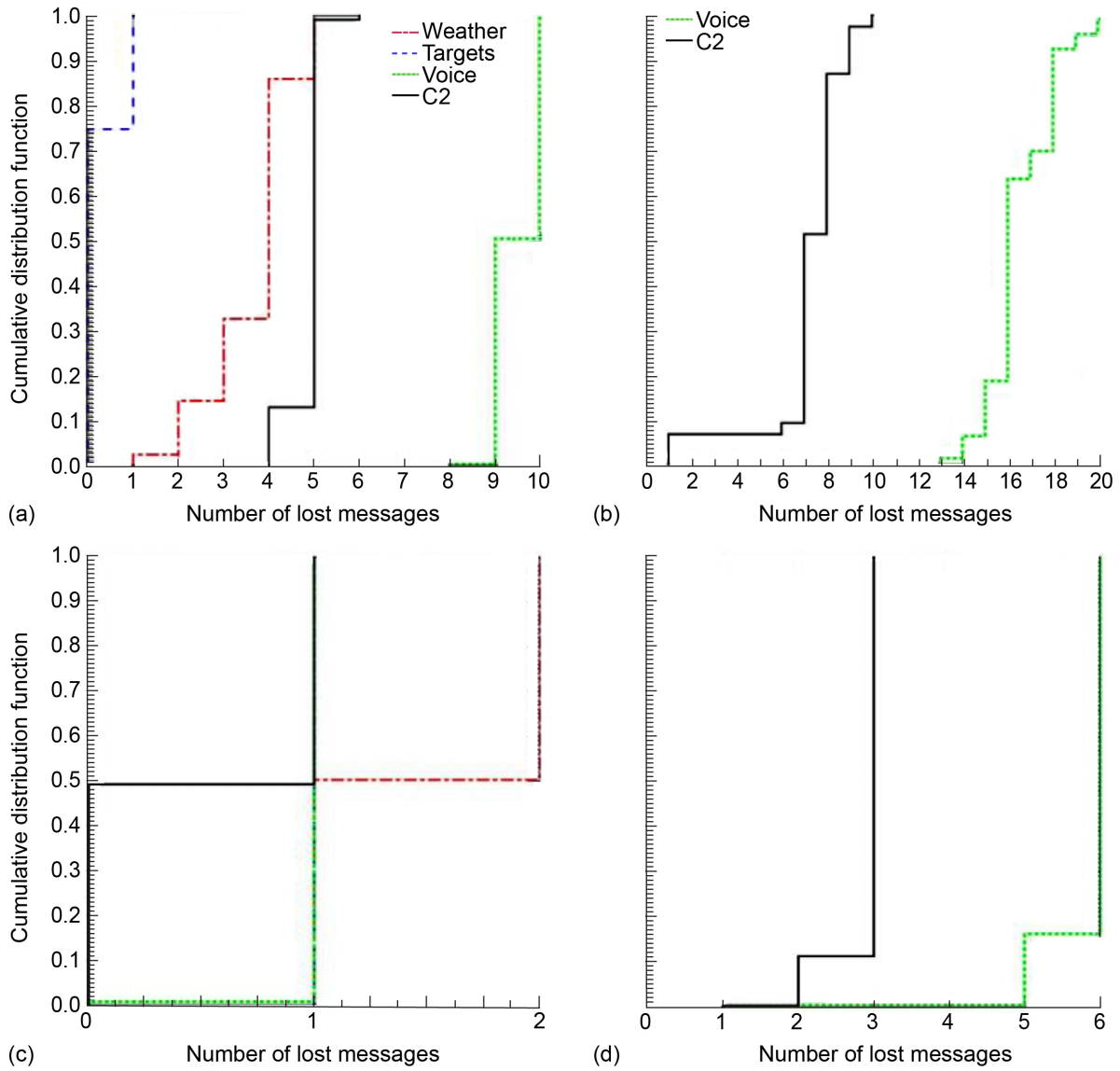


Figure 61.—Number of lost messages for the 10-hour switchover tests. Command and control (C2). (a) Untuned downlink. (b) Untuned uplink. (c) Tuned downlink. (d) Tuned uplink.

## 6.0 Conclusions

The successful completion of the Generation 7 Control and Non-Payload Communications (CNPC) radio flight test campaign and the delivery of data to the RTCA, Inc., Subcommittee (SC)–228 Working Group 2 mark the conclusion of the Unmanned Aircraft Systems Integration in the National Airspace System (UAS in the NAS) Command and Control (C2) Communications Subproject within NASA. As a result of project Phases 1 and 2, NASA Glenn Research Center researchers were able to capture and provide valuable data to support development of unmanned aircraft (UA) systems for the United States. Specific flight data was delivered to other U.S. Government agencies and used in preparation and validation of comprehensive technical standards. Additionally, the UAS C2 Subproject has led efforts to advance CNPC radio technology toward commercial application in relevant flight environments.

No propagation models or flight test data were previously available to provide the important information needed by RTCA and the technical community, so the flight tests described in this report were undertaken. The data produced in Phase 2 of the UAS in the NAS C2 Subproject covered operating ranges up to 60 nmi in flat, hilly, and over-water terrain settings, and at aircraft elevation angles that cleared the local terrain by 1.0°, 1.5°, 2.0°, and 3.0°. Data were also acquired for UA operations on airport surfaces, data which again proved to be both illuminating and highly valuable to the national community.

A complete data package providing C-band radio propagation measurement performance in multiple terrain settings was submitted to RTCA SC–228 Working Group 2 for use in preparing DO–362 Minimum Operational Performance Standards (MOPS) Revision A. In addition, the network switchover test results and data latency test results produced by Glenn were utilized by RTCA members to validate technical requirements within the DO–377 companion document entitled “Minimum Aviation System Performance Standards (MASPS) for C2 Link Systems Supporting Operations of Unmanned Aircraft Systems in U.S. Airspace.”

The Generation 7 C2 Subproject effort has demonstrated that the CNPC function can be successfully migrated to a smaller, lighter, and more efficient radio platform suitable for midsize UA. Multiuser waveforms with close channel spacing further demonstrate that radios can be used in a higher density flight environment. Laboratory and ground testing indicated that the Generation 7 Gaussian Minimum Shift Keying (GMSK) radios were able to achieve full air-ground radio-to-radio connectivity to a slant range in excess of the 35-nmi range required in the RTCA C2 MOPS document.

The Generation 7 prototype CNPC–5000E radios supplied to NASA require further maturing in order to be suitable for production units and to meet all requirements of Reference 5. The radios were determined to be highly effective for propagation and data flow investigations.

Several important NASA-centric accomplishments were also realized:

- Aeronautical communications competency—In addition to codevelopment of the CNPC radios, all other test instrumentation, electronic test support equipment, communications and data transfer systems, and test infrastructure was designed, assembled, installed, tested, and successfully operated by NASA Glenn. This included preparation of multiple mobile and fixed ground stations, data acquisition systems, aircraft flight payloads, and the UAS Flight Test Control Center. Data collection, processing, storage, and analysis processes were refined and validated. Highly unique and specialized measurement and instrumentation systems were regularly prepared for specific tests, garnering significant respect from technical experts across the United States. As a result of the skilled laboratory test capabilities and a highly successful flight test campaign, the UAS C2 team at NASA Glenn became established as a valued and well-respected independent test authority.

- Aircraft operations—The UAS C2 engineers believed that the key to the successful flight test campaign was the ability to rapidly reconfigure the test equipment and flight plans for frequent, iterative testing that became progressively more complex. The cycle of repeated test adjustments and regular reflight opportunities made possible by research aircraft and crew based at NASA Glenn provided researchers with the ability to build broad datasets and also examine specific test conditions. Fast data processing and direct communications with the aircraft allowed real-time test adjustments, retests, or refinements, even when the aircraft was in flight. This approach proved to be a very effective and efficient means of acquiring large amounts of data that specifically target customer needs and engineering goals of the project. All flight test operations were conducted safely and without incident, attesting to the skills of the UAS team members.

## References

1. RTCA, Inc.: Command and Control (C2) Data Link Minimum Operational Performance Standards (MOPS) (Terrestrial). RTCA DO-362, 2016.
2. Shalkhauser, Kurt A., et al.: Control and Non-Payload Communications Generation 1 Prototype Radio Flight Test Report. NASA/TM-2014-218099, 2014. <http://ntrs.nasa.gov>
3. Ishac, Joseph A., et al.: Control and Non-Payload Communications Prototype Radio—Generation 2 Flight Test Report. NASA/TM-2014-218391, 2014. <http://ntrs.nasa.gov>
4. Shalkhauser, Kurt A., et al.: Control and Non-Payload Communications (CNPC) Prototype Radio Validation Flight Test Report. NASA/TM-2017-219379, 2017. <http://ntrs.nasa.gov>
5. RTCA, Inc.: Command and Control (C2) Data Link Minimum Operational Performance Standards (MOPS) (Terrestrial). RTCA Paper No. DO-362A, 2020.
6. Johnson, M.E.; and Geirhart G.D.: Applications Guide for Propagation and Interference Analysis Computer Programs (0.1 to 20 GHz). DOT Report FAA-RD-77-60, 1978.





